R. A. Lohnes, F. W. Klaiber, B. H. Kjartanson, T. A. Austin,
G. A. Heilers, B. C. Morgan, E. A. Peiffer

Design Methodology for Corrugated Metal Pipe Tiedowns: Phase II

June 1995

Sponsored by the
Iowa Department of Transportation Highway Division
and the Iowa Highway Research Board

Iowa DOT Project HR-362
ISU-ERI-Ames-96401

Iowa Department of Transportation

report

College of Engineering
Iowa State University

The opinions, findings, and conclusions expressed in this publication are those of the authors and not necessarily those of the Highway Division of the Iowa Department of Transportation.

R. A. Lohnes, F. W. Klaiber, B. H. Kjartanson, T. A. Austin,
G. A. Heilers, B. C. Morgan, E. A. Peiffer

Design Methodology for Corrugated Metal Pipe Tiedowns: Phase II

Sponsored by the
Iowa Department of Transportation Highway Division
and the Iowa Highway Research Board

Iowa DOT Project HR-362
ISU-ERI-Ames-96401

engineering research institute
iowa state university

ABSTRACT

This investigation is the final phase of a three part study whose overall objectives were to determine if a restraining force is required to prevent inlet uplift failures in corrugated metal pipe (CMP) installations, and to develop a procedure for calculating the required force when restraint is required.

In the initial phase of the study (HR-306), the extent of the uplift problem in Iowa was determined and the forces acting on a CMP were quantified. In the second phase of the study (HR-332), laboratory and field tests were conducted. Laboratory tests measured the longitudinal stiffness of CMP and a full scale field test on a 3.05 m (10 ft) diameter CMP with 0.612 m (2 ft) of cover determined the soil-structure interaction in response to uplift forces.

Reported herein are the tasks that were completed in the final phase of the study. In this phase, a buried 2.44 m (8 ft) CMP was tested with and without end-restraint and with various configurations of soil at the inlet end of the pipe. A total of four different soil configurations were tested; in all tests the soil cover was constant at 0.61 m (2 ft). Data from these tests were used to verify the finite element analysis model (FEA) that was developed in this phase of the research. Both experiments and analyses indicate that the primary soil contribution to uplift resistance occurs in the foreslope and that depth of soil cover does not affect the required tiedown force.

Using the FEA, design charts were developed with which engineers can determine for a given situation if restraint force is required to prevent an uplift failure. If an engineer determines restraint is needed, the design charts provide the magnitude of the required force. The design charts are applicable to six gages of CMP for four flow conditions and two types of soil.

TABLE OF CONTENTS

LIST OF TABLES

Page

LIST OF FIGURES

Page

1. INTRODUCTION

1.1 Problem Statement

Engineers have utilized Corrugated Metal Pipe (CMP) culverts since the late 1800's as an economical alternative to bridges. In recent years, CMP have experienced inlet uplift that limits the serviceability and safety of CMP (Federal Highway Administration, 1974 and Pestonik, 1976). In many instances, the uplift caused the roadway above the pipe to fail.

Pore water pressures acting beneath the CMP are thought to be the cause of the longitudinal uplift. The pore pressure develops from a hydraulic head difference, created by high flows and/or partial blockage, between the CMP inlet and outlet (Federal Highway Administration, 1974).

Many state Departments of Transportation have design guidelines for determining the magnitude of force required to restrain CMP against these uplift forces. A previous study showed that the required restraint force determined from the various guidelines varied as much as 500% for a 3.05 m (10 ft) diameter CMP. Furthermore, no evidence was provided on the experimental or analytical basis for the various state specifications.

1.2 Objective and Scope of Investigation

The objective of this investigation is to provide a design method to determine the required force for restraining a CMP against inlet uplift. Chapter 2 of this report details the design method, and Appendix A contains examples of how to apply the method. A summary of the experimental and analytical work that provides the rational for these design guidelines is presented in Chapters 3 and 4.

1.3 Previous Experimental and Analytical Work

Full field tests were conducted on pipes ranging in diameter from 1.2 m (4 ft) to 3.05 m (10 ft). Three tests were completed to determine the longitudinal flexural stiffness and strength of the pipes without soil cover (Havens, 1993 and Klaiber et al, 1993) and one test undertaken to determine the uplift response of a 3.05 m (10 ft) diameter CMP under 0.6 m (2 ft) of soil cover with a 2:1 foreslope (McCurnin, 1993 and Klaiber et al, 1993).

Five full scale field tests focused on foreslope and restraint conditions (Morgan, 1995). Two and three dimensional finite element methods (FEM) and finite difference methods (FDM), respectively, were used to analyze the soil-structure interaction in these tests. The two dimensional model analyzed the resisting forces attributed to soil properties, cover depth, and CMP diameter (Heilers, 1994). The three dimensional FEM model was used to investigate soil properties as well as pipe properties (Peiffer, 1995) and is the basis for the design method presented here. Data from the previously noted full scale model tests were used to calibrate the FEM. The experimental and analytical work not described in previous reports (Austin et al, 1990 and Klaiber et al, 1993) to the Iowa Department of Transportation Highway Research Advisory Board is discussed in Chapters 3 and 4 of this report.

2. DESIGN METHOD FOR UPLIFT RESTRAINT

2.1 Assumptions and Limitations of the Design

The method presented in this chapter is based on a three dimensional FEM analysis that is described in detail by Peiffer (1995). The CMP is modeled as a smooth shell pipe with equivalent properties and the soil is assumed to be linearly elastic. The model was applied for different combinations of pipe stiffness, pipe diameter, soil characteristics, foreslopes, depth of cover, and hydraulic conditions. A hydraulic load was included in the model, with the inlet restrained, to determine the amount of resisting force needed to prevent uplift.

The following assumptions were made in this FEM analysis:

1. The toe of the slope is at the end of the pipe.
2. The roadway width is 9 m (30 ft).
3. Uplift force results from pore pressure with the maximum head equal to the pipe diameter at the inlet. The pressure dissipates linearly to zero at the outlet.
4. Backfill soil ranges from a stiff glacial till with an elastic modulus of 16.5 MPa (2400 psi) to a medium consistency alluvial clay with an elastic modulus of 2.9 MPa (425 psi).
5. Restraining force is based on a maximum allowable deflection of 12.5 mm (0.5 in) -1/2 the CMP corrugation depth - at the inlet. This allows the restraining force, pipe stiffness, and soil stiffness to be mobilized.

The FEM analysis also has the following limitations:

1. The method applies only for 75 mm x 25 mm (3 in. x 1 in.) corrugation style.
2. Design procedure applies only to pipes between 1.2 m (4 ft) and 3.05 m (10 ft) in diameter.
3. The analysis is for a projecting (not beveled) inlet.
4. The design charts are based on 2:1 foreslopes, but additional analyses indicate 3:1 foreslopes require a restraining force 1.5 times greater than 2:1 slopes.

2.2 Procedure for Determining Required Restraining Force

The flowchart in Figure 2.1 provides an outline of the procedure to determine if a restraining force is needed and the magnitude of such a force if required. The design method is explained in the following sections, along with comments to aid in the process. Several design examples are presented in Appendix A.

2.2.1 Retrofitting an existing culvert

This design procedure can be applied to culverts that are already in use. Follow the retrofit path on the right side of the flowchart in Figure 2.1 to determine if restraint is required for an existing culvert. If restraint is needed, the procedure can be used to determine the magnitude of restraining force.

2.2.2 Determine site geometry and characteristics

The first step in the design process is to determine the required pipe length. The roadway width and elevation, elevation and slope of flow line, and the foreslope angle establish the CMP length based on the assumption that the end of the pipe is at the toe of the slope. A minimum soil cover of 0.6 m (2 ft) is required. Analyses conducted with varying depths of cover indicated that the depth of soil is not critical in determining the required restraining force. The largest resistance to the uplift occurs within the foreslope; therefore, increases in the depth of cover have no effect on the restraining force.

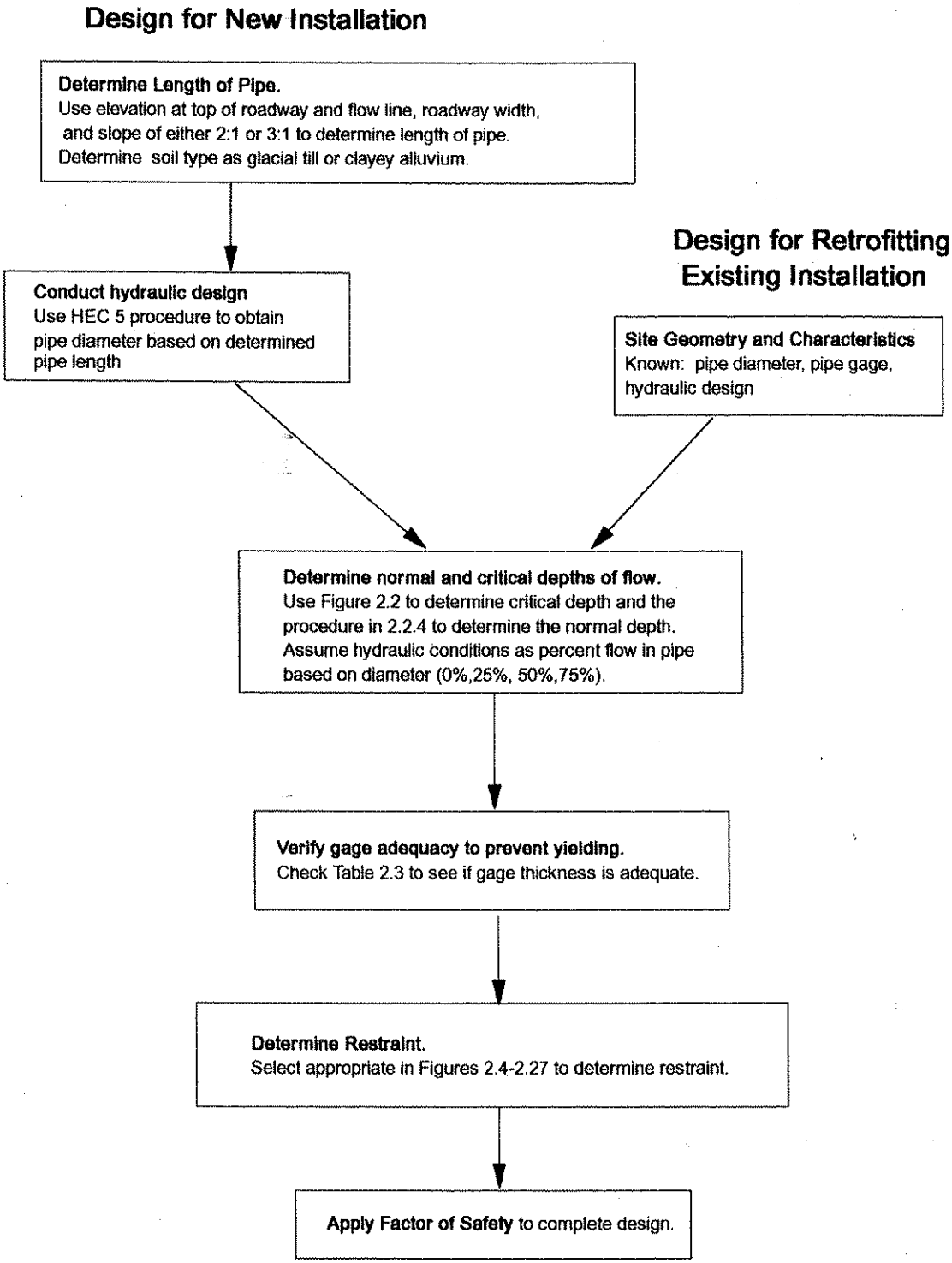

Figure 2.1 Flowchart for design process to determine restraining force.

2.2.3 Hydraulic design of culvert

The design discharge is estimated from the drainage area flowing into the culvert using the Iowa DOT runoff chart. With the length of pipe and design discharge known, the diameter of the culvert, CMP, is determined using HEC-5 (FHWA 1985). Concern for uplift is more significant under inlet control since the pipe will be flowing partially full during inlet control. Select a diameter that will produce a headwater (HW) less than the allowable headwater (AHW) established at the site. For projecting inlets, the HW equal to the pipe diameter (D) seems to be critical. If the design HW is greater than D, determine the flow rate, Q, from the inlet control charts in HEC-5 using HW/D = 1. Use this Q in the next steps.

Once the diameter of the culvert has been determined, select the gage of CMP according to the procedure recommended by the American Iron and Steel Institute (1983).

2.2.4 Determine critical and normal depths of flow

To determine the critical depth of flow, use the discharge from Section 2.2.3 used in HEC-5 and go to Figure 2.2. From the discharge, extend a vertical line to the pipe diameter, from this point extend a horizontal line to the ordinate to determine the critical depth. Critical depth will occur near the entrance of a culvert flowing under inlet control.

The process for determining the normal flow depth is an iterative process which solves Manning's equation. Manning's equation can be written as follows:

$$Q = \frac{X}{n} AR^{2/3} S^{1/2} \qquad 2.1$$

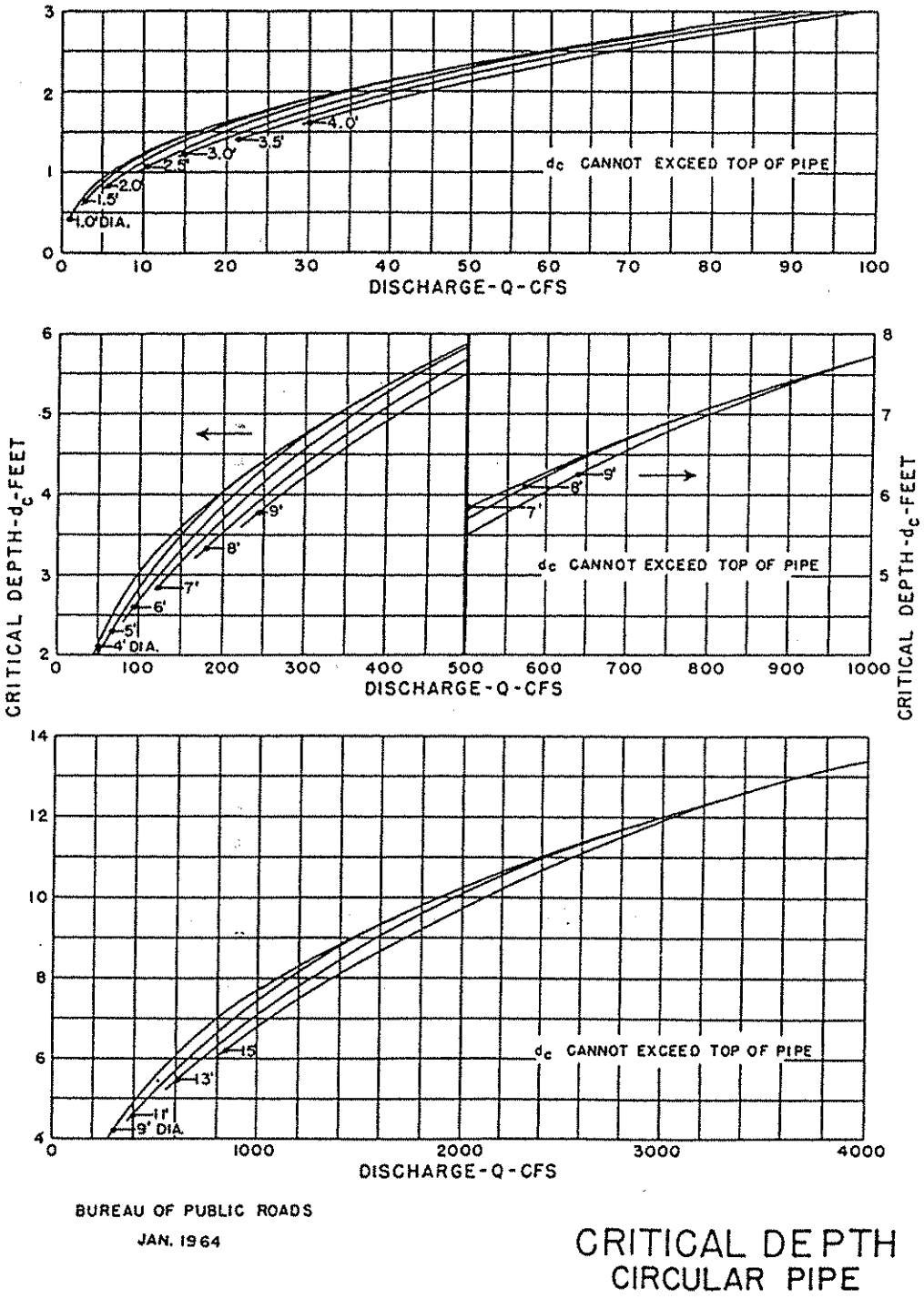

Figure 2.2. Determination of critical depth (After FHWA 1965,1986).

where:

Q = Discharge, m^3/s

X = 1.0 for SI units or 1.49 for English units

n = roughness coefficient (typical value for corrugated metal pipe is 0.024)

A = cross sectional area, m^2

R = mean hydraulic radius (wetted area/wetted perimeter), m

s = slope of channel

To determine the normal depth of flow, Manning's equation is rewritten as:

$$AR^{2/3} = \frac{Qn}{Xs^{1/2}} \qquad 2.2$$

The cross sectional area (A) and the hydraulic radius (R) are functions of the normal depth, Dn. For a rectangular channel cross section, A = (Dn x w), where w is the channel width, and R = A/((2 x Dn)+ w). Different shaped channel cross sections produce different values of A and R. The wetted perimeter, which is (2 x Dn+w), is that portion of the channel cross section which is in contact with flowing water. The solution for the normal depth, Dn, is obtained by placing the variables into Table 2.1 and iterating with different values of Dn until the values in the last two columns are equal. This is easily achieved by using a computer spreadsheet.

Table 2.1 Format for iterative solution for normal depth of flow, Dn.

Cycle	Dn	A	Wetted perimeter	R	$AR^{2/3}$	$Qn/Xs^{1/2}$
1						
2						

Flow in a long culvert pipe of constant slope will approach normal depth.

2.2.5 Determining assumed flow in pipe

Based upon the CMP diameter and the critical and normal depths of flow, the assumed depth of flow in the pipe is determined by matching either the critical or normal depth of flow to water levels in the pipe of 0%, 25%, 50%, and 75% of the pipe diameter. Another possibility is to use the average of critical and normal depths of flow.

The amount of restraining force required is reduced if water is flowing in the pipe. Austin et al (1990) presented methods to determine flow profiles that occur in CMP, but these computed profiles are difficult to include within finite element programs; therefore, the analyses for determining restraint forces were conducted with constant water levels in the pipe of 0%, 25%, 50%, and 75% of the pipe diameter, as shown in Figure 2.3.

The selection of normal or critical flow to match the percentages of flow is left to the judgment of the engineer. Experience is the basis for determining if a no flow condition is likely. During floods, smaller diameter pipes have a greater possibility of becoming blocked due to debris while in larger diameter pipes there is less likelihood of complete blockage.

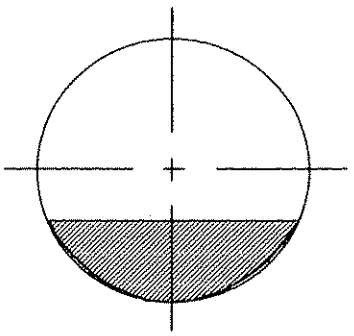

(a) Flow at 25% of pipe diameter

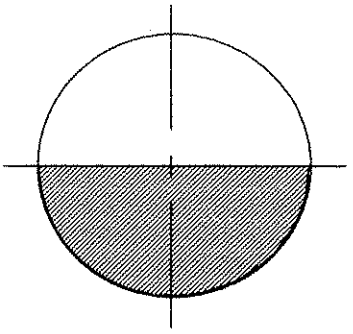

(b) Flow at 50% of pipe diameter

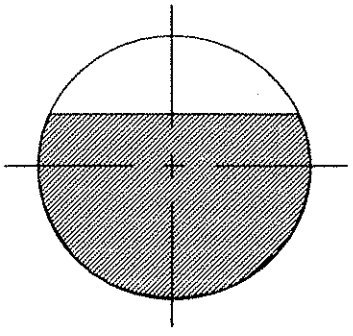

(c) Flow at 75% of pipe diameter

Figure 2.3. Cross sectional view of assumed flow conditions.

2.2.6 Adequacy of selected gage thickness

The hydraulic loading can create a maximum negative moment in the CMP between the restraint and the soil embankment. In some instances, the gage of steel selected from the American Iron and Steel Institute (1983) manual may not provide the flexural strength needed to withstand this moment. If the moment is too great, the longitudinal bending stiffness of the pipe is exceeded, and the steel in the pipe will yield, causing excessive deflections in the pipe.

Using the pipe diameter and assumed flow condition, yielding of the steel can be prevented by following the guidelines in Table 2.2. If the previously determined pipe gage is not in the suggested range, yielding can be prevented by selecting a gage which is in the recommended range. If in retrofitting a culvert the gage of steel is found to be inadequate to prevent yielding, the engineer can employ alternate structural modifications to increase the longitudinal stiffness of the CMP and thus prevent negative moment yielding.

Table 2.2 Pipe gage required to prevent negative moment yielding.

Diameter	Assumed Flow Conditions			
	No Flow	25% Flow	50% Flow	75% Flow
1.2 m (4 ft)	*	*	*	*
1.8 m (6 ft)	8 - 14	8 - 16	*	*
2.7 m (8 ft)	8 - 12	8 - 12	8 - 16	*
3.0 m (10 ft)	8 - 10	8 - 12	8 - 18	*

* All gages are acceptable

2.2.7 Determination of required restraint

The soil type and stiffness, pipe gage, and assumed flow conditions within the CMP are needed to determine the required restraining force. Select the appropriate design chart from Figures 2.4-2.27 which corresponds to the correct pipe gage and assumed flow conditions. Table 2.3 identifies the appropriate design chart for a given pipe gage and assumed flow condition. The conversion factor for the pipe diameter is 1 m = 3.3 ft.

Using the appropriate design chart, the restraining force is determined by extending a vertical line from the pipe diameter to the curve for the type of backfill material over the CMP. From this intersection, extend a horizontal line to the ordinate. This value on the ordinate is the amount of restraining force required. If the backfill material used at the site has stress strain (stiffness) characteristics between those of glacial till and alluvial clay, an interpolation between the two curves based on experience is appropriate.

Note in Figure 2.27 that the required restraining force is independent of soil type for 18 gage pipe with 75% flow. Figures 2.7 and 2.11 indicate that no restraint is required if a stiff glacial till backfill material is used.

The design charts are based on 2:1 foreslopes, but as previously noted 3:1 foreslopes are accommodated by multiplying the restraining force determined for the 2:1 foreslope by a factor of 1.5.

Installation of the culvert and surrounding backfill material shall follow current Iowa DOT Specifications (1993). FEM analyses were conducted with soil properties of a stiff glacial till, E=16.5 Mpa (2400 psi), and a medium consistency clayey alluvium, E=2.9 Mpa (425 psi). These two soil

Table 2.3. Location of design charts.

CMP Gage	Flow Condition	Figure Number	Page
8	0%	2.4	14
	25%	2.5	14
	50%	2.6	15
	75%	2.7	15
10	0%	2.8	16
	25%	2.9	16
	50%	2.10	17
	75%	2.11	17
12	0%	2.12	18
	25%	2.13	18
	50%	2.14	19
	75%	2.15	19
14	0%	2.16	20
	25%	2.17	20
	50%	2.18	21
	75%	2.19	21
16	0%	2.20	22
	25%	2.21	22
	50%	2.22	23
	75%	2.23	23
18	0%	2.24	24
	25%	2.25	24
	50%	2.26	25
	75%	2.27	25

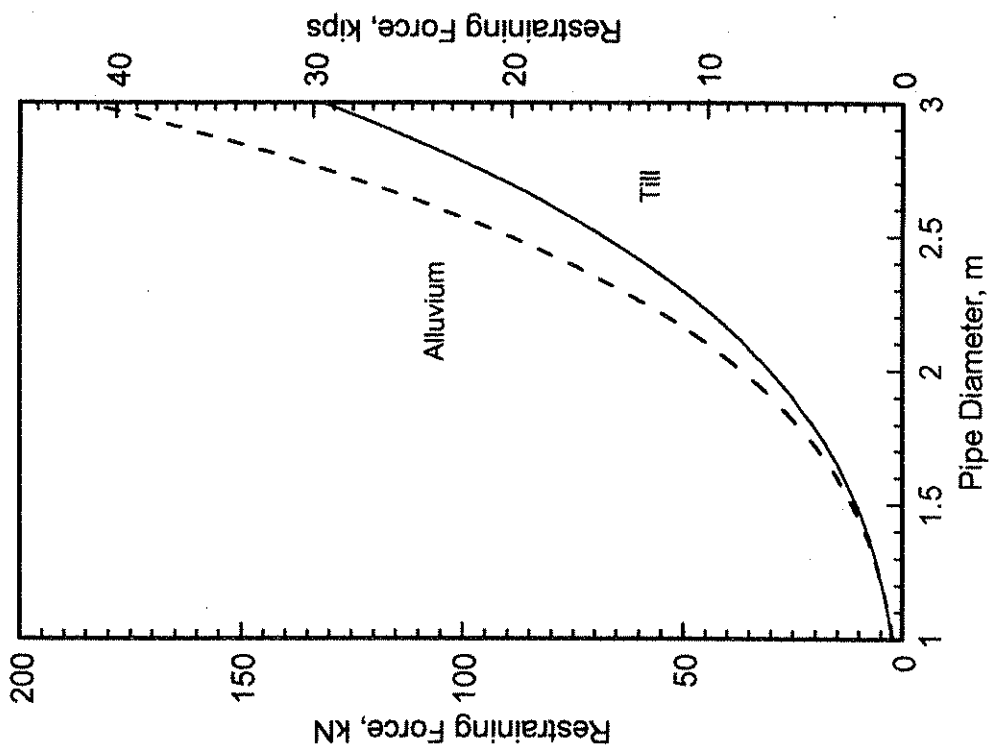

Figure 2.5. Design chart for 8 gage pipe with 25% flow

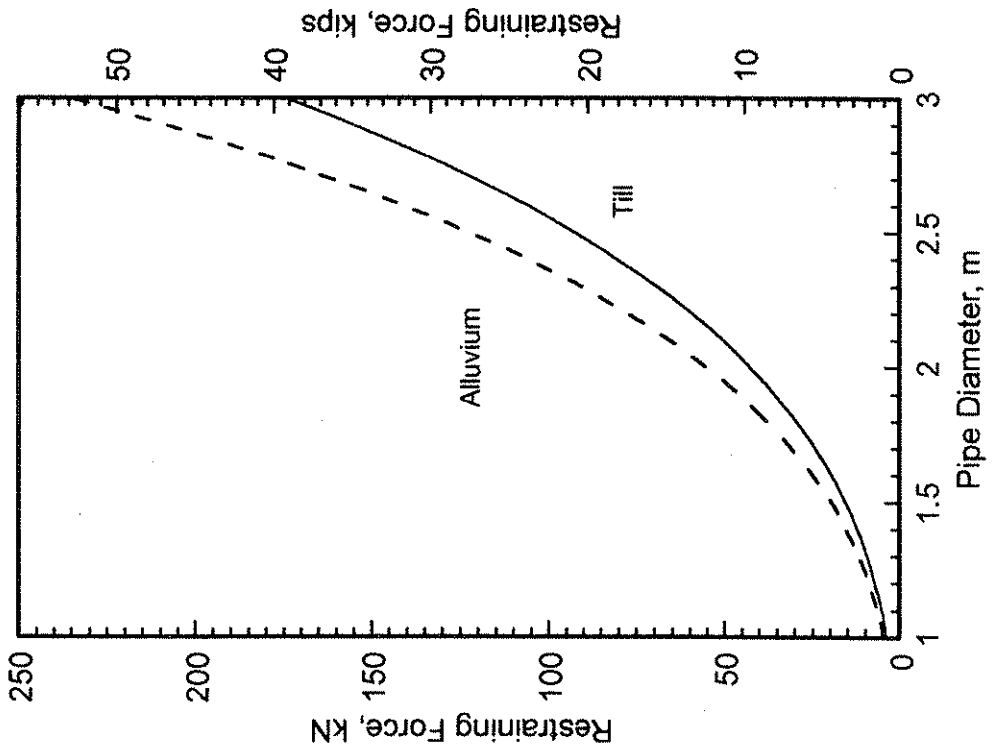

Figure 2.4. Design chart for 8 gage pipe with no flow

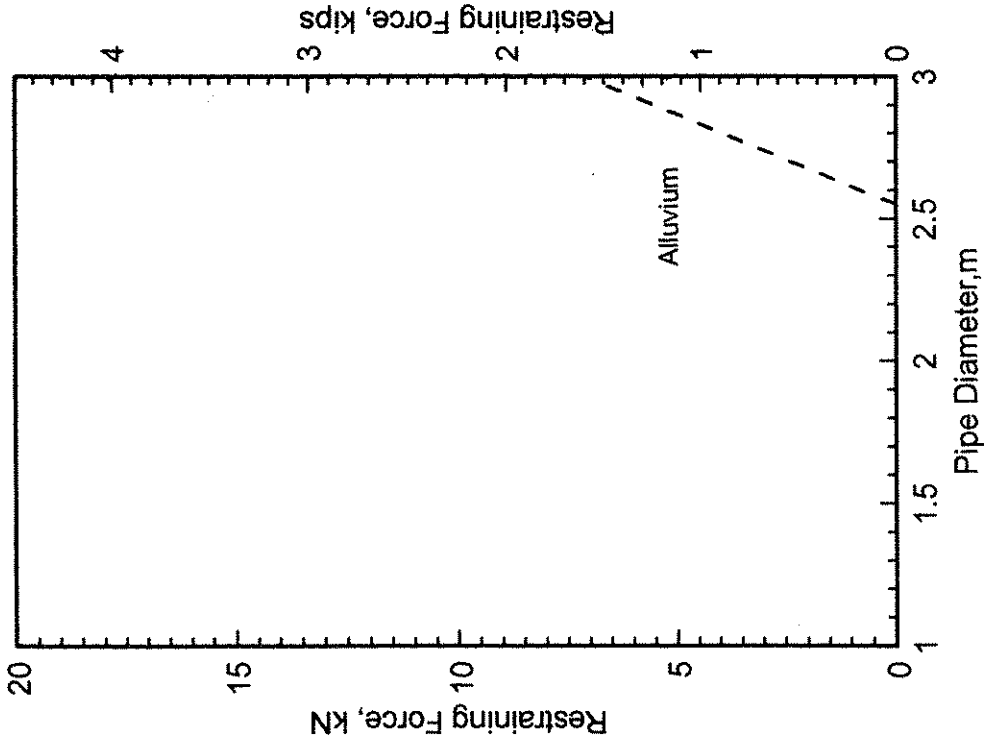

Figure 2.7 Design chart for 8 gage pipe with 75% flow.

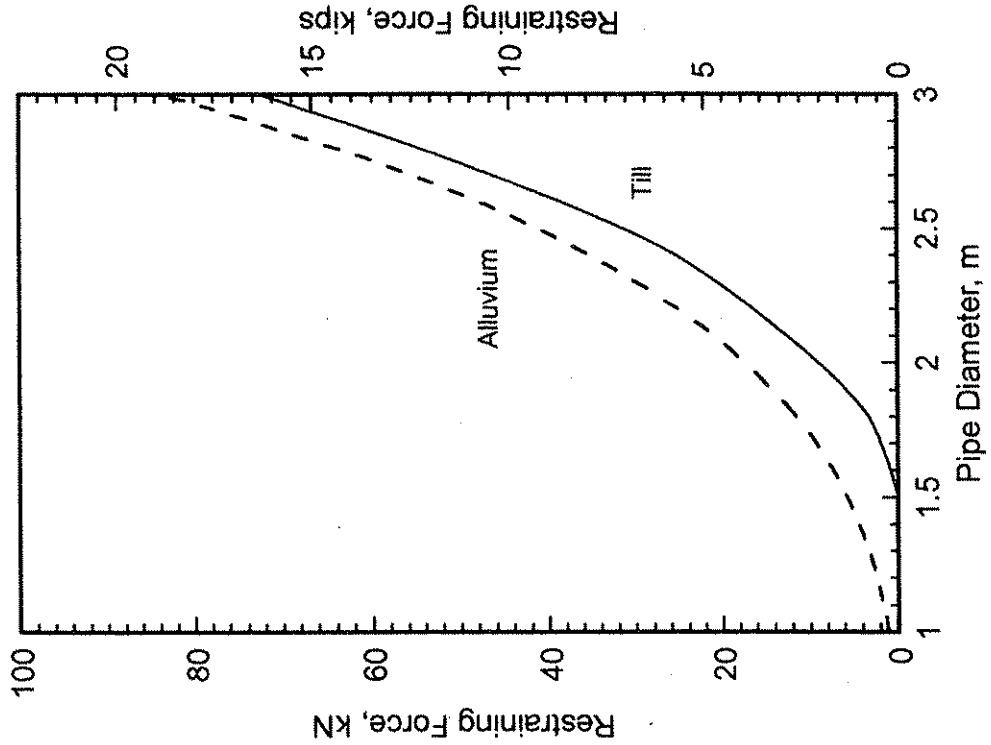

Figure 2.6 Design chart for 8 gage pipe with 50% flow.

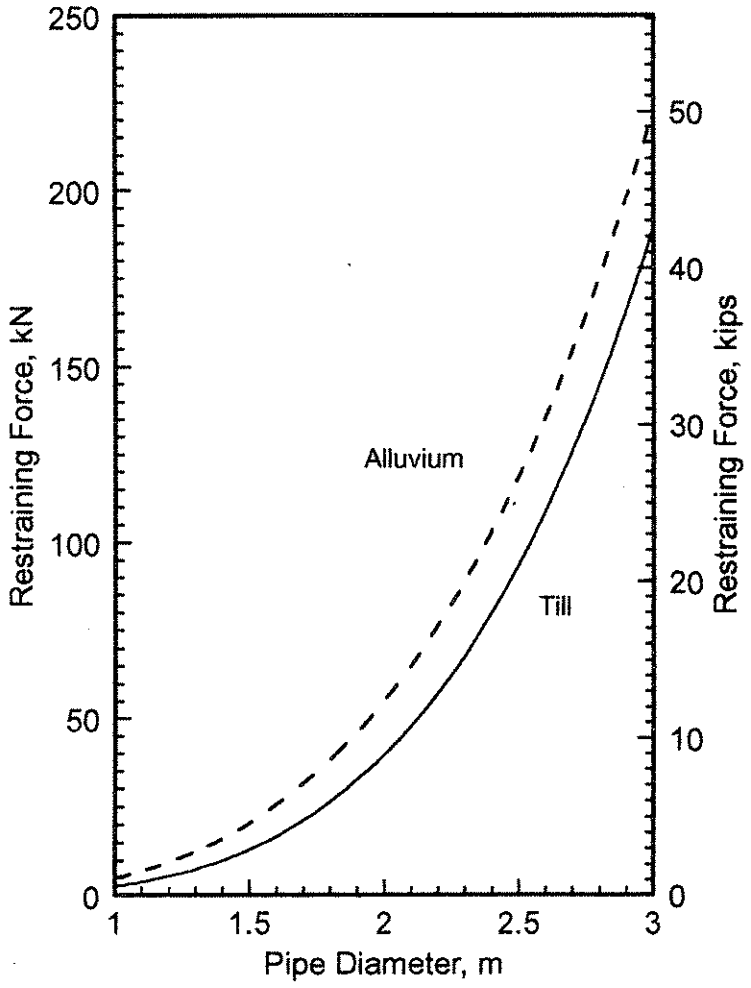

Figure 2.8. Design chart for 10 gage pipe with no flow.

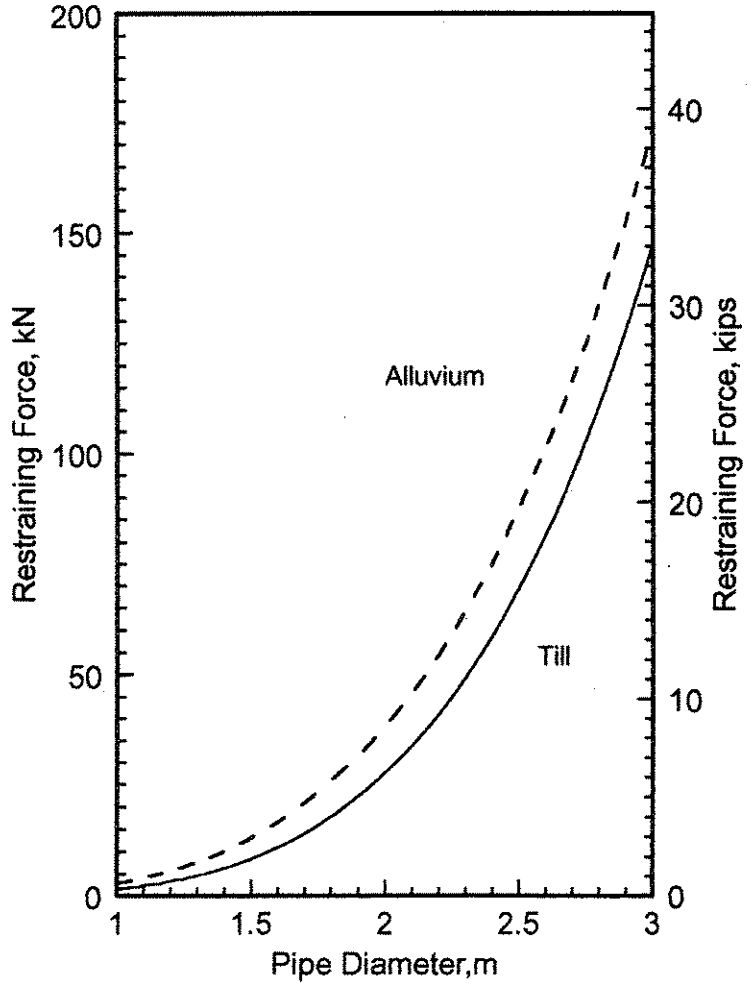

Figure 2.9. Design chart for 10 gage pipe with 25% flow.

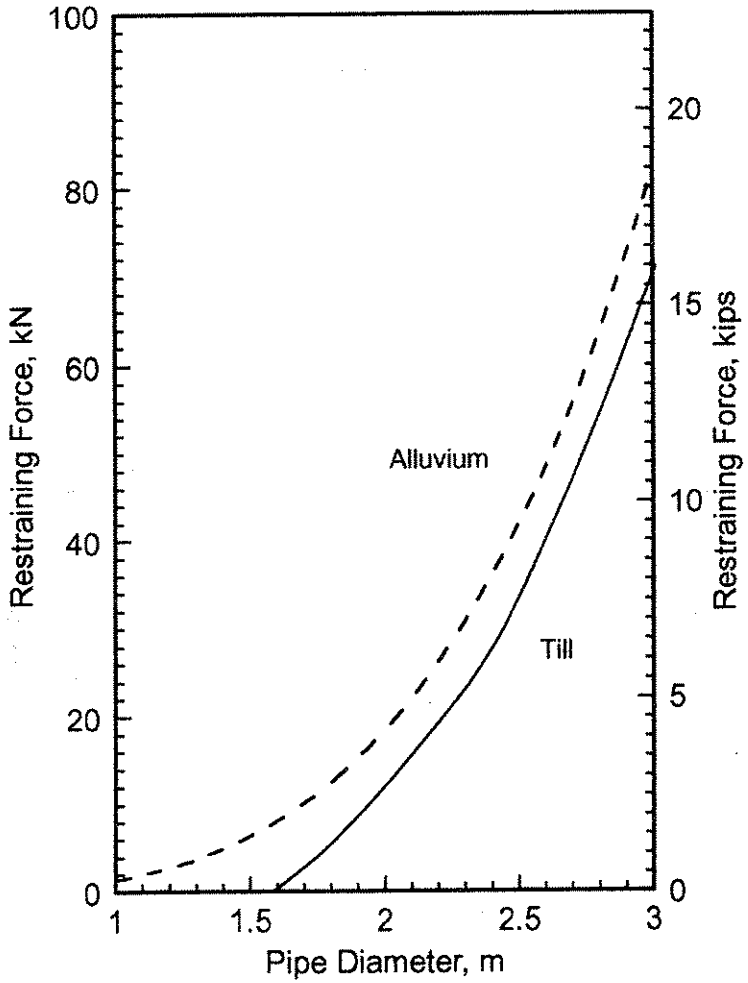

Figure 2.10. Design chart for 10 gage pipe with 50% flow.

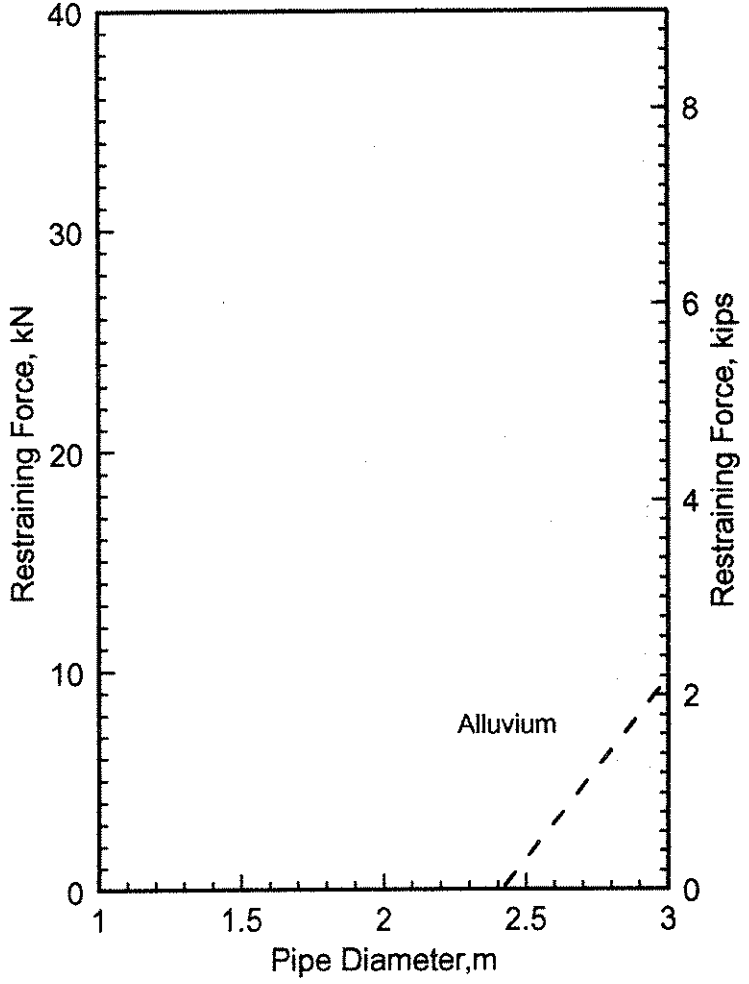

Figure 2.11. Design chart for 10 gage pipe with 75% flow.

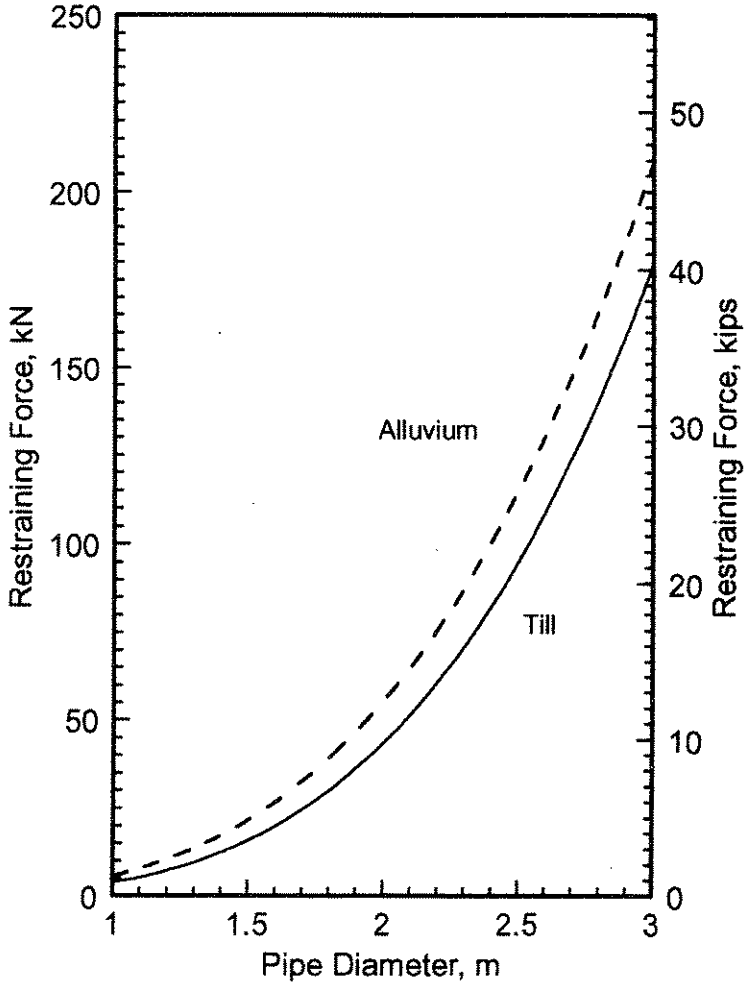

Figure 2.12. Design chart for 12 gage pipe with no flow.

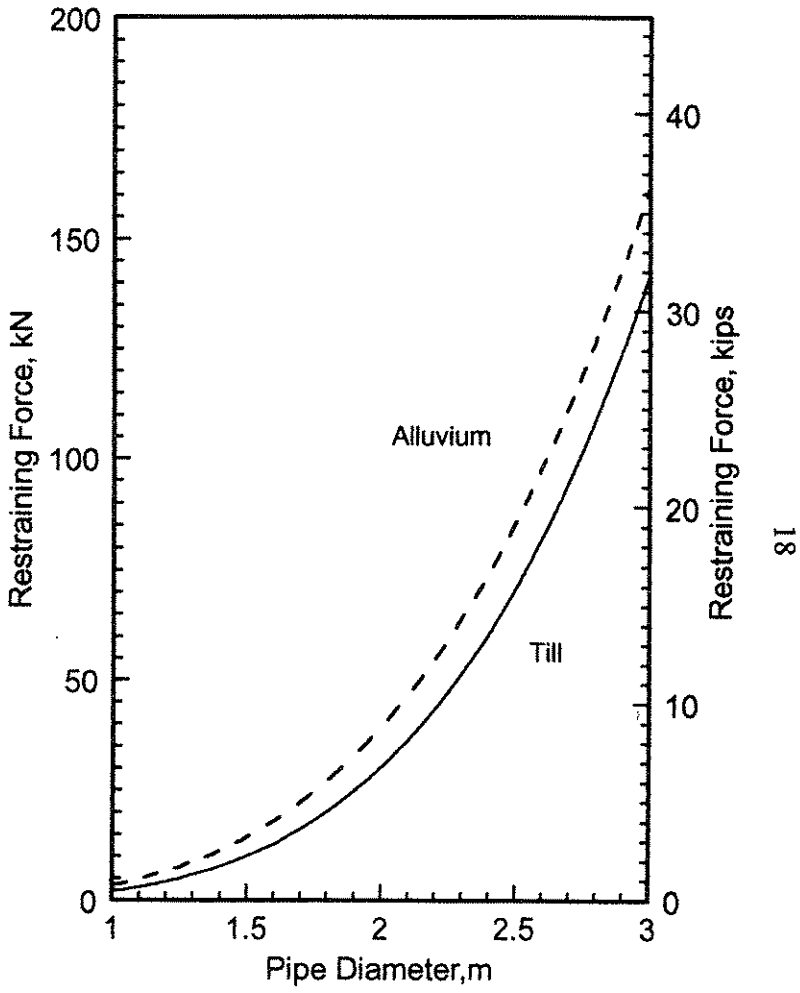

Figure 2.13. Design chart for 12 gage pipe with 25% flow.

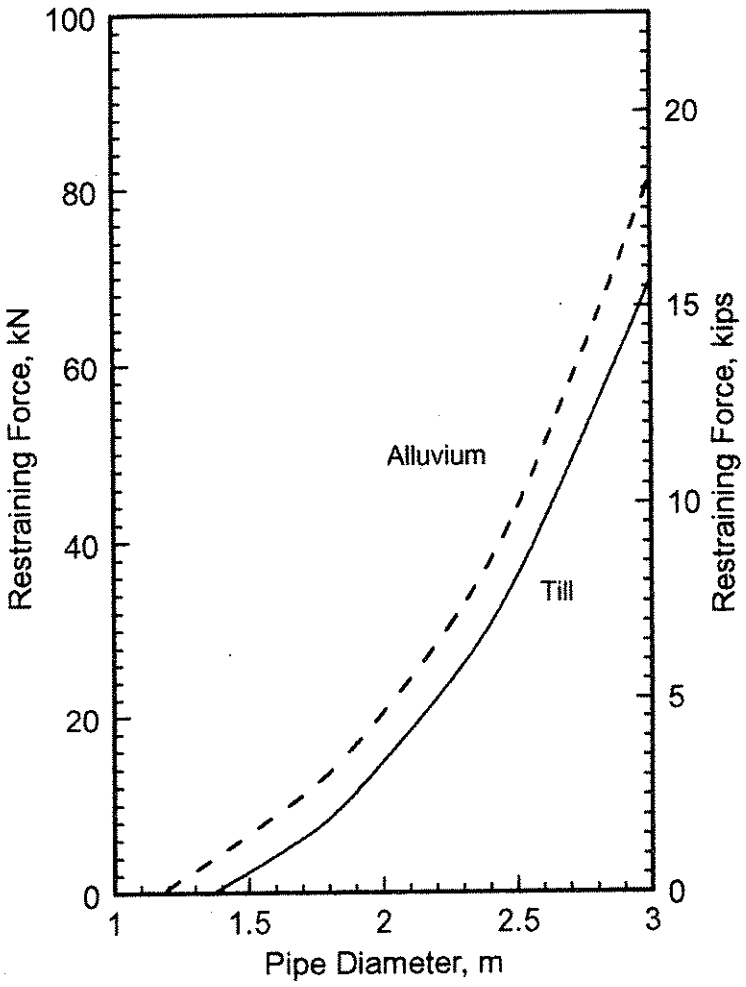

Figure 2.14. Design chart for 12 gage pipe with 50% flow.

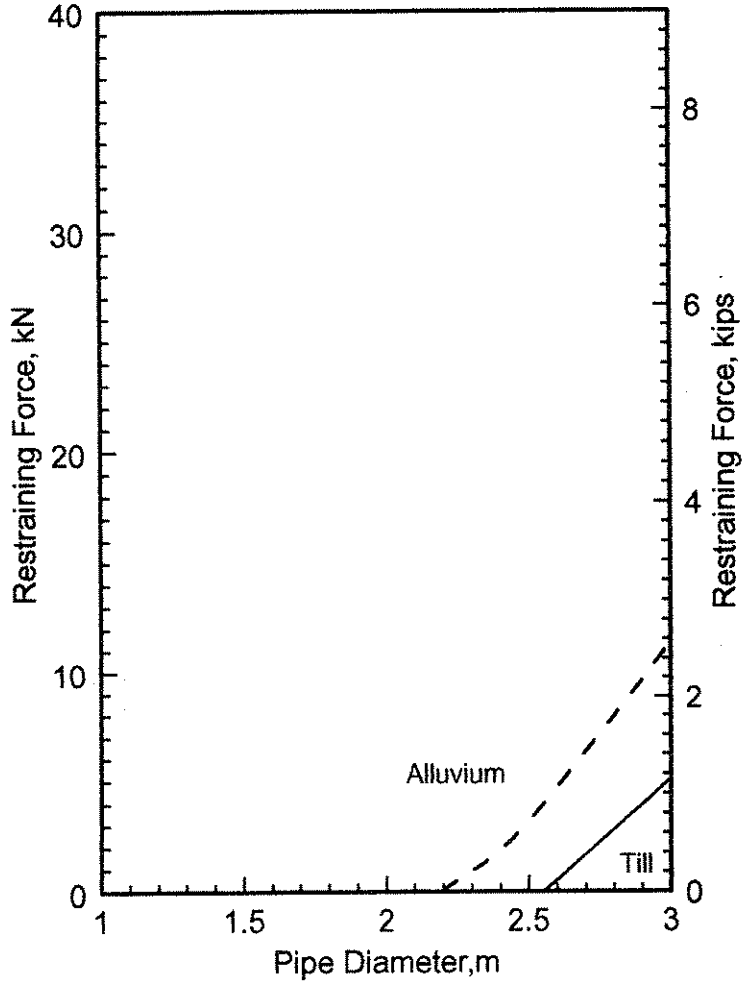

Figure 2.15. Design chart for 12 gage pipe with 75% flow.

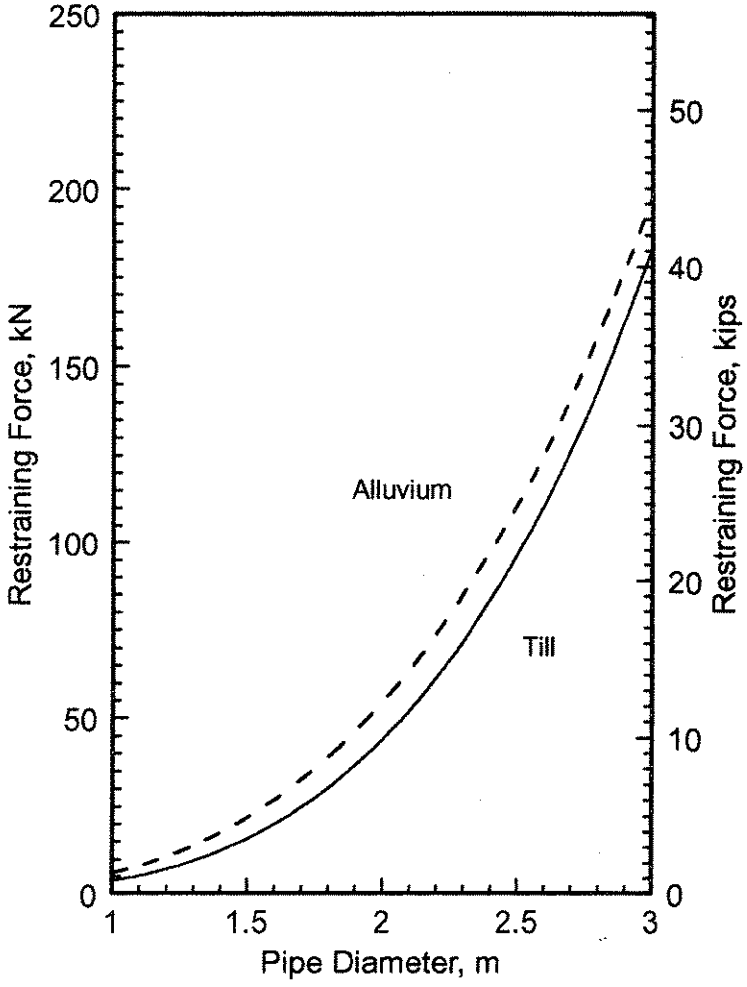

Figure 2.16. Design chart for 14 gage pipe with no flow.

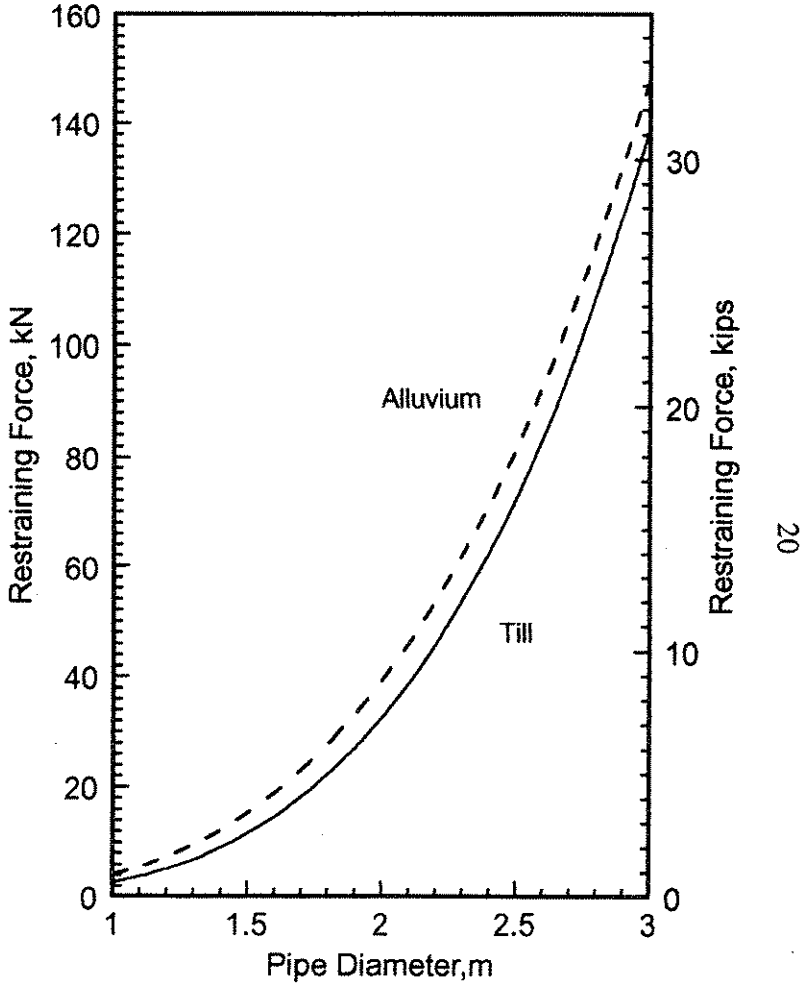

Figure 2.17. Design chart for 14 gage pipe with 25% flow.

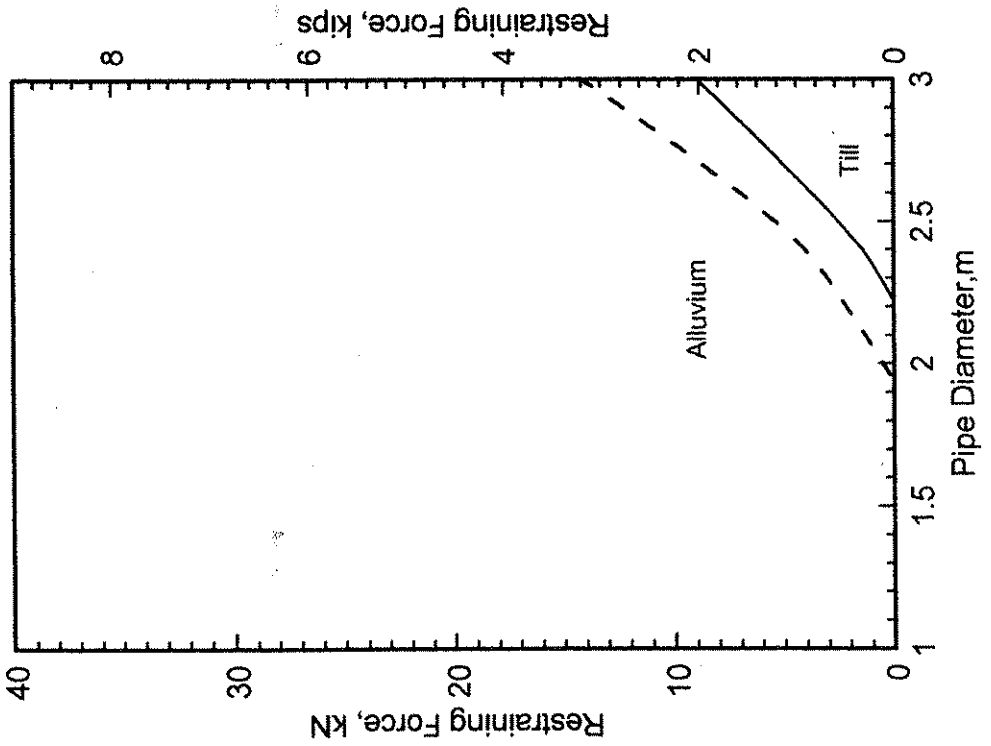

Figure 2.19. Design chart for 14 gage pipe with 75% flow.

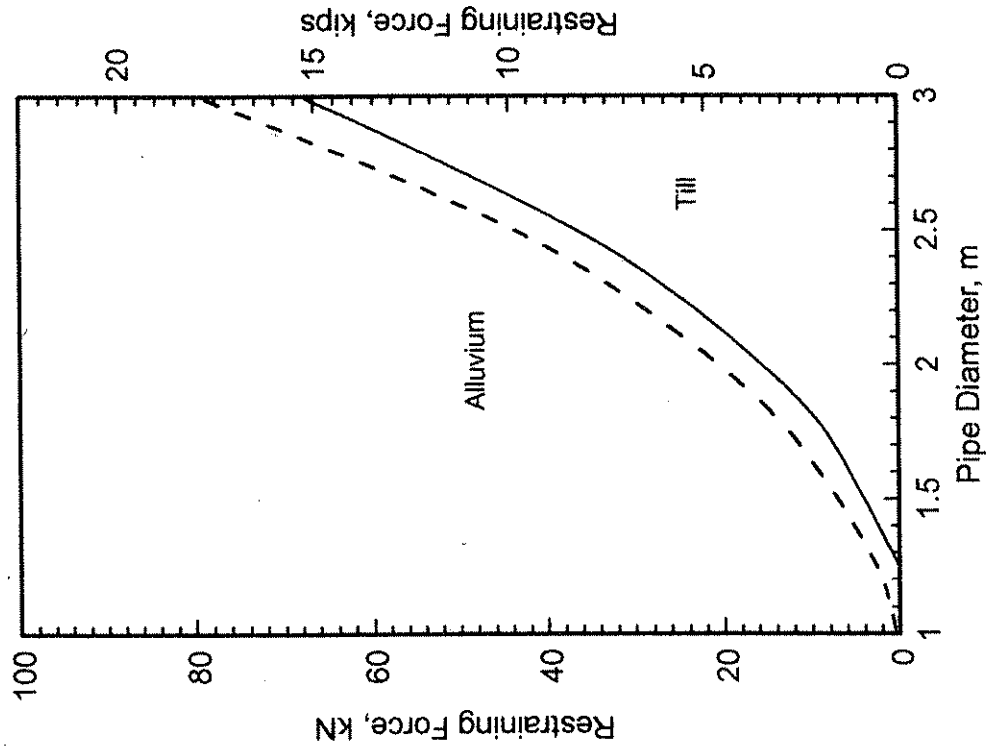

Figure 2.18. Design chart for 14 gage pipe with 50% flow.

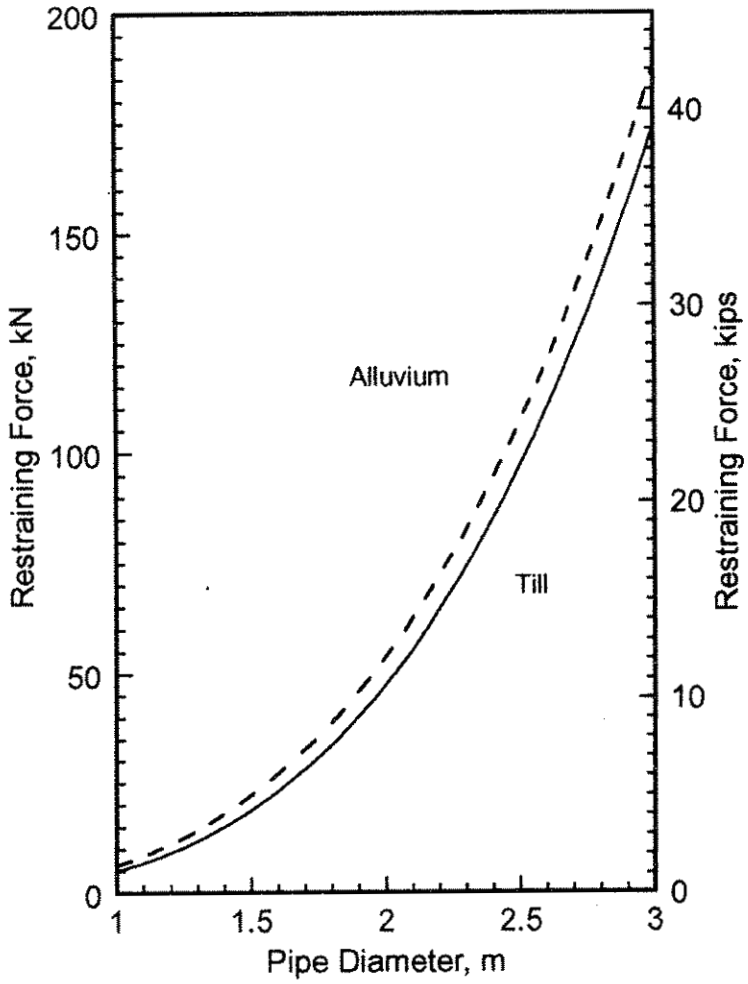

Figure 2.20. Design chart for 16 gage pipe with no flow.

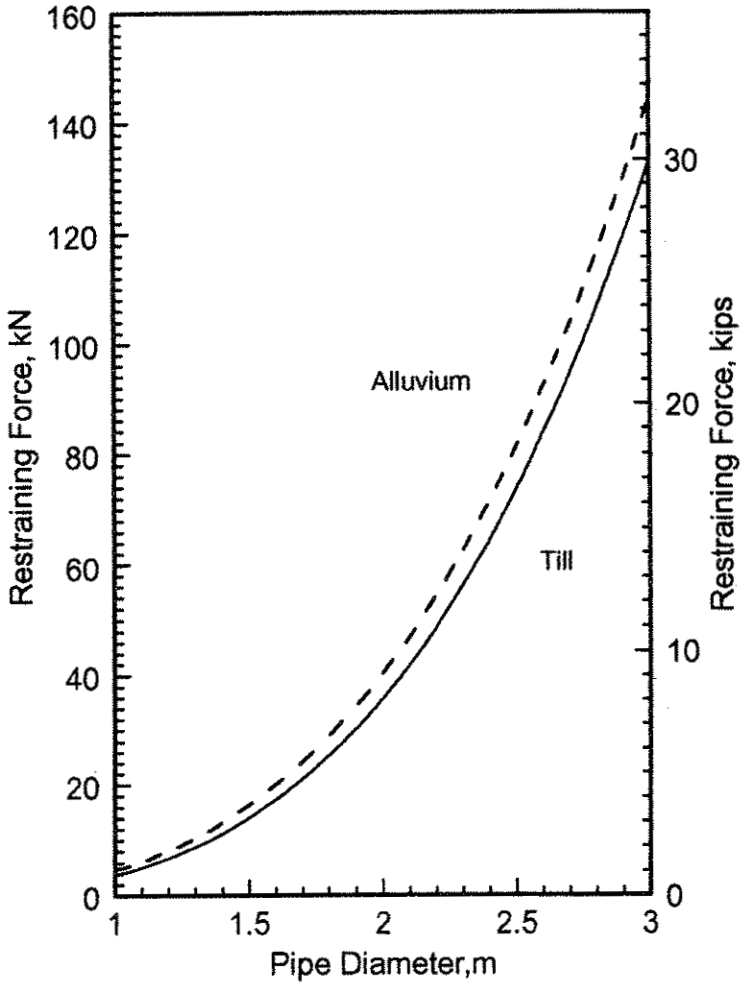

Figure 2.21. Design chart for 16 gage pipe with 25% flow.

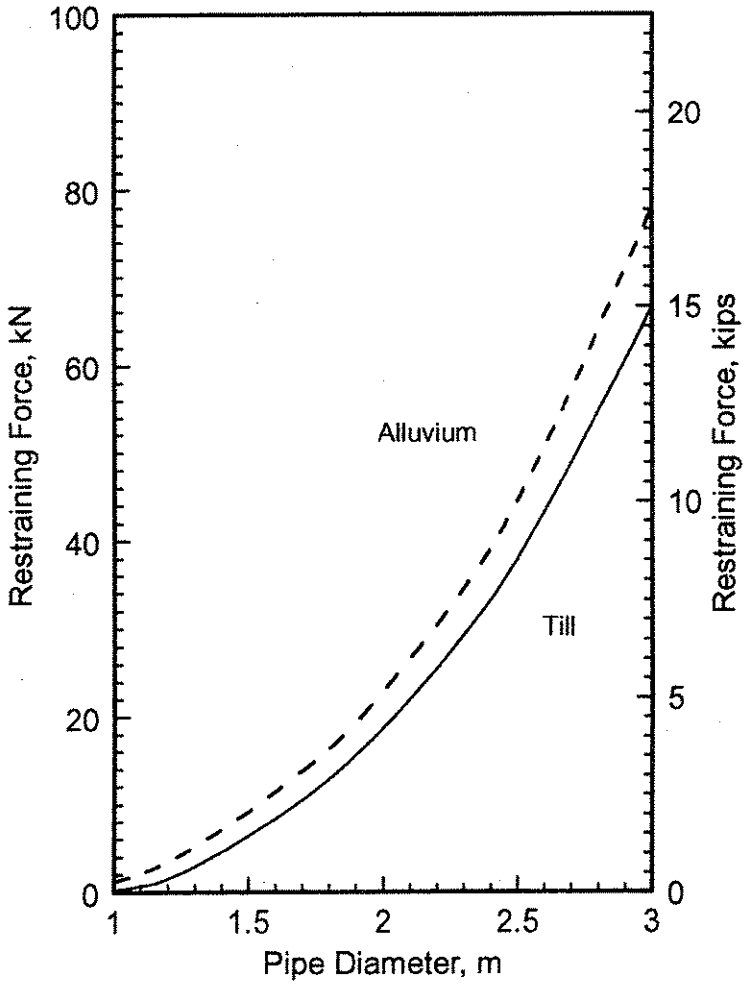

Figure 2.22. Design chart for 16 gage pipe with 50% flow.

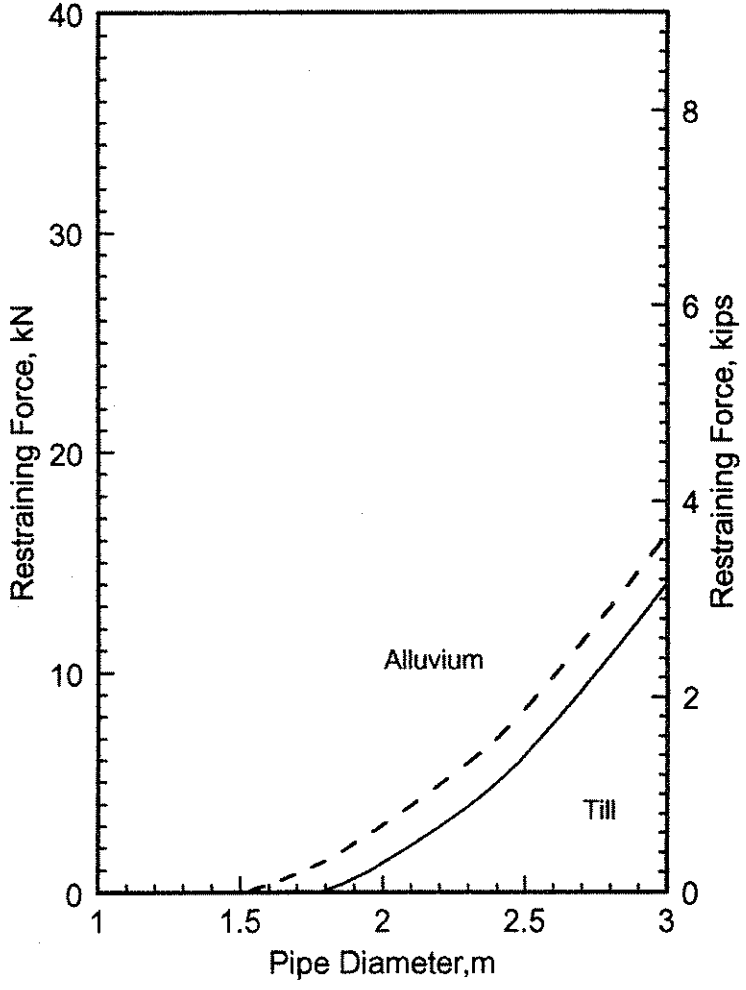

Figure 2.23. Design chart for 16 gage pipe with 75% flow.

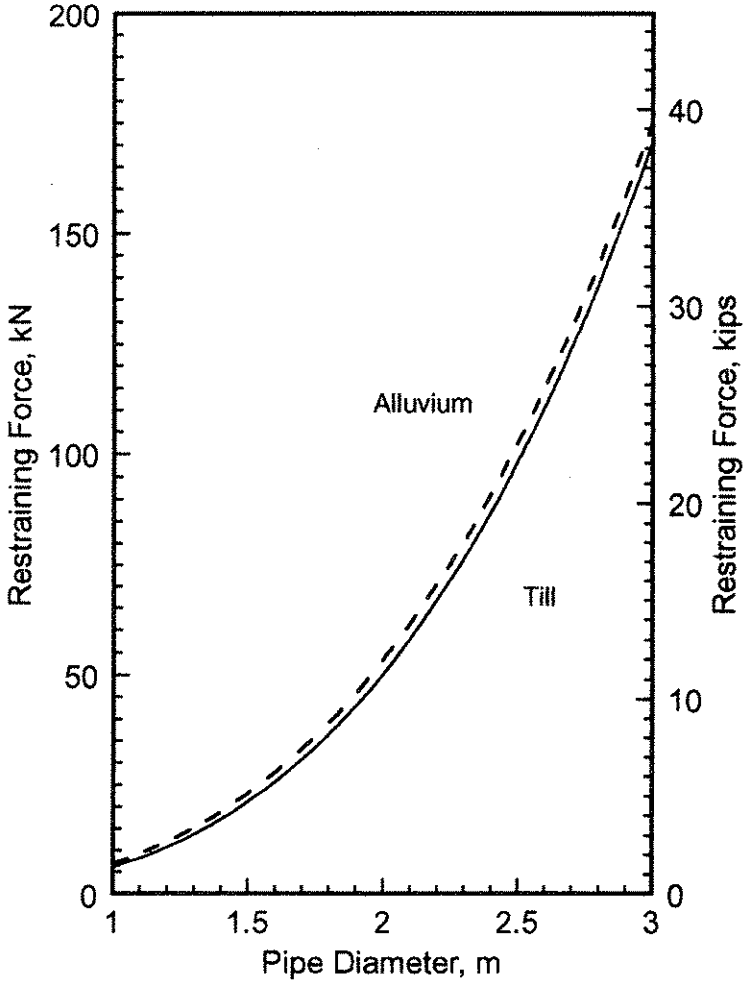

Figure 2.24. Design chart for 18 gage pipe with no flow.

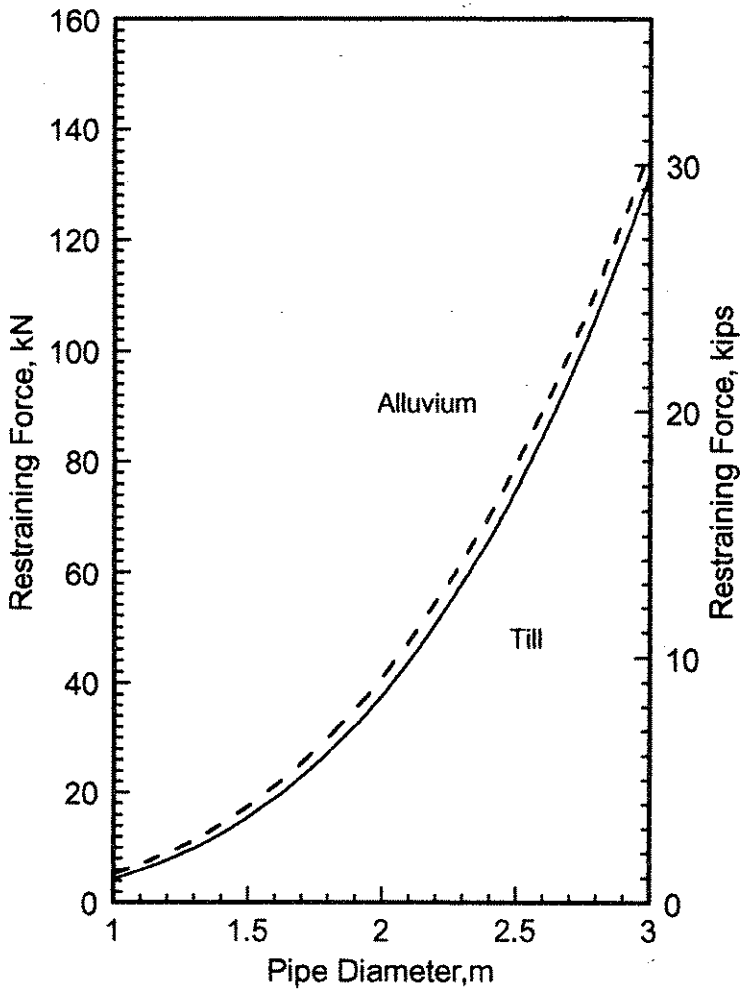

Figure 2.25. Design chart for 18 gage pipe with 25% flow.

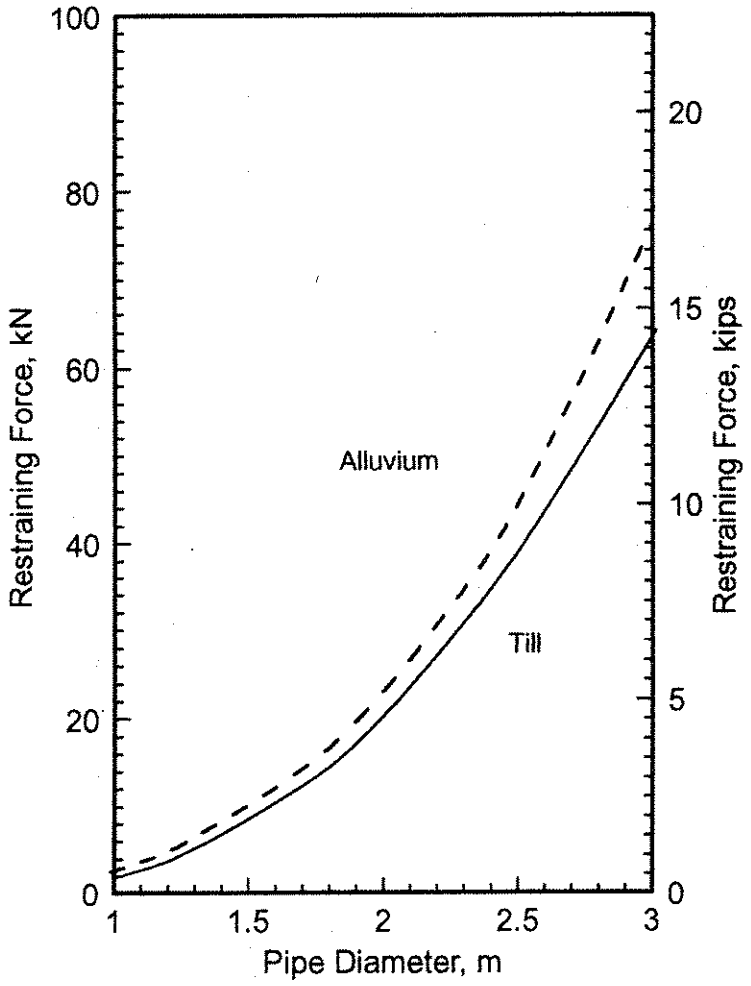

Figure 2.26 Design chart for 18 gage pipe with 50% flow.

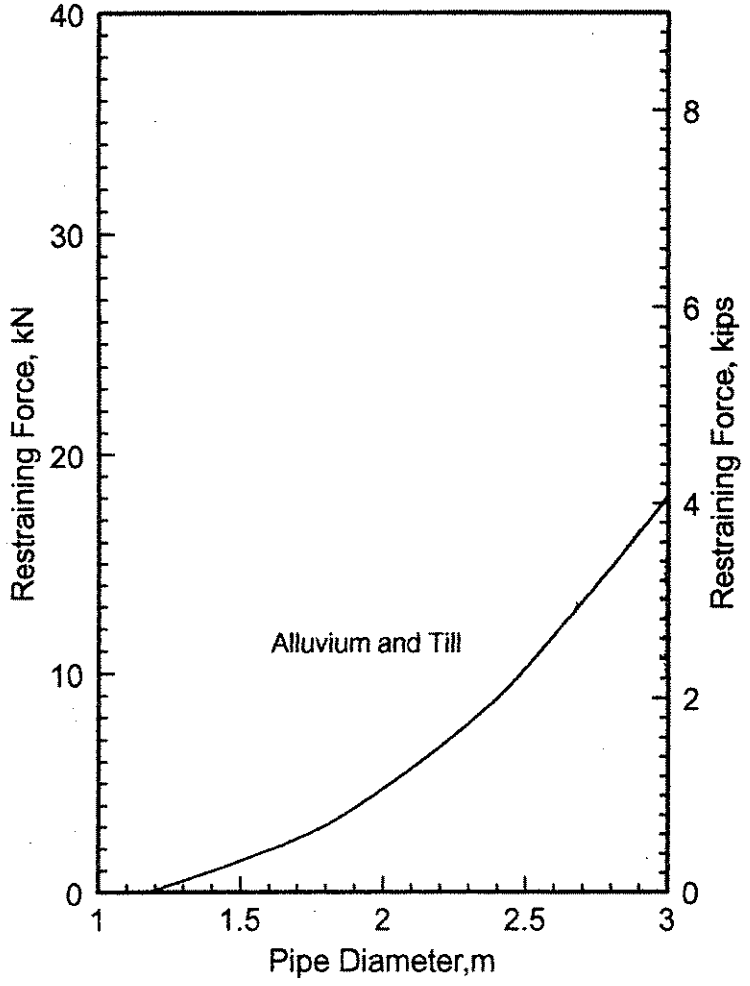

Figure 2.27 Design chart for 18 gage pipe with 75% flow.

types are commonly found in Iowa. The curve for stiff glacial till represents an upper bound of backfill stiffness, while the curve for clayey alluvium represents a lower bound. Backfill softer than the lower bound should not be used.

2.2.8 Factor of safety and additional considerations

The design charts presented are based on analyses conducted with no safety factor applied in any of the steps; therefore an appropriate factor of safety should be applied to complete the design. In general, the assumptions and limitations (see Section 2.1) underlying the design method should be reviewed when selecting a safety factor.

One consideration when determining the factor of safety is the assumed flow condition in the CMP. If it is thought that the pipe may never become plugged, the safety factor should be less than if the culvert is likely to be subjected to the most severe uplift condition.

Another aspect to consider is the grade of the foreslope. As the slope angle decreases, the net uplift force increases; therefore, small slopes (i.e. those with small slope angles) require a larger factor of safety.

Economics and constructability of a required restraint also should be taken into consideration. If a large factor of safety is used, the solution obtained from the design methodology may be unfeasible.

The hugger band used to connect segments of CMP presents a potential weakness with regard to longitudinal bending. To avoid problems, it is recommended that the connection between CMP segments be placed in a region of full soil cover, preferably in the central portion of the embankment.

3. FIELD TESTS

3.1 Objective

Continued investigation of the soil-structure interaction of buried CMP, beyond that described in McCurnin, (1993) and Klaiber et al (1993), is described here. Five field tests were conducted on a 2.43 m (8 ft) diameter CMP specimen. The first test consisted of uplifting the pipe with a soil cover of 0.6 m (2 ft) and a foreslope of 2:1, referred to as 8SC (8 ft diameter CMP with soil cover). In the next two tests, the CMP was lifted with no soil cover. One test involved lifting the CMP with only the front strap (Test 8NC1), while the following test (8NC2) used both straps to lift the pipe (see Figure 3.1).

Following 8NC, the pipe was backfilled without a foreslope to leave approximately 5.3 m (16 ft) of the upstream end of the pipe without soil restraint. This test, 8NF, was to determine the effect of the foreslope on uplift response. Finally, a restraint was constructed at the inlet and the specimen was retested for the fifth time. This test is referred to as 8R. After Test 8SC, soil was removed from the CMP and the pipe was rotated "end for end" so that the end furthest from the loaded end now became the loaded end of the pipe. Instrumentation in the test indicated the end furthest from the loaded end was essentially stress free in all tests. Thus, by rotating the CMP for the last four tests, the loaded segment was essentially stress free ("new").

3.2 Test Specimen

The CMP used for the field tests was galvanized steel, 2.4 m (8 ft) in diameter with 75 mm x 25 mm (3 in. x 1 in.) helical corrugation, with continuously welded seams. Two 7.9 m (26 ft) segments, 12 gage in thickness, were used to construct the 15.8 m (52 ft) long test specimen. The

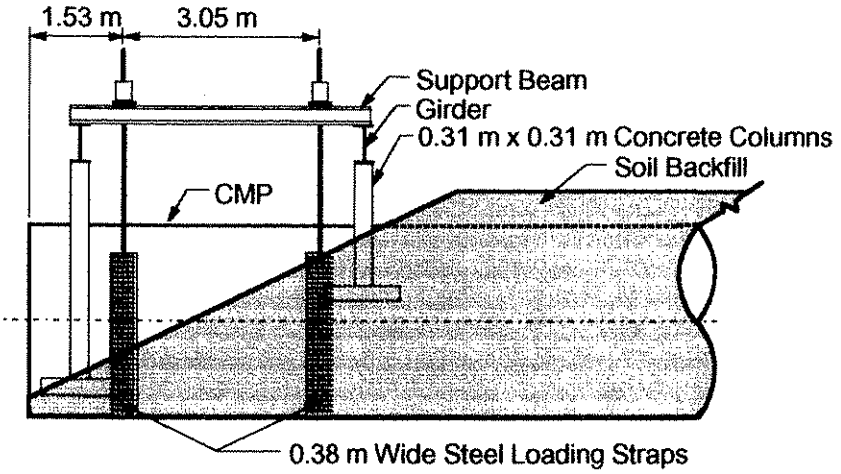

(a) Profile of load frame

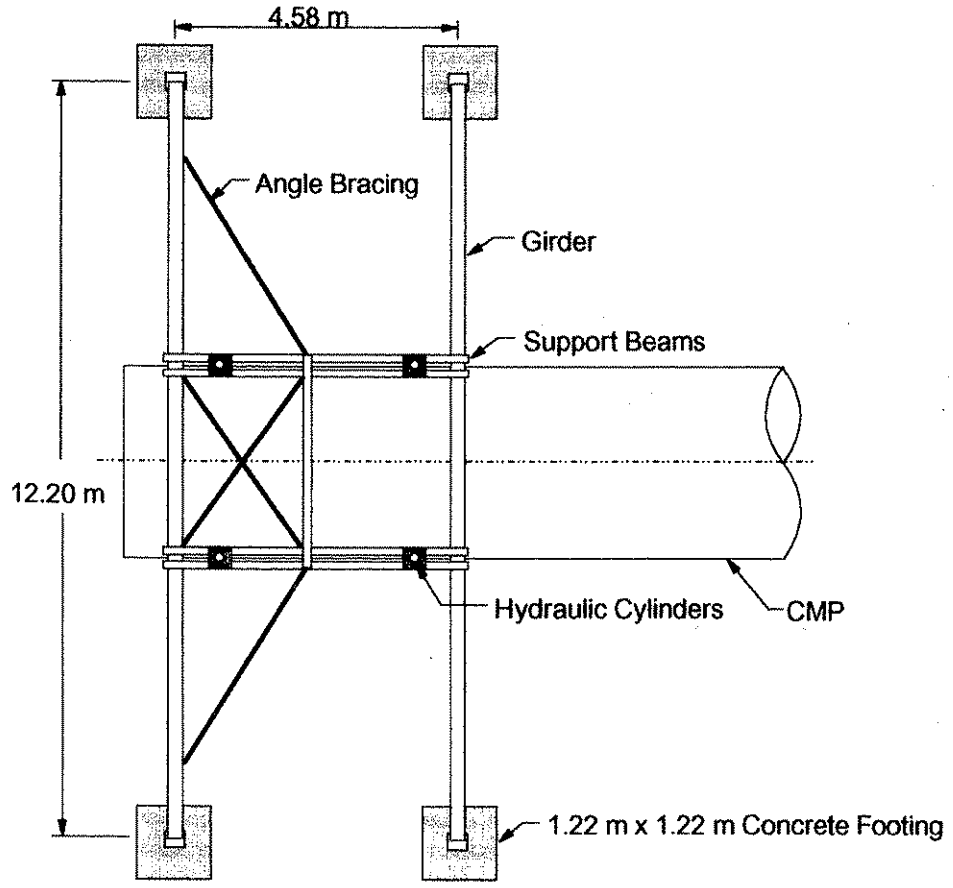

(b) Plan view of load frame

Figure 3.1. Load frame description.

two segments of pipe were connected together by a 0.25 m (10 in.) hugger band and reinforced with welded bars described later.

3.3 Bedding Preparation

The testing was conducted at Spangler Geotechnical Laboratory, the same site of the previous research phase (McCurnin, 1993 and Klaiber et al, 1993). The soil at the site is a glacial till which is described elsewhere (Heilers, 1994). After the previous specimen was removed, the excavated trench was approximately 4.6 m (15 ft) wide with slopes of 2:1. The base of the trench was prepared according to Class C bedding (Iowa DOT 1992). This specification requires that 10% of the pipe height rest below the adjacent ground level. A 0.24 m (9.6 in.) deep template was used to shape a concave saddle cut from the compacted bedding.

3.4 Placing the Pipe

Pipe segments were placed in the saddle with a backhoe. Loose soil was placed in the saddle to insure voids between corrugations were filled. The two pipe segments were aligned by the concave saddle. After the specimens were aligned, the 0.25 m (10 in.) hugger band was placed around the pipe segments and tightened to join the two segments. As with the previous tests, 26 plate stiffeners (305 mm x 63.5 mm x 6.5 mm (12 in. x 2.5 in. x 0.25 in.)) were welded to the pipe to increase the strength and stiffness of the joint to insure that the pipe would not separate at the joint during the uplift testing.

3.5 Loading System

The loading system previously described in detail by McCurnin (1993) and Klaiber et al (1993) was also used for this work. Two loading points located 1.5 m (5 ft) and 4.6 m (15 ft) from the upstream end of the CMP allowed the simulation of pore pressure loading that is thought to be the cause of the inlet uplift failures. The uplift force at 1.5 m (5 ft) from the inlet was twice that at the point 4.6 m (15 ft) from the inlet. Uplift forces were provided by the use of four hollow core hydraulic cylinders reacting on the overhead frame shown in Figures 3.1 and 3.2a. The loads were transferred to the CMP through a system of prestressing cables and 380 mm (15 in.) wide steel bands which passed beneath the CMP. A grout mix was placed between the straps and pipe corrugations to insure that the load from the bands would be evenly distributed to the CMP. Photographs of field Tests 8SC, 8NF, and 8R are shown in Figures 3.2b, 3.2c and 3.2d, respectively.

3.6 Instrumentation

Data collected during each test consisted of strains on the inner surface of the CMP, pipe cross section deformations, and applied loads. These data were continuously recorded during the testing with a Hewlett Packard data acquisition system. Vertical deflections of the crown of the pipe and the overlying backfill due to the CMP uplift were recorded manually using surveying equipment. Data were collected during the backfilling process as well as during the uplift stage.

3.6.1 Strain gages

Initially, six sections along the length of the pipe were instrumented with strain gages. Two additional sections were instrumented for the final restraint test to measure strains close to the tiedown and maximum moment location. At each section, the gages were placed at the top and

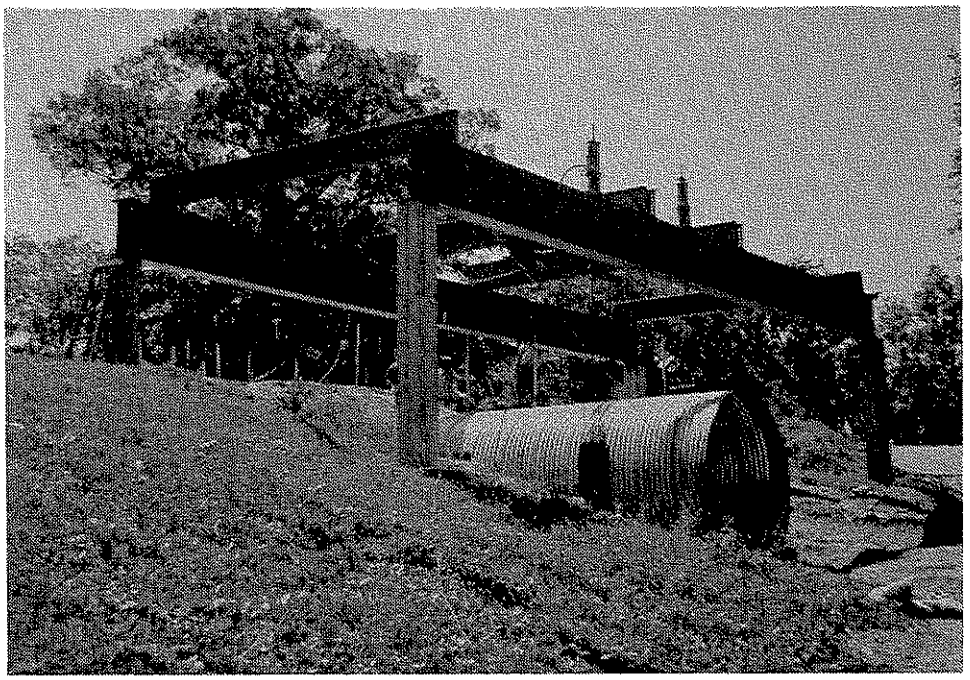

(a) Overall view of test frame and CMP test specimen.

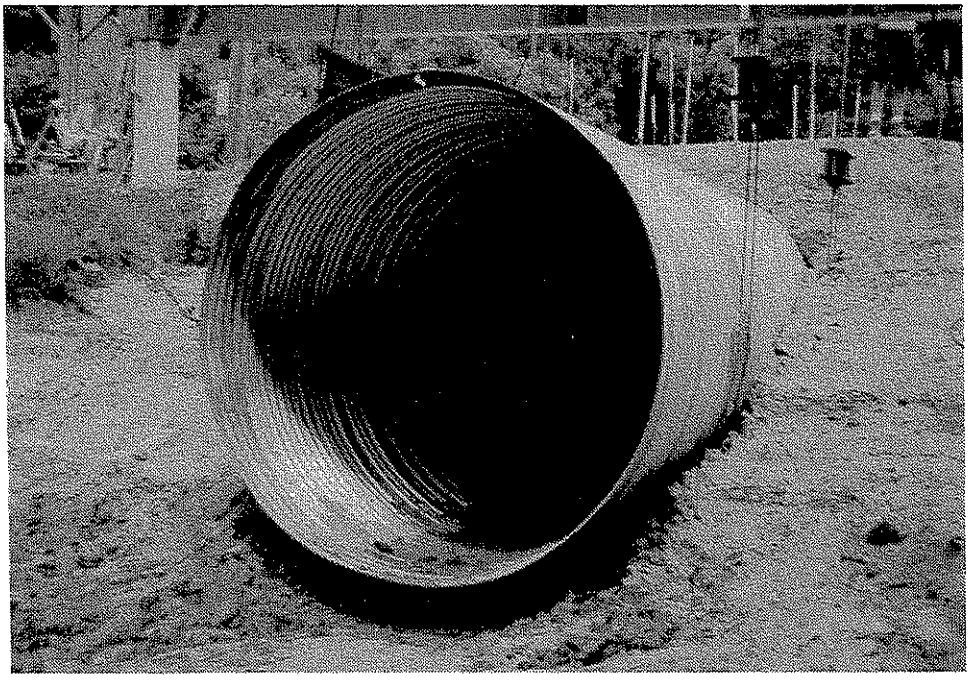

(b) 2:1 slope for Test 8SC.

Figure 3.2. Photographs of field tests.

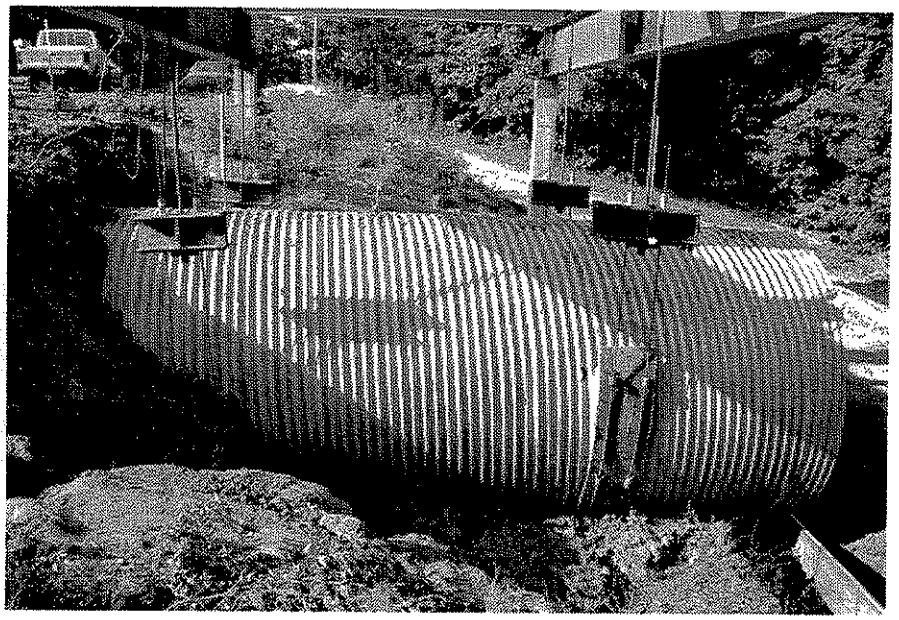

(c) Test setup for Test 8NF.

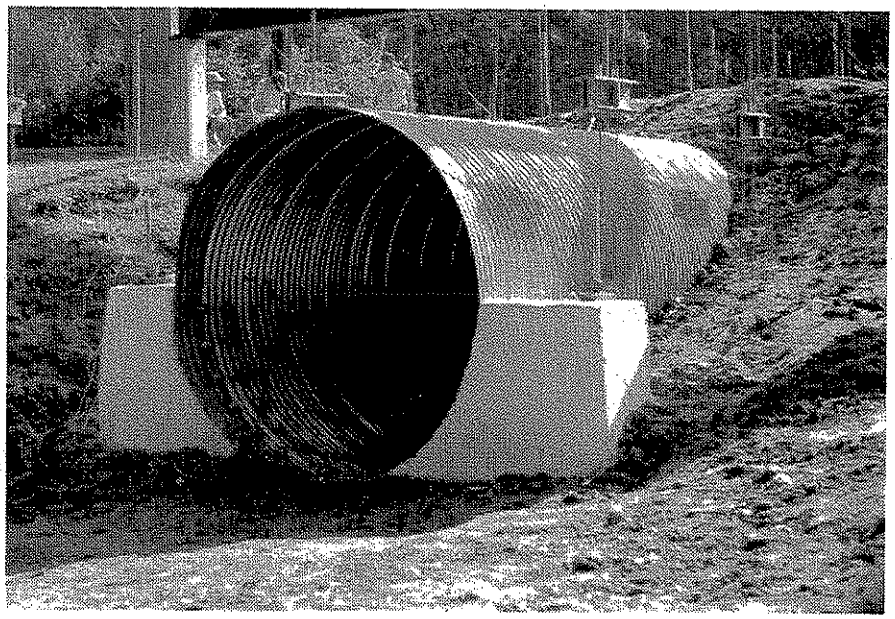

(d) Restraint for Test 8R.

Figure 3.2. Photographs of field tests (continued).

bottom of the CMP, and at the ends of the horizontal diameter. The gages were placed to measure hoop and longitudinal strains thus at each section there were eight gages. Gage locations can be seen in Figure 3.3. Gaged Sections A and B refer to the two additional sections.

3.6.2 Cross sectional deformation measurements

CMP cross section deformations were measured using Celescos, which are voltage potentiometers. The Celescos were attached to the inside of the CMP near the six original strain gage locations. The Celescos were offset slightly to avoid introducing stress concentrations; however, the Celesco locations are referenced according to strain gaged sections. Detail of this instrumentation is shown in Figure 3.4.

3.6.3 Vertical deflection measurements

Vertical deflections of the pipe were measured using steel rods (attached to the CMP) that extended above the fill. Engineering scales were attached to the steel rods and read with surveying levels during uplift testing. Locations of the deflection rods are shown in Figure 3.5.

3.7 Backfilling

It has been noted that the specimen was used for four tests; 8SC, 8NC, 8NF, and 8R. The specimen was backfilled for Test 8SC and after testing was completed, the backfill material was excavated and the specimen was then lifted with a crane, rotated 180 degrees and placed into the existing cradle. After Test 8NC was completed, the specimen was backfilled with the exception of the foreslope for Test 8NF. The backfilling procedures before Tests 8SC and 8NF will be referred to as Backfill 1 and Backfill 2, respectively.

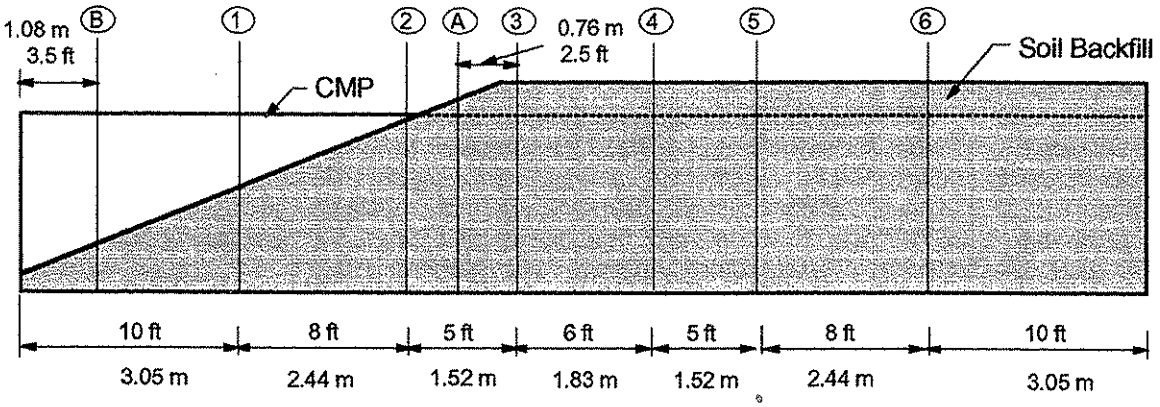

(a) Location of Strain gaged sections

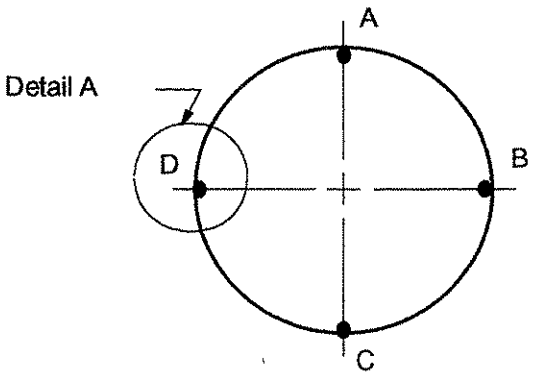

(b) Strain gage locations

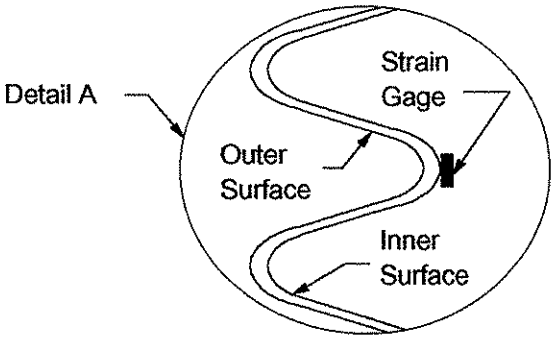

(c) Detail A

Figure 3.3. Placement of strain gages

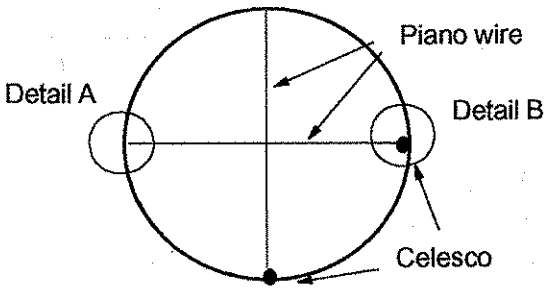

(a) Celesco Configuration

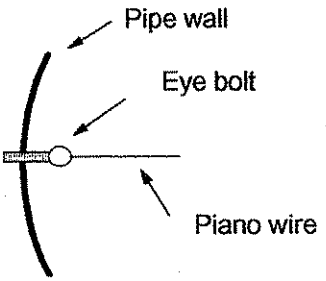

(b) Detail A

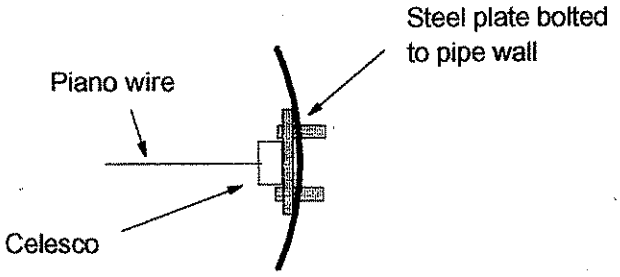

(c) Detail B

Figure 3.4. Instrumentation to measure diameter change.

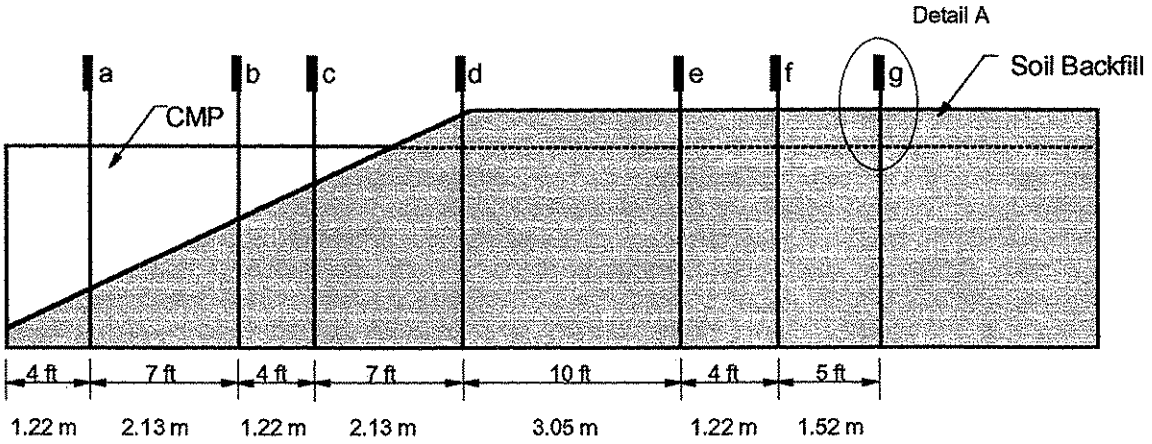

(a) Location of vertical deflection rods

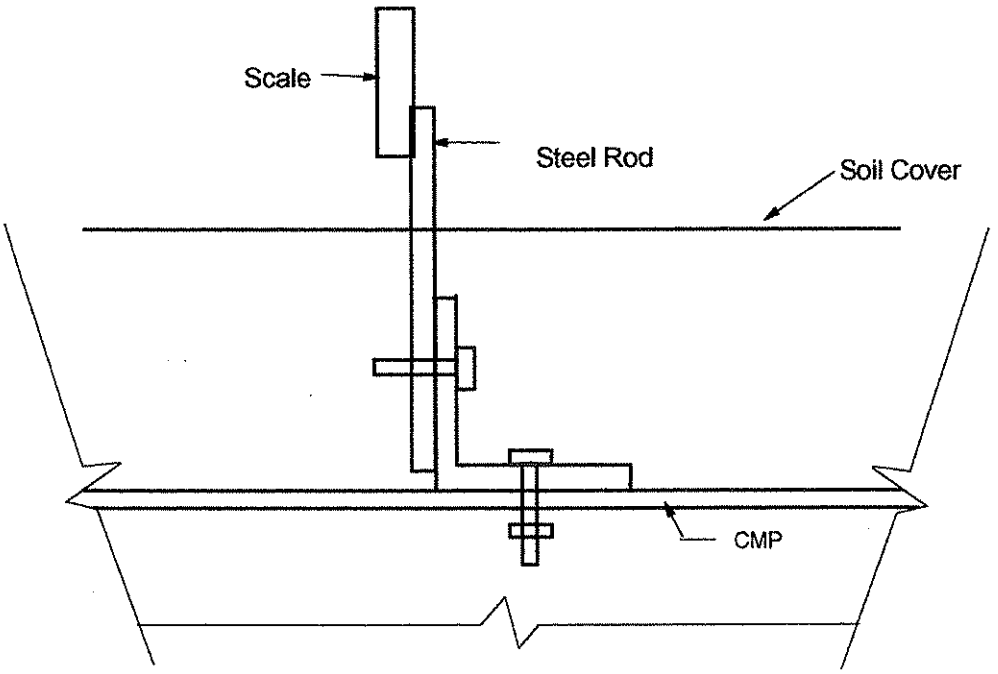

(b) Detail A

Figure 3.5. Vertical deflection rods.

Specifications require the fill material to be compacted to 90% of the maximum dry density obtained from a standard Proctor density test (Iowa DOT 1992). The glacial till has a maximum dry density of 18.9 kN/m^3 (120 lb/ft^3) and an optimum moisture content of 12%.

The first stage of the backfilling process required the haunch areas near the base of the pipe to be compacted. These areas were compacted by hand using 2 x 4 wood studs. As the fill depth increased, more space was available for larger mechanical tampers. Loose lifts of soil approximately 305 mm (12 in.) deep were evenly spread and then compacted by the use of a backhoe mounted vibratory plate. Gasoline powered, hand operated mechanical tampers were also used along the sides of the CMP. Backfilling alternated from side to side so that the two fills were kept at approximately the same height. A transverse section of the finished fill is shown in Figure 3.6a.

As noted, standard Proctor density tests indicated that the fill has a maximum dry density of 18.9 kN/m^3 (120 lb/ft^3) at a moisture content of 12%. A nuclear density gage was used to check specification compliance for Backfill 1 in Test 8SC, while the sand cone method was used for Backfill 2 in Tests 8NF and 8R. Errors were made with the sand cone, so the density data for Backfill 2 are unreliable.

Backfill 1 was wet from heavy rainfall and winter snow melt, and so dryer soil from on site was mixed with the wetter material to reduce the moisture content. The nuclear density data indicate densities ranging from 16.7 kN/m^3 (106 lb/ft^3) at 17% moisture to 17.7 kN/m^3 (113 lb/ft^3) at 16% moisture. These data indicated that Backfill 1 was overcompacted.

Although density data are unavailable for Backfill 2, moisture contents ranging from 14.5% to 16.8% suggested that Backfill 2 was dryer and likely to be closer to maximum dry density because identical compaction techniques were used for both fills.

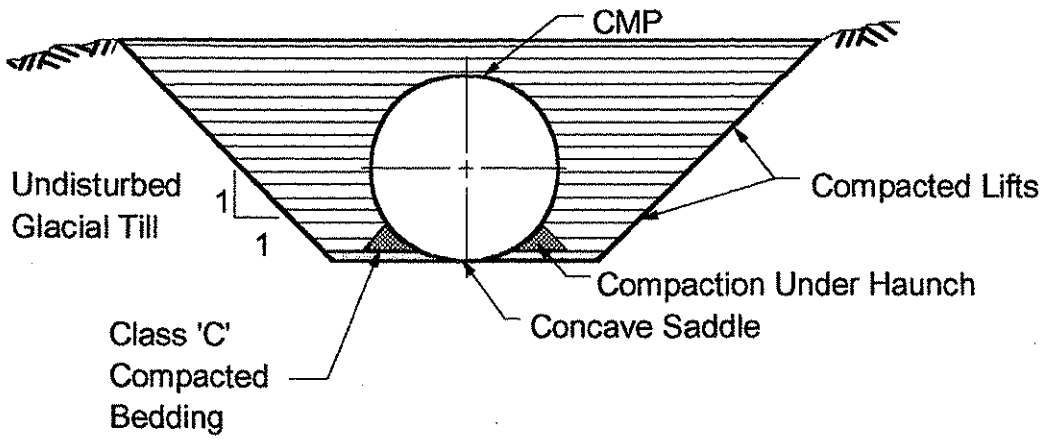

(a) Transverse Section - CMP Installation - Showing excavation and backfill compaction details

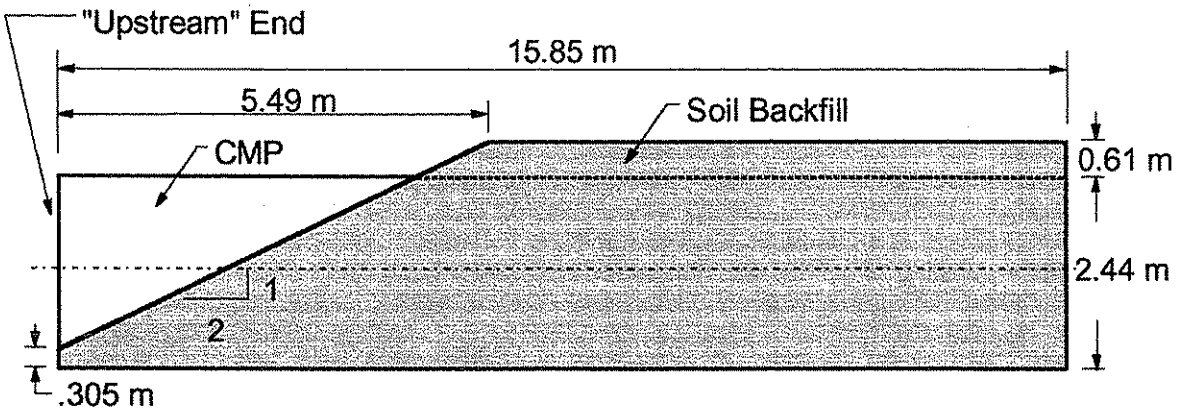

(b) Longitudinal profile

Figure 3.6. CMP test installation.

During placement of Backfill 1, a slope of 2:1 was formed. The slope extended from the inlet to the top of the embankment where a cover of 0.61 m (2 ft) was constructed. This profile simulates a typical highway embankment with minimum cover and typical foreslope as shown in Figure 3.6b.

During Backfill 2 for Test 8NF, the specimen was backfilled without the formation of the foreslope. The first 5.3 m (16 ft) of pipe were left exposed, while the remaining length of pipe had 0.61 m (2 ft) of cover. After the completion of Test 8NF a 2:1 slope was placed for Test 8R.

3.8. Pipe Response During Backfill

3.8.1 Cross sectional deformations

Both horizontal and vertical diameter changes were monitored during the backfilling process. As the level of fill increased, changes in diameter were evident. The compacted soil exerted enough lateral force on the pipe to cause a decrease in the horizontal diameter and an increase in the vertical diameter. The deflections resulting from Backfill 1 are considerably greater than those of Backfill 2, as shown in Figure 3.7 (positive values indicate an increase in diameter, while negative values indicate a decrease in diameter). The key used in this figure (2V, 2H, 6H, etc.) is the number indicates the section (illustrated in Figure 3.3) and V and H indicate changes in vertical and horizontal diameters, respectively. This discrepancy probably results from the lower density of Backfill 1 providing less restraint. The results from Backfill 2 compare closely with those presented by McCurnin for the 3.05 m (10 ft) diameter pipe. When the fill was near the springline, the deflections were the greatest and decreased as the fill approached the top of the pipe. As the fill deepened more confinement was provided by the soil.

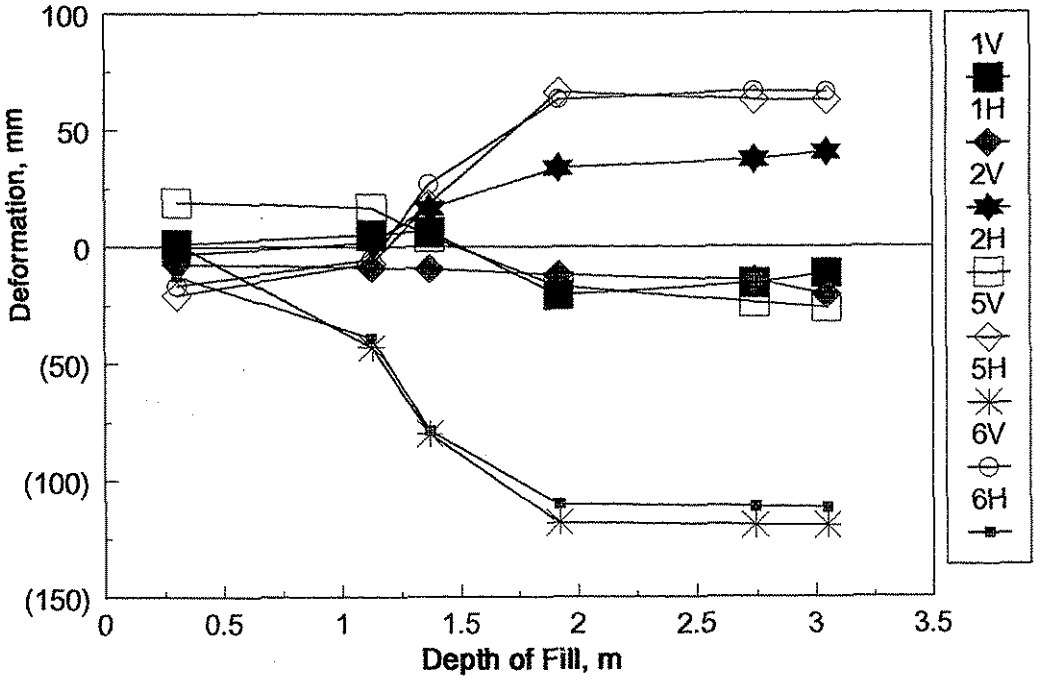

(a) Backfill1 deformation

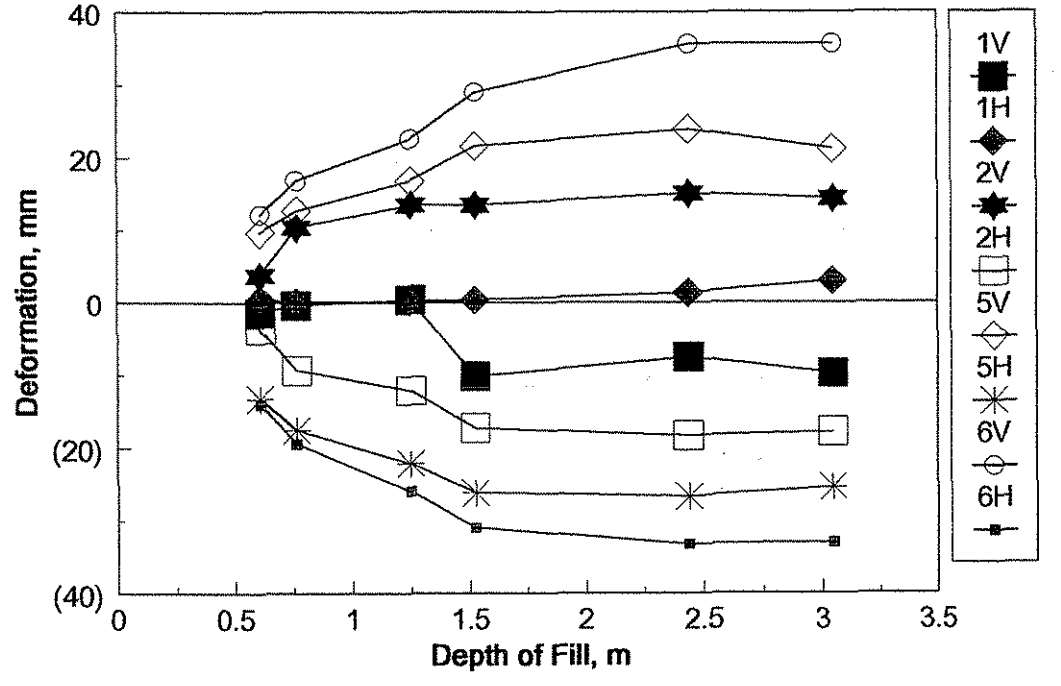

(b) Backfill2 deformation

Figure 3.7. Deformations during backfilling.

The horizontal deformations, at a given section, were nearly equal to the vertical deformation at that section (see Figure 3.7). The deformations in Sections 5 and 6 were the largest while the smallest deflections occurred on Sections 1 and 2. Sections 5 and 6 are completely backfilled (0.61 m (2 ft) of cover) whereas Sections 1 and 2 occur within the sloped region of the embankment.

3.8.2 Strain data

Representative strain data from Backfill 1 and Backfill 2 are shown in Figures 3.8 to 3.11 where strains at Sections 2, 4, and 6 are shown. The key used in these figures (4-CH, 4-BL, etc.) is the number indicates the section (see Figure 3.3a), the first letter indicates location on section (see Figure 3.3b), and the second letter (H or L) indicates hoop and longitudinal strains, respectively. Comparison of Figures 3.9 and 3.11 show that the hoop strains were significantly higher than the longitudinal strains during backfilling. The strain values for Backfill 1 were greater than those of Backfill 2 due to the larger displacement which occurred during Backfill 1. This correlates with the measured cross sectional deformations.

The strains within the pipe were consistent with the deformations. As shown in Figures 3.8 to 3.10 hoop strains were positive at gage locations B and D indicating that the inside of the pipe wall is in tension, associated with an inward movement of the horizontal diameter. At the same time, the strains at gage locations A and C were negative, indicating compressive behavior. As with the deformation data, the strains remained nearly constant as the depth of fill approached the top of the pipe.

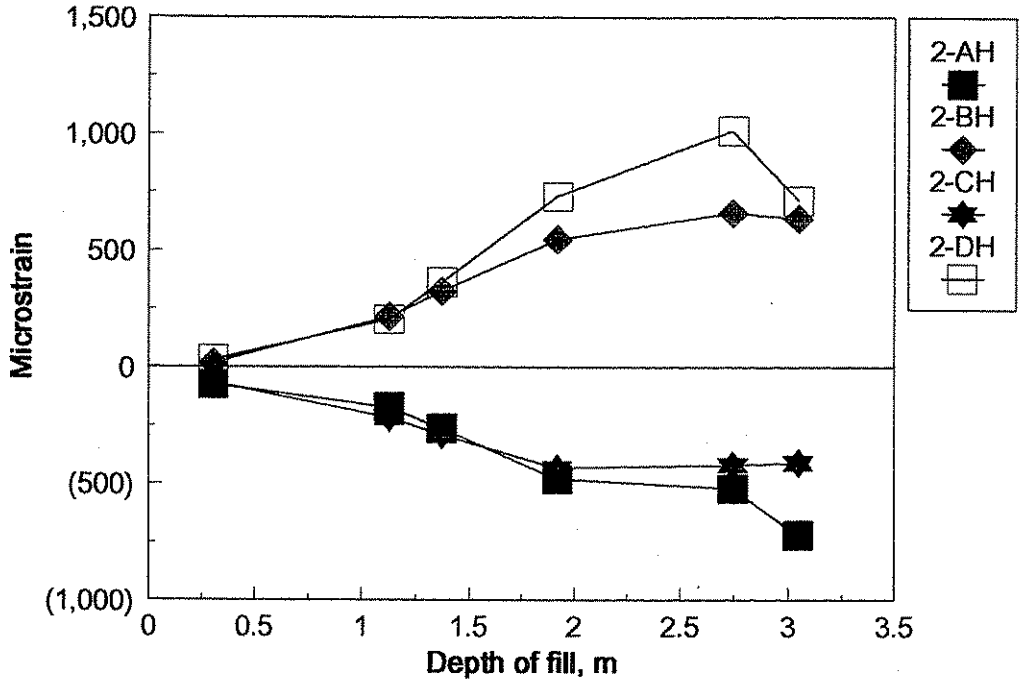

(a) Backfill1 strains at section 2

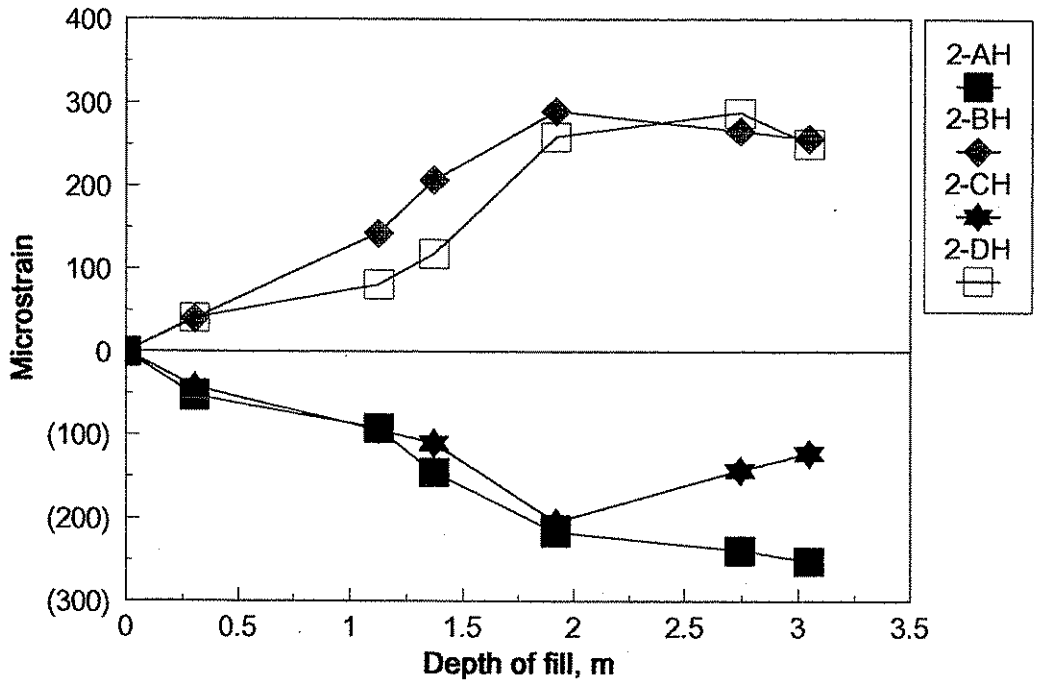

(b) Backfill2 strains at section 2

Figure 3.8. Backfill hoop strains for section 2.

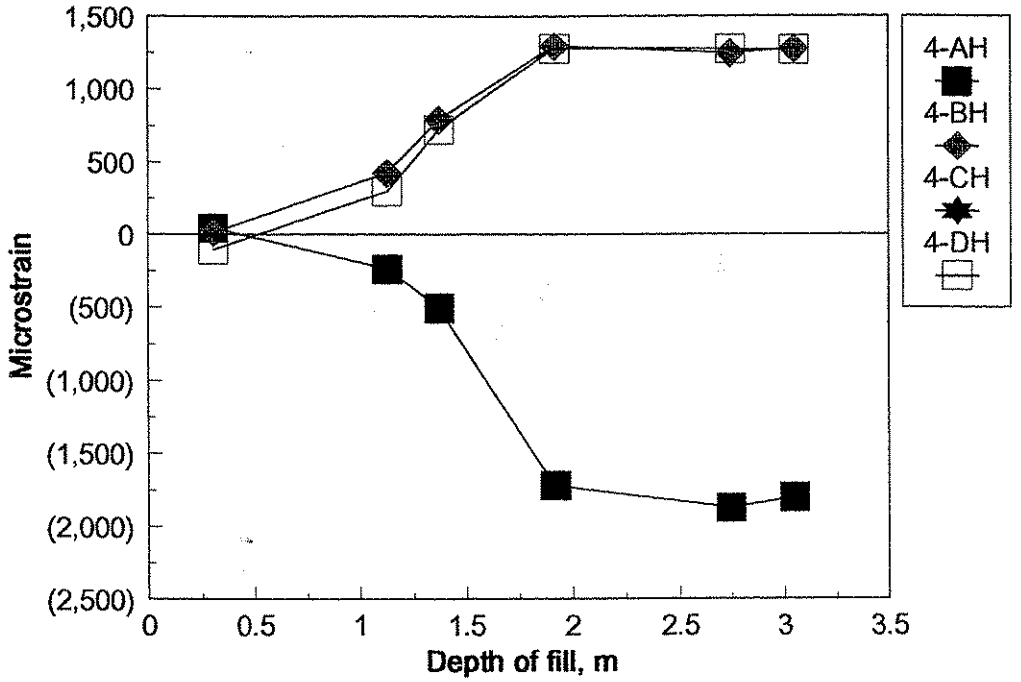

(a) Backfill1 strains at section 4

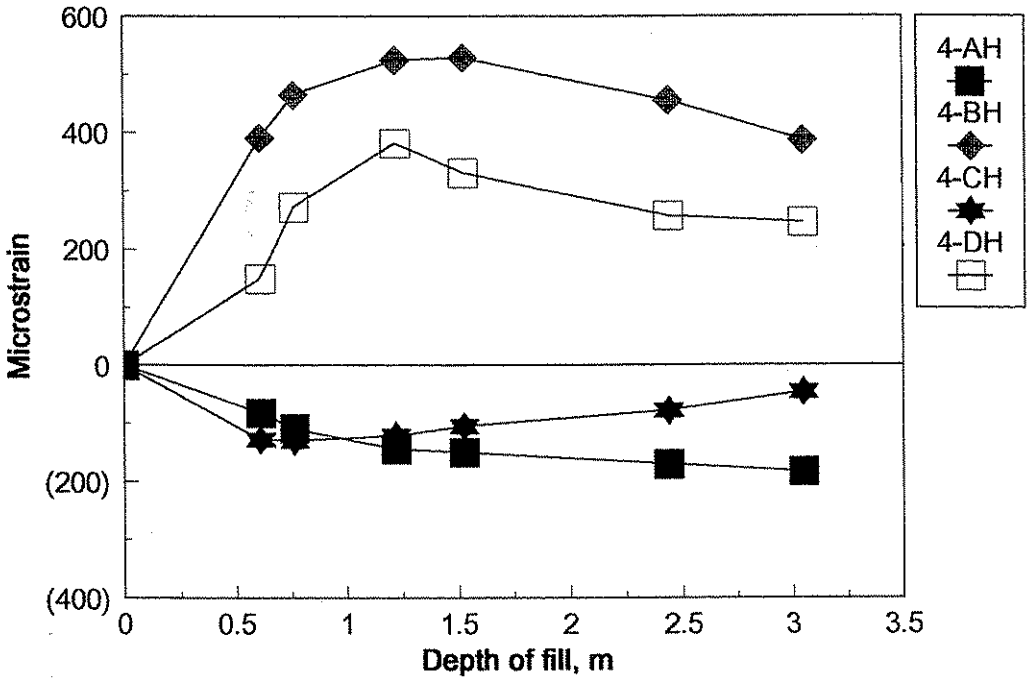

(b) Backfill2 strains at section 4

Figure 3.9. Backfill hoop strains for section 4.

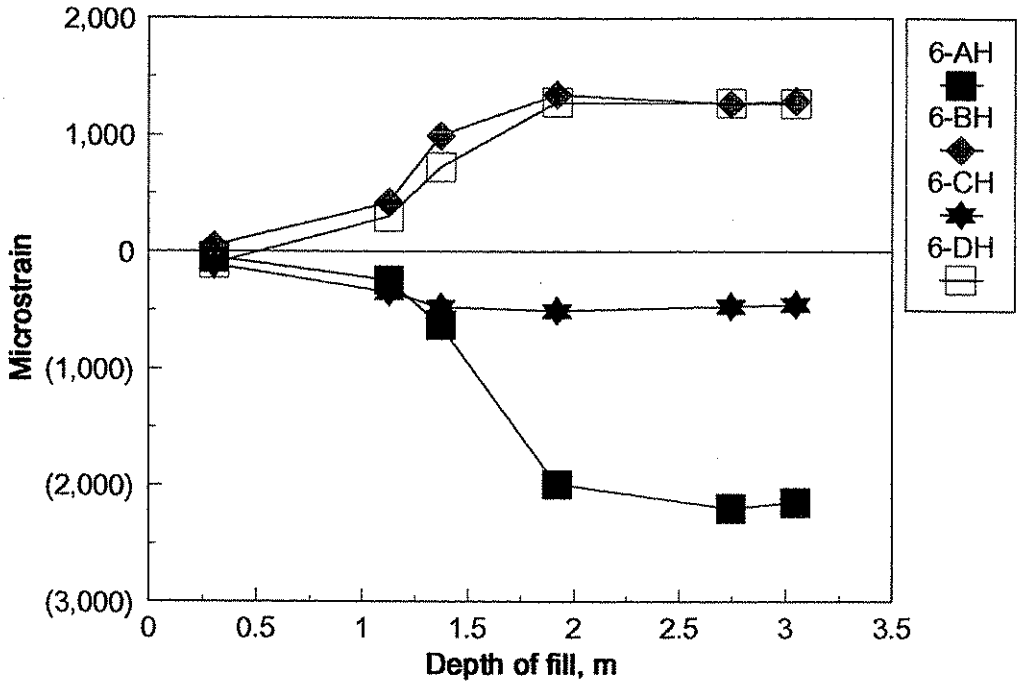

(a) Backfill1 strains at section 6

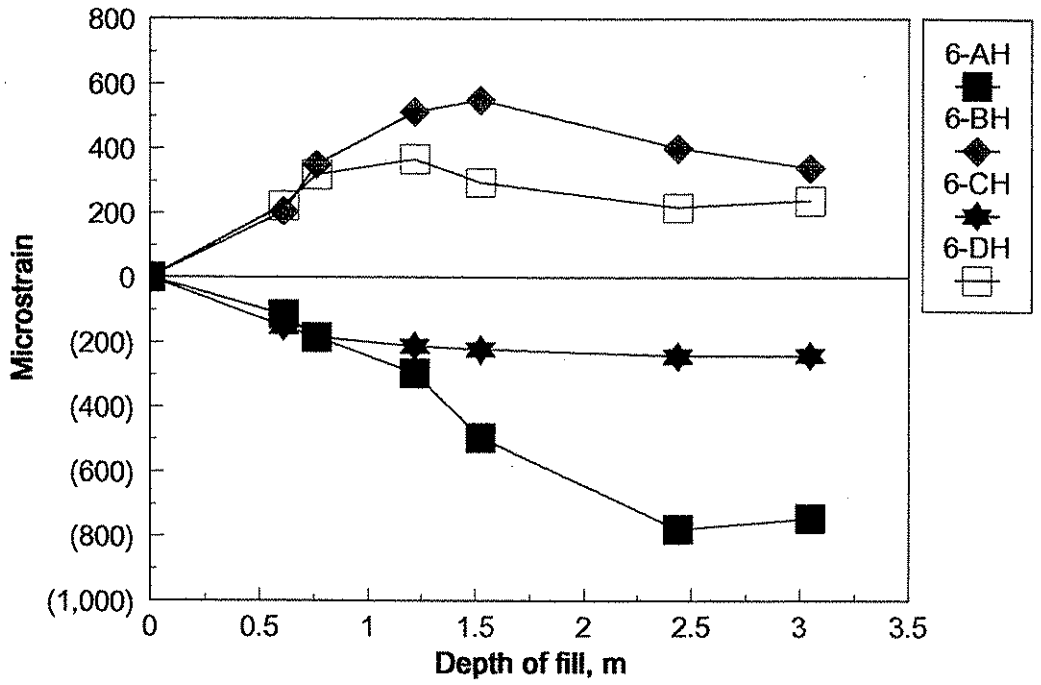

(b) Backfill2 strains at section 6

Figure 3.10. Backfill hoop strains for section 6.

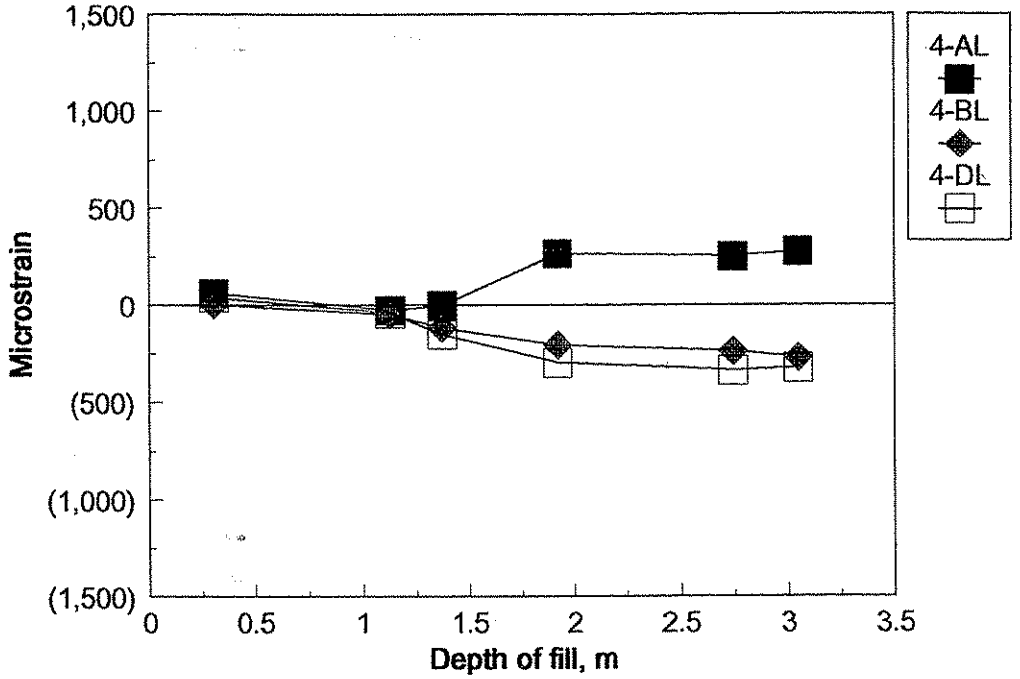

(a) Backfill1 strains at section 4

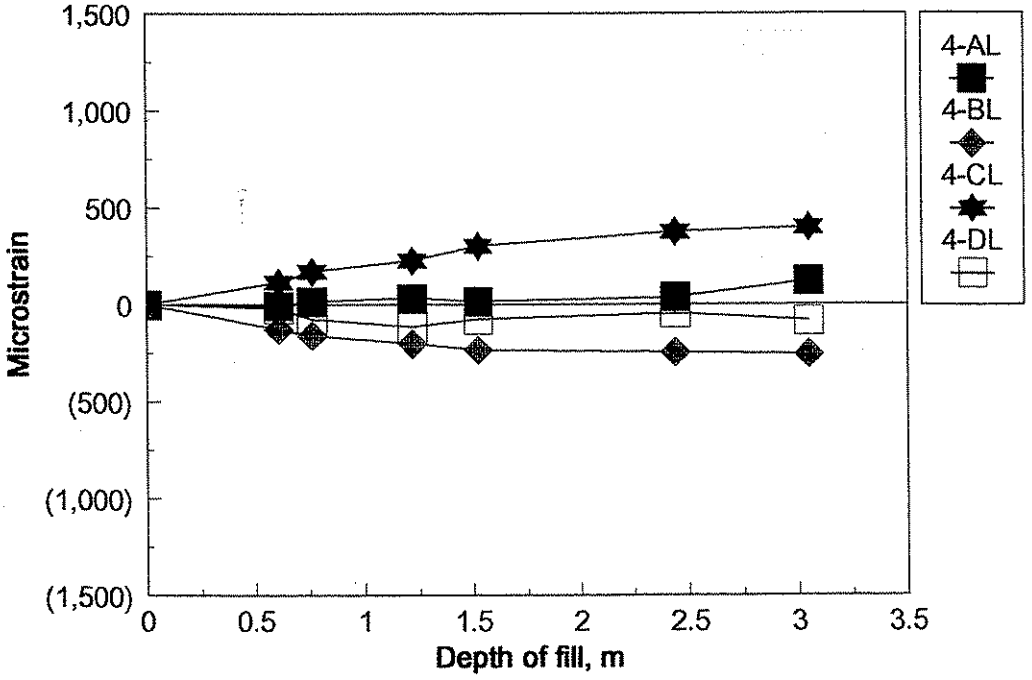

(b) Backfill2 strains at section 4

Figure 3.11 Backfill longitudinal strains for section 4.

The hoop strains generated at the top of the pipe were larger than those at the bottom of the pipe. The bottom of the pipe was properly bedded and movement was prevented while the top of the pipe had little soil to resist deformation.

3.9 Restraint Description

For Test 8R, a concrete tiedown was placed at the inlet of the CMP. The design force of the restraint was obtained from Iowa DOT headwall recommendations with a weight of 120 KN (27 kips) of concrete and constructed as shown in Figure 3.12. A photograph of this weight in place was previously shown in Figure 3.2d.

3.10 Uplift Results

3.10.1 Vertical deflections

Vertical deflections along the top of the pipe were recorded during each test and plotted against the corresponding load as shown in Figure 3.13 and 3.14. The key in these figures (Rod A, Rod E, etc.) refers to the locations shown in Figure 3.5. Very little movement was observed at Section d, while no movement was evident in Sections e, f, and g for Tests 8SC, 8NF, and 8R. In Test 8NC, the entire pipe experienced uplift with very little bending. In comparing Tests 8SC, 8NF, and 8NC at the same deflection, it is evident that the amount of soil affects the response of the system. Test 8SC required more load for a given deflection than 8NF, while 8NC essentially required only enough load to lift the pipe.

Figures 3.15 and 3.16 show defections along the length of the pipe at different loads. For Tests 8SC and 8NF, the deflection data indicate that pipe bending is occurring near the crest of the

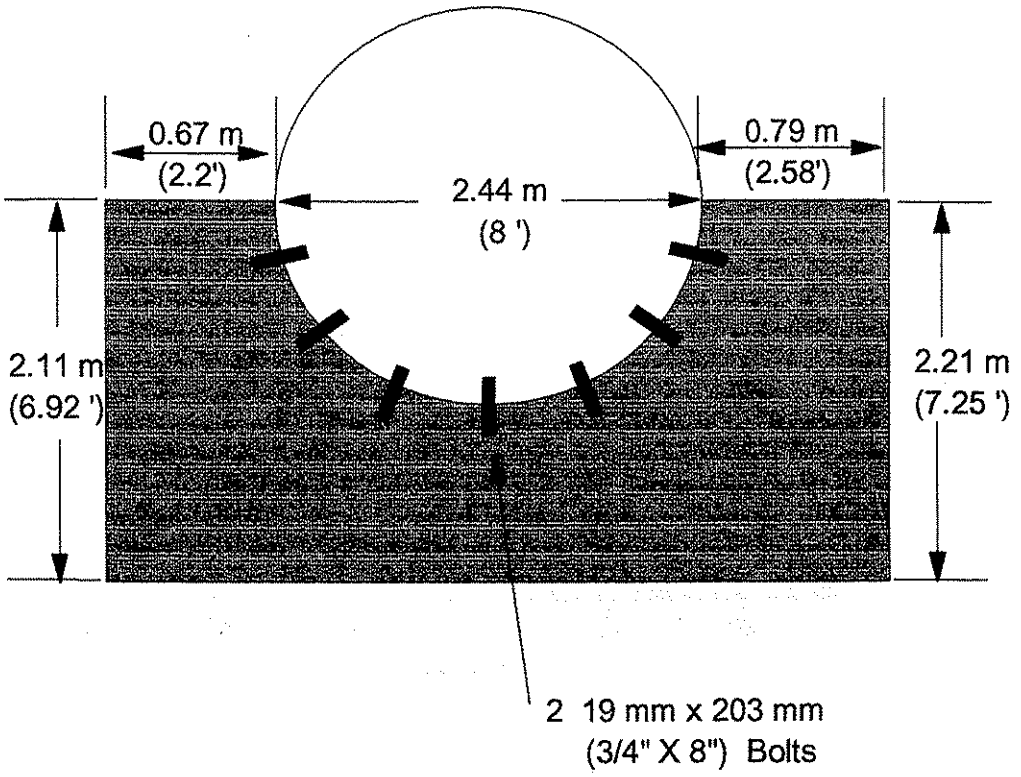

(a) Plan veiw of concrete restraint.

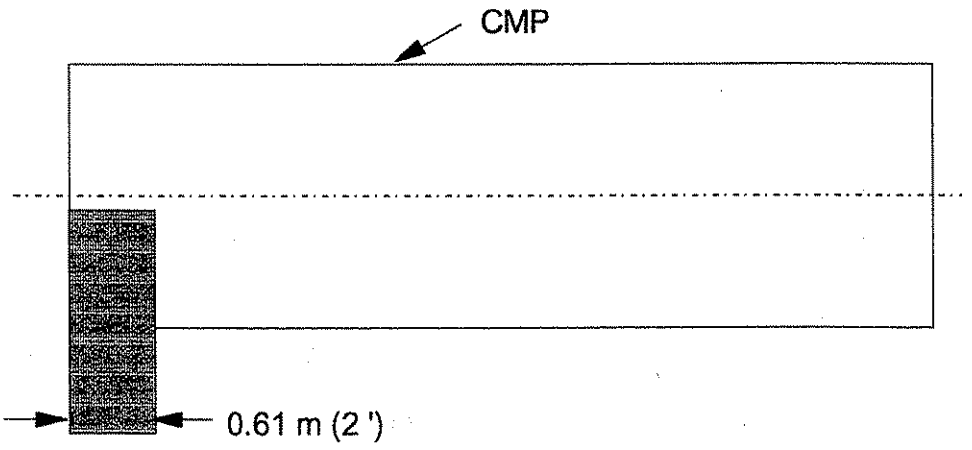

(b) Profile view of concrete restraint.

Figure 3.12. Concrete restraint system.

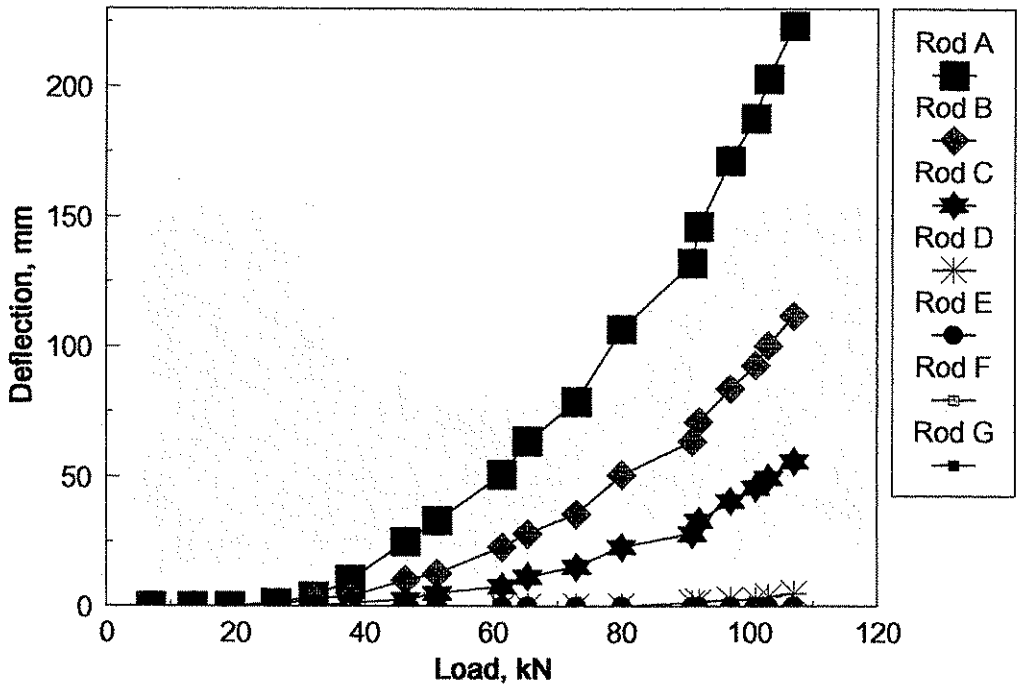

(a) Test 8SC

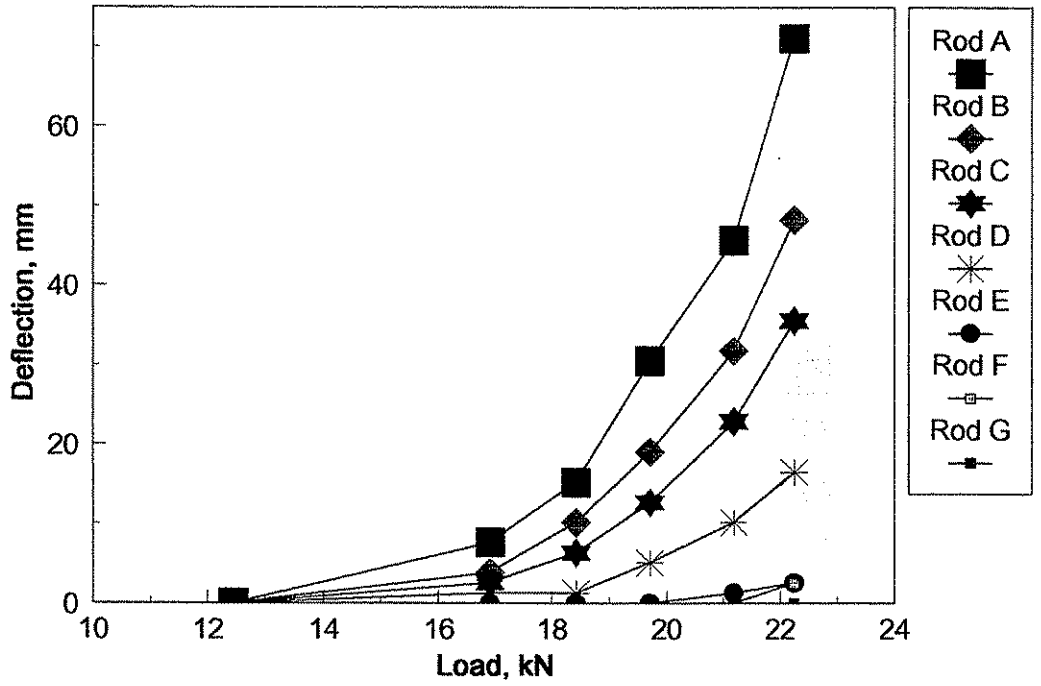

(b) Test 8NC

Figure 3.13. Load vs. deflection of vertical deflection rods for test 8SC and 8 NC.

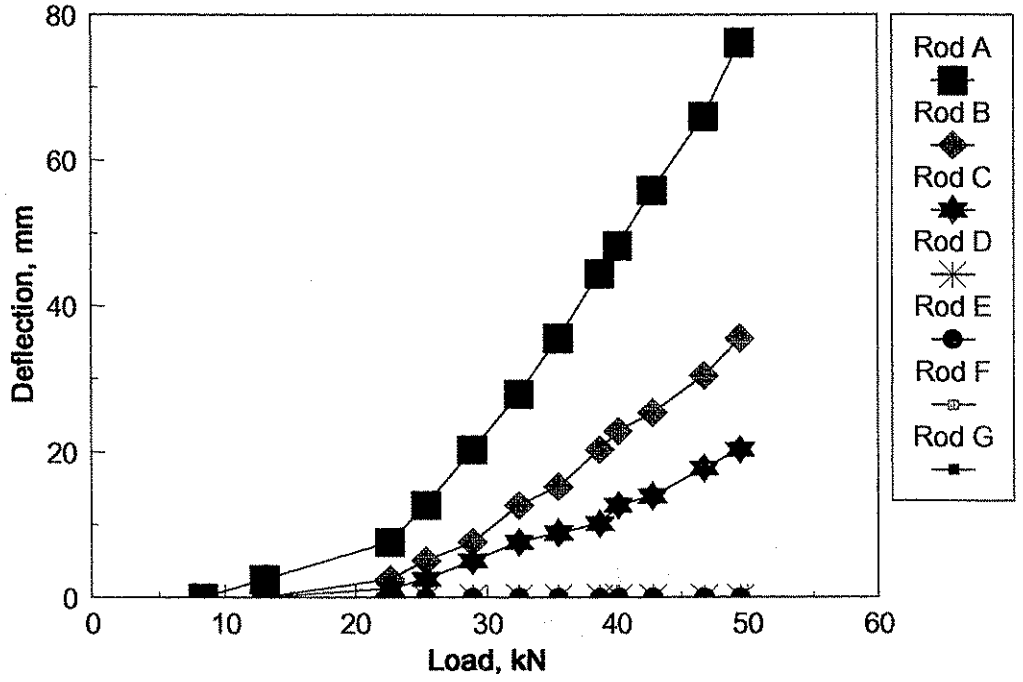

(a) Test 8NF

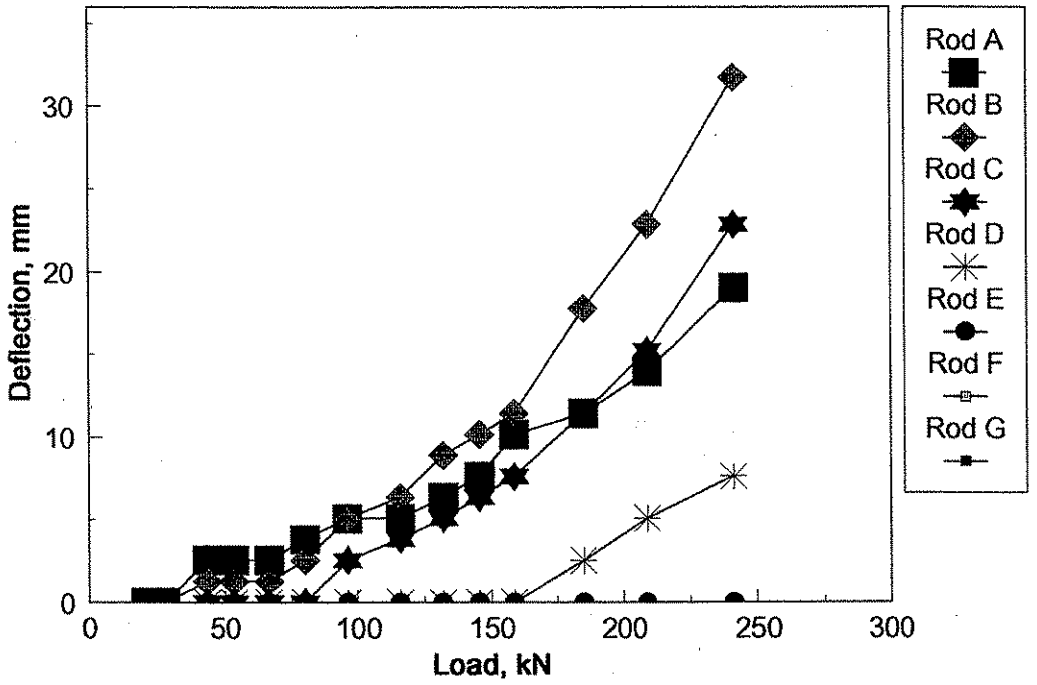

(b) Test 8R

Figure 3.14. Load vs. deflection of vertical deflection rods for test 8NF and 8R.

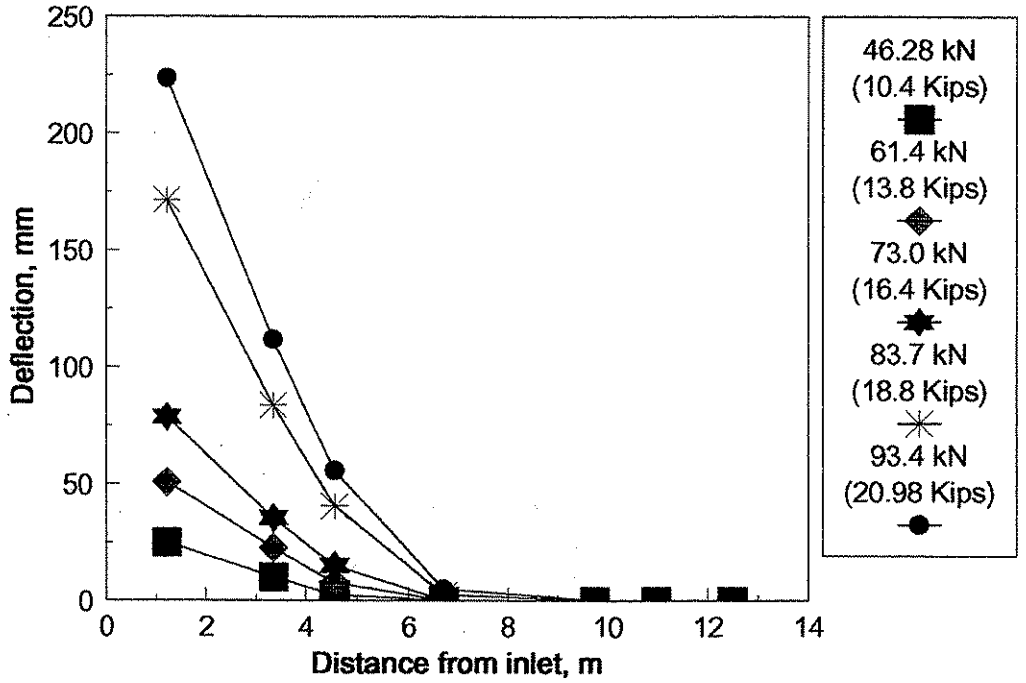

(a) Test 8SC

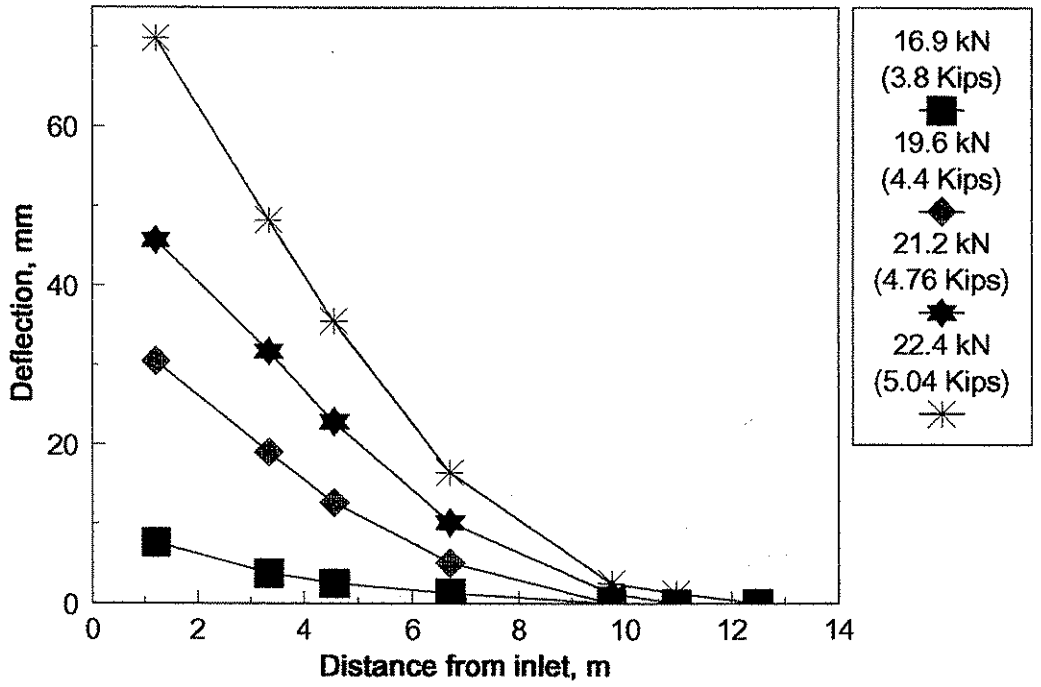

(b) Test 8NC

Figure 3.15. Deflections vs. distance from inlet.

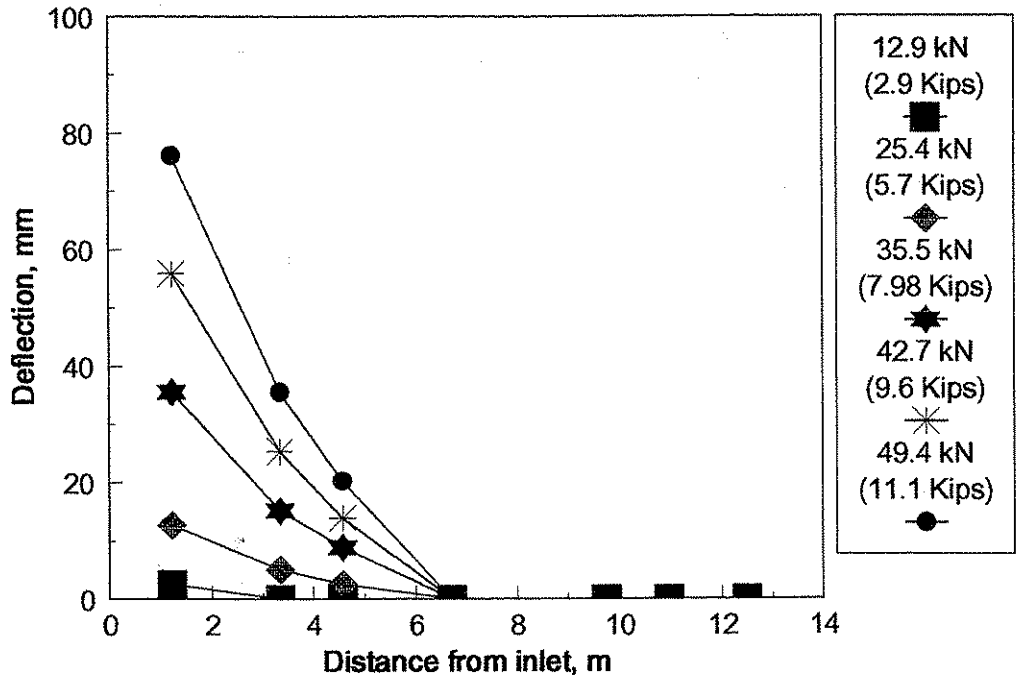

(a) Test 8NF

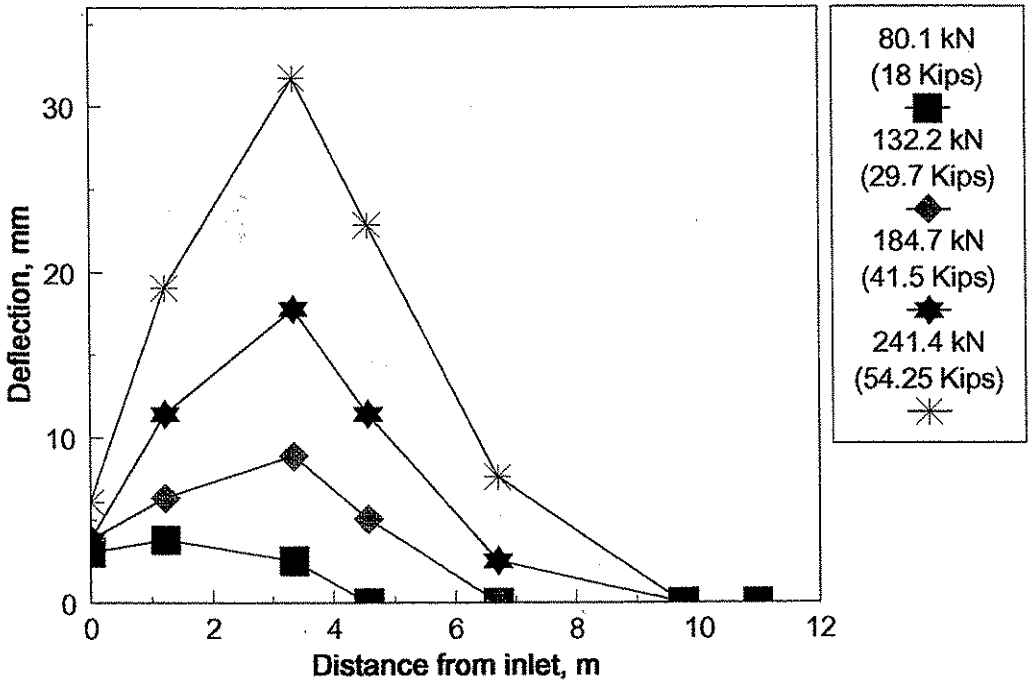

(b) Test 8R

Figure 3.16. Deflections vs. distance from inlet.

embankment. In the restraint test, 8R, the maximum deflection is closer to the loading and away from the inlet as indicated in Tests 8SC and 8NF.

Figure 3.17 compares deflection data from Tests 8SC and 8R and illustrates the effect a restraint has on the longitudinal bending characteristics of CMP subjected to uplift. Figure 3.17 shows deflections for the largest loads applied in those two tests. Although approximately 2.5 times more load was applied in Test 8R, it can be seen that the deflections in Test 8R are very small compared to those of Test 8SC.

3.10.2 Strain data

Strain readings were recorded for each load increment. Representative samples of the strain data recorded are presented and discussed in this section. Longitudinal and hoop strains for Sections 2 and 4 are presented in Figures 3.18 - 3.25. The key for these figures is the same as was used in Figures 3.8 - 3.11. The longitudinal strains were much larger than the hoop strains, as expected, due to the direction of applied loading. The magnitude of the strains in the longitudinal direction at gaged Locations B and D (springline of the pipe) were very small relative to the strains at gaged Locations A and C (top and bottom of the pipe respectively (see Figure 3.3a)). This implies that the neutral axis of the CMP remained near the mid height of the pipe during loading. Because the strain gages were on the inside of the pipe, tensile (positive) strains were recorded on the top of the pipe while compressive (negative) strains were recorded on the bottom of the pipe during uplift loading.

Throughout the loading sequence, the magnitude of the strains at Locations A and C were nearly equal. The longitudinal strains at Section 2 were greater than those at Section 4. This can be explained by the manner in which the pipe is bending. As seen in Figure 3.16a the pipe is bending at

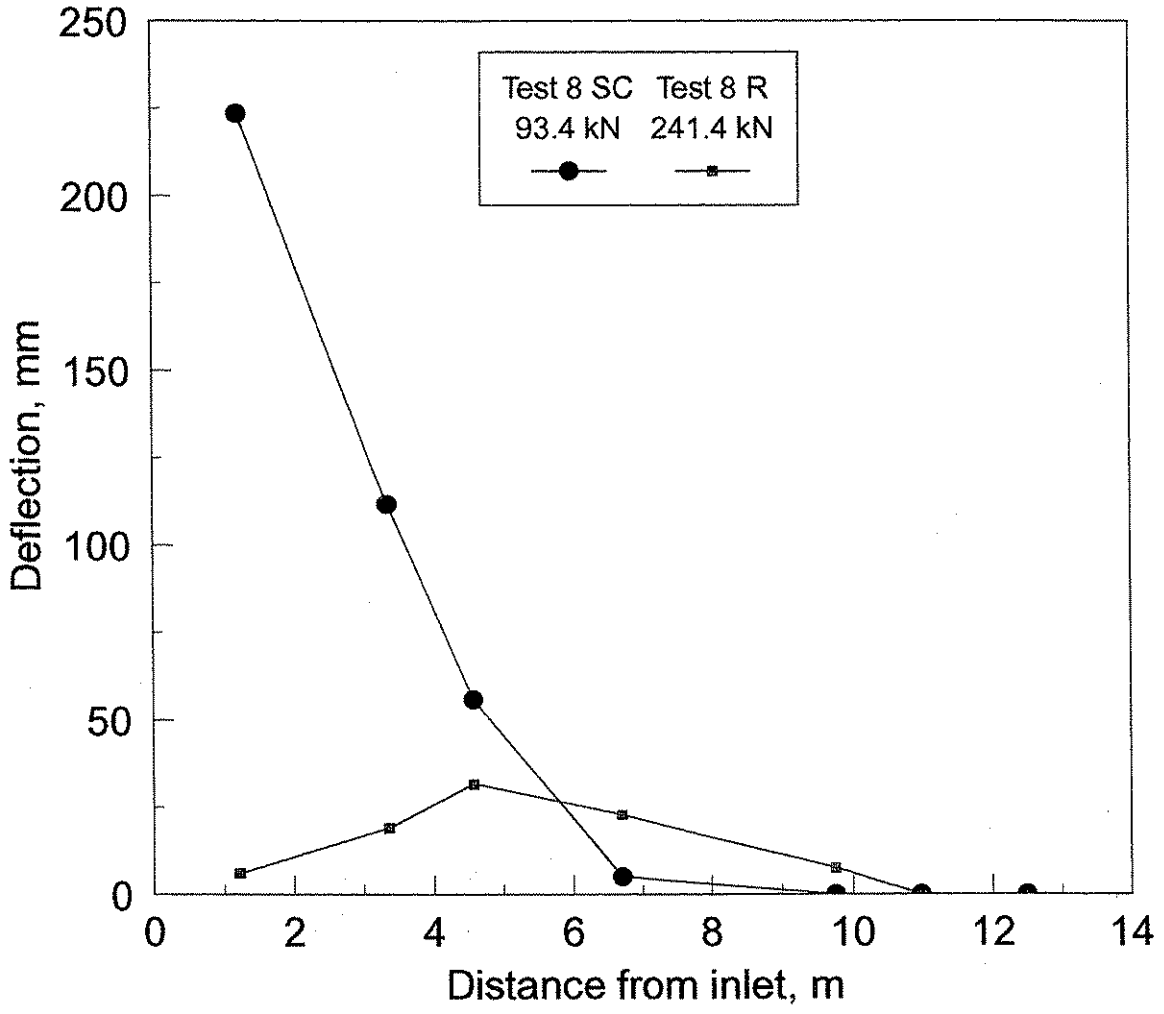

Figure 3.17. Comparison of field tests 8 SC and 8 R deflections.

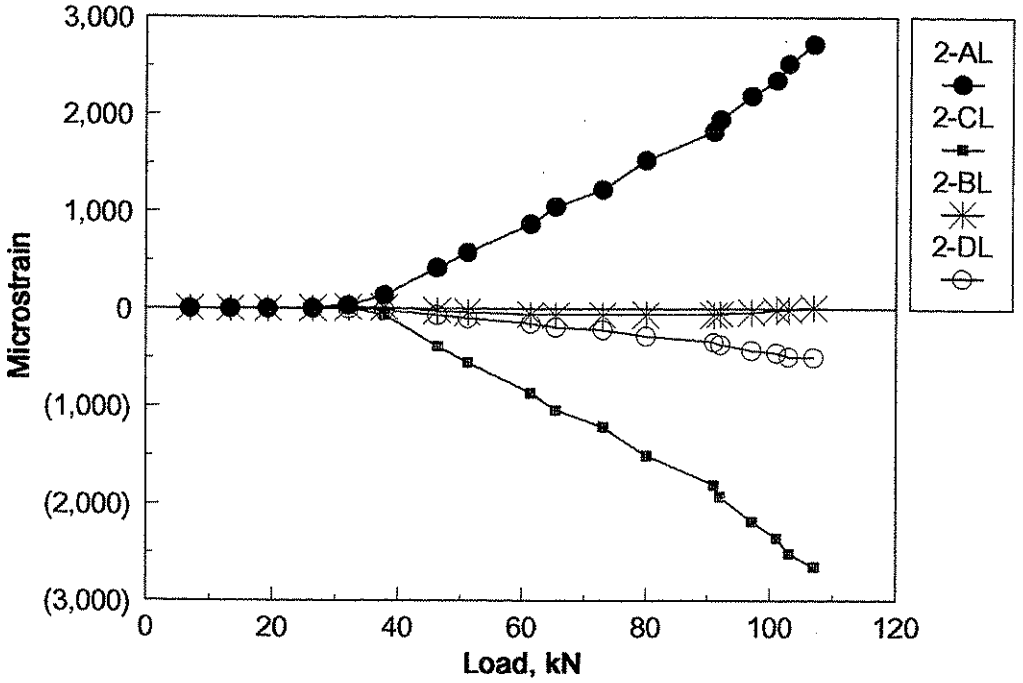

(a) Longitudinal Strain

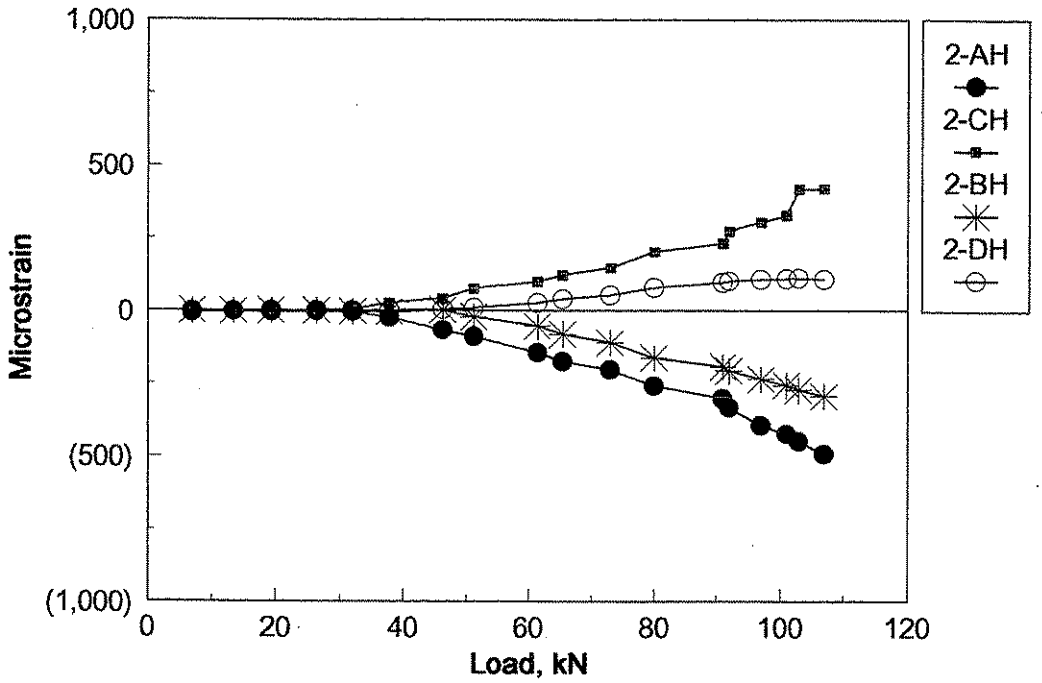

(b) Hoop Strain

Figure 3.18. Test 8SC strain readings at section 2.

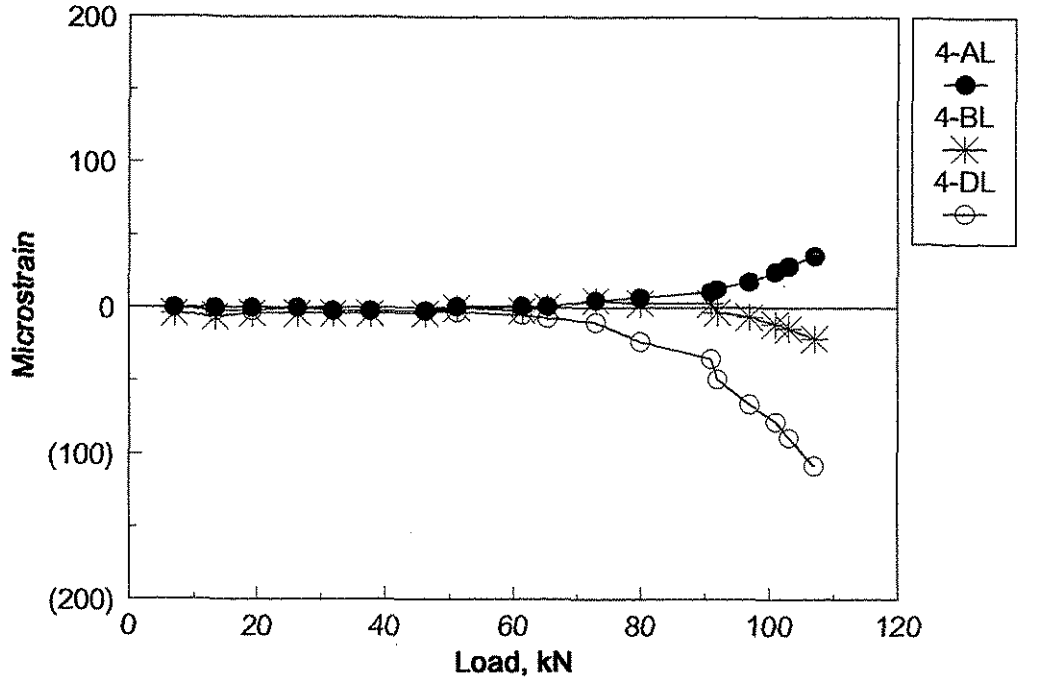

(a) Longitudinal Strain

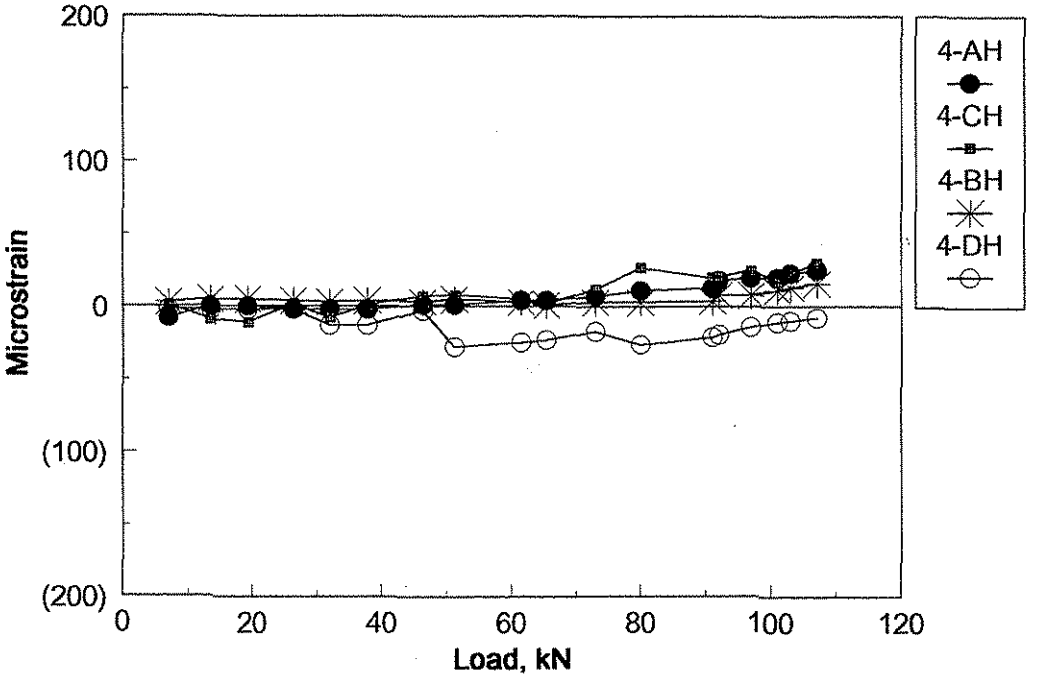

(b) Hoop Strain

Figure 3.19. Test 8SC strain readings at section 4.

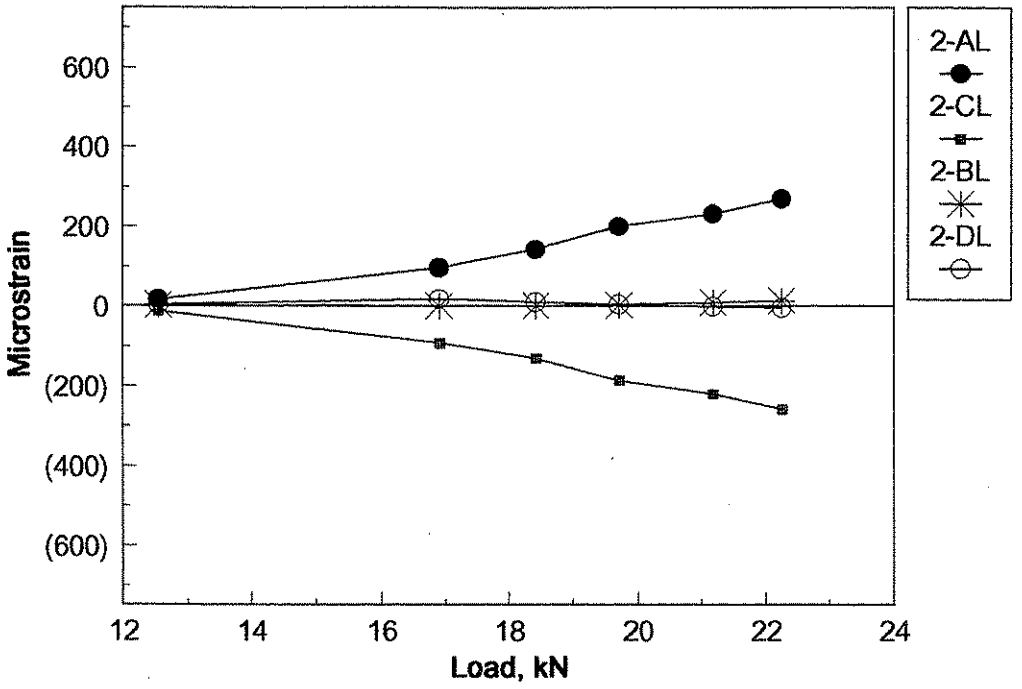

(a) Longitudinal Strain

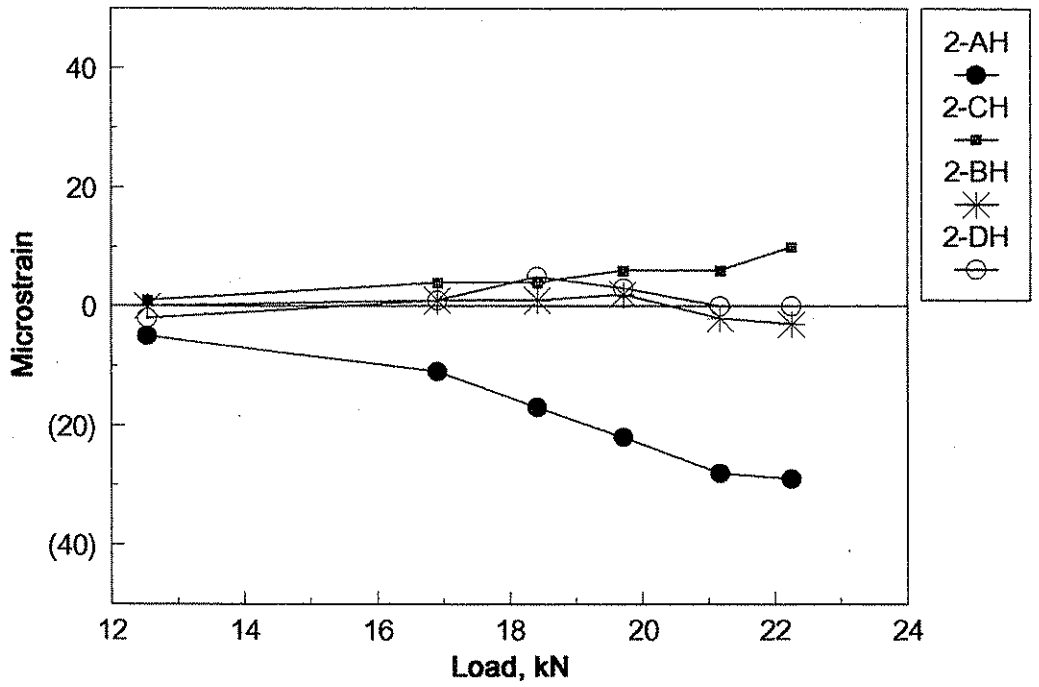

(b) Hoop Strain

Figure 3.20. Test 8NC strain readings at section 2.

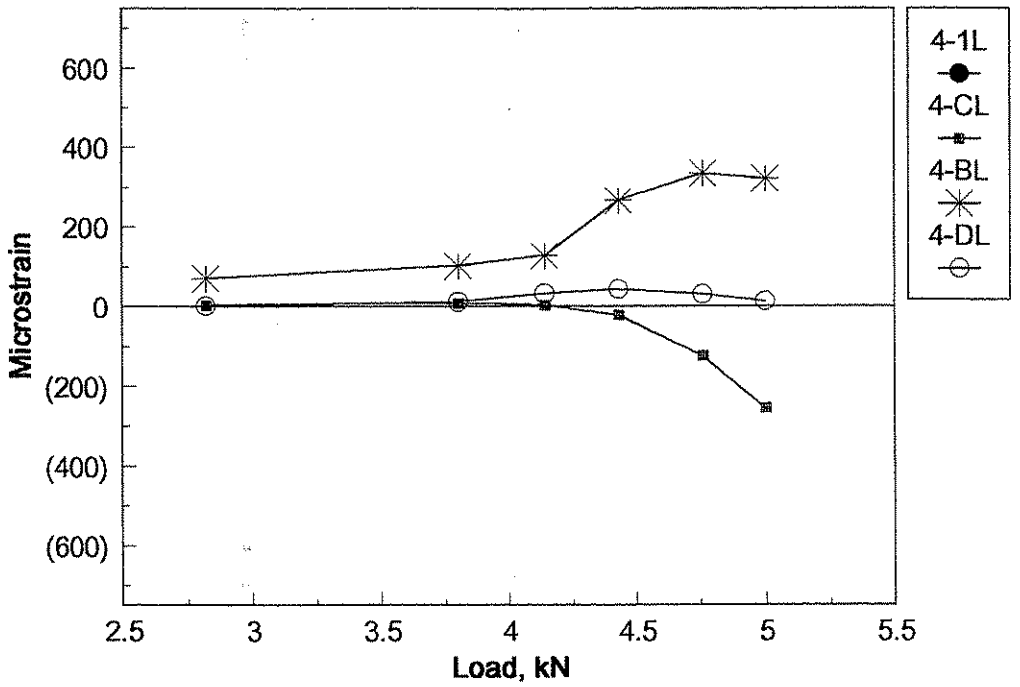

(a) Longitudinal Strain

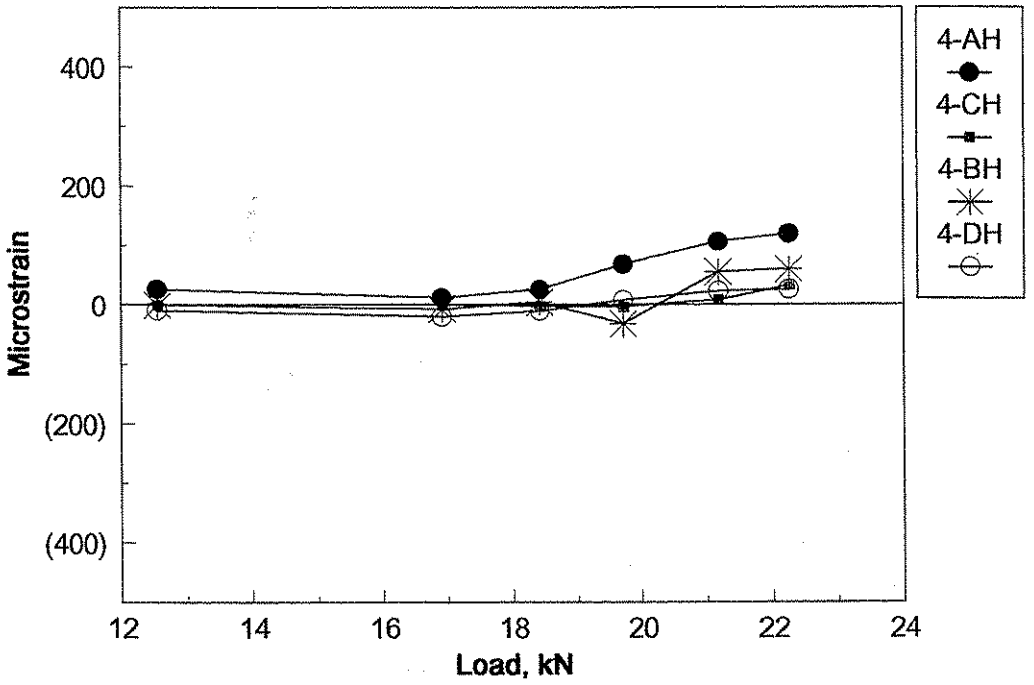

(b) Hoop Strain

Figure 3.21. Test 8NC strain readings at section 4.

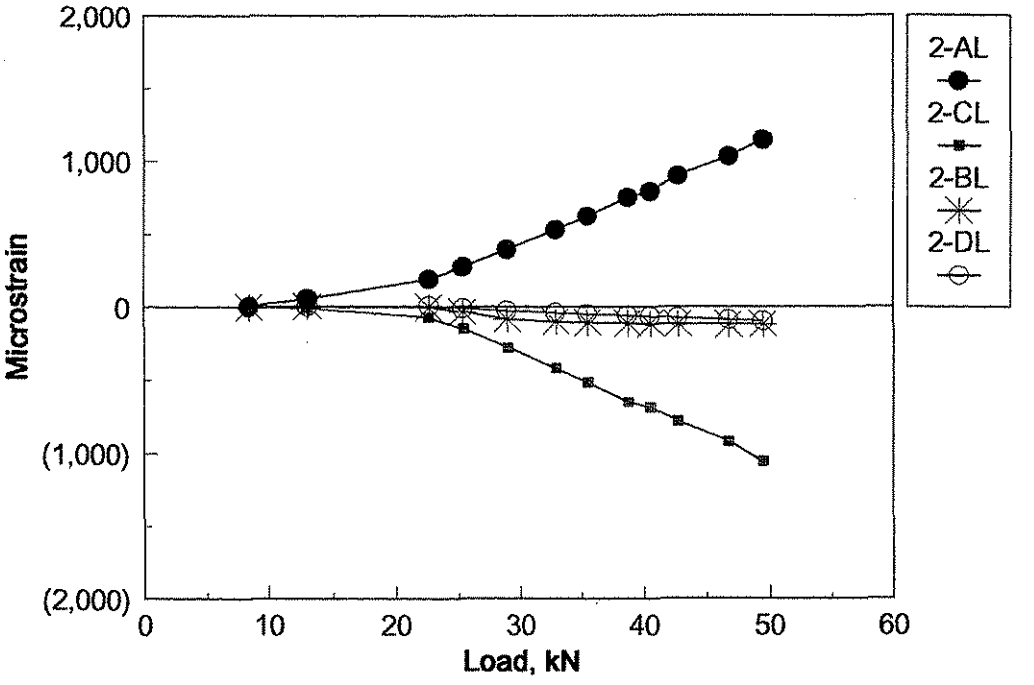

(a) Longitudinal Strain

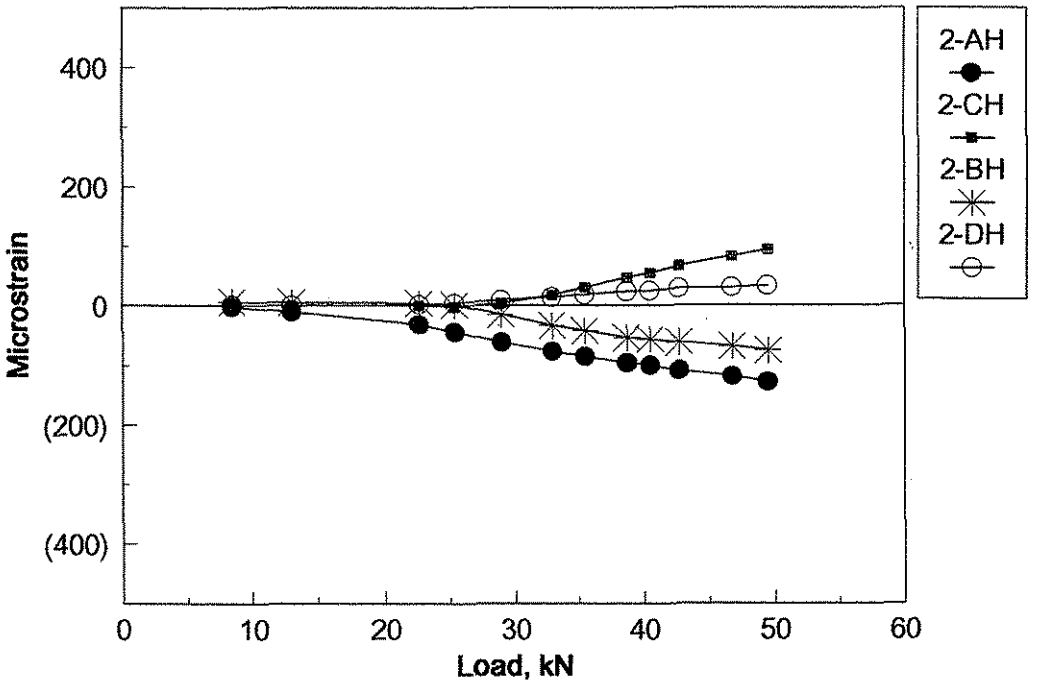

(b) Hoop Strain

Figure 3.22. Test 8NF strain readings at section 2.

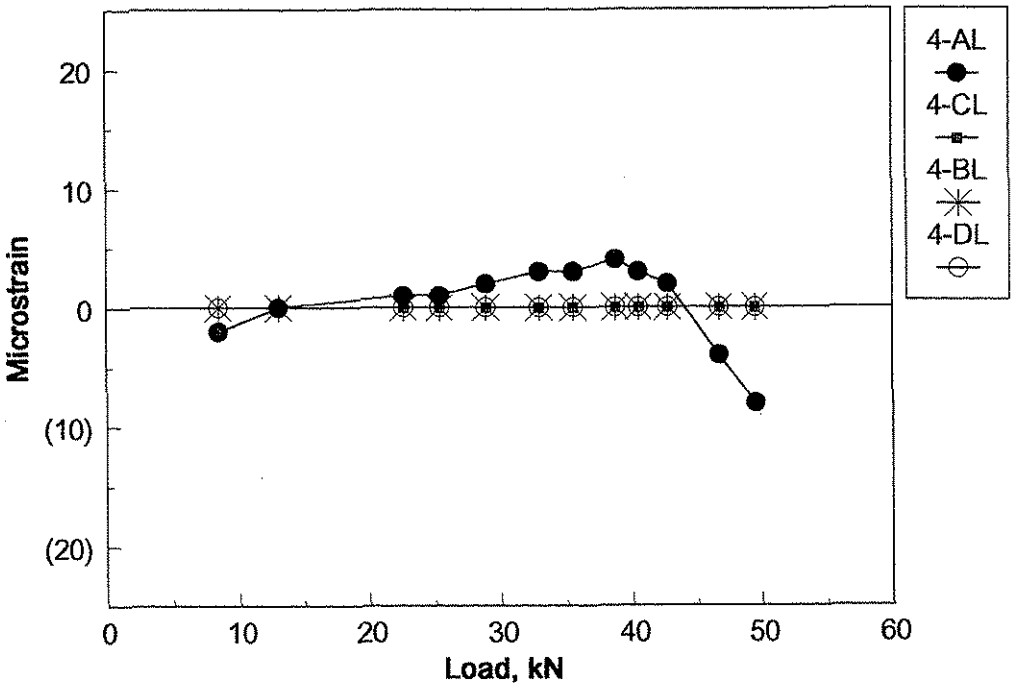

(a) Longitudinal Strain

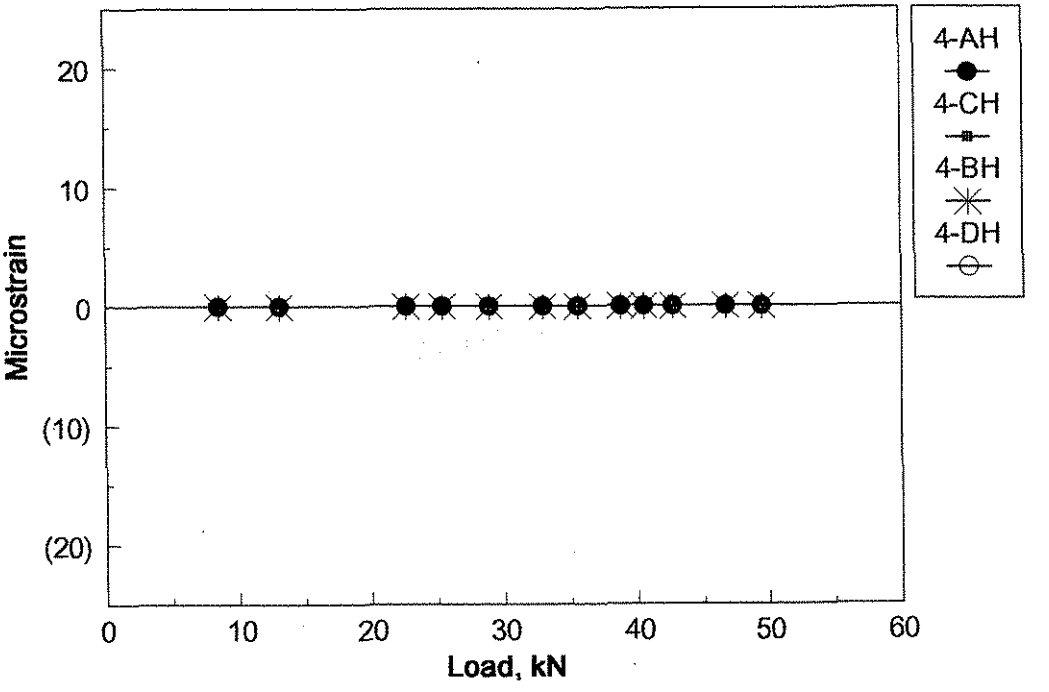

(b) Hoop Strain

Figure 3.23. Test 8NF strain readings at section 4.

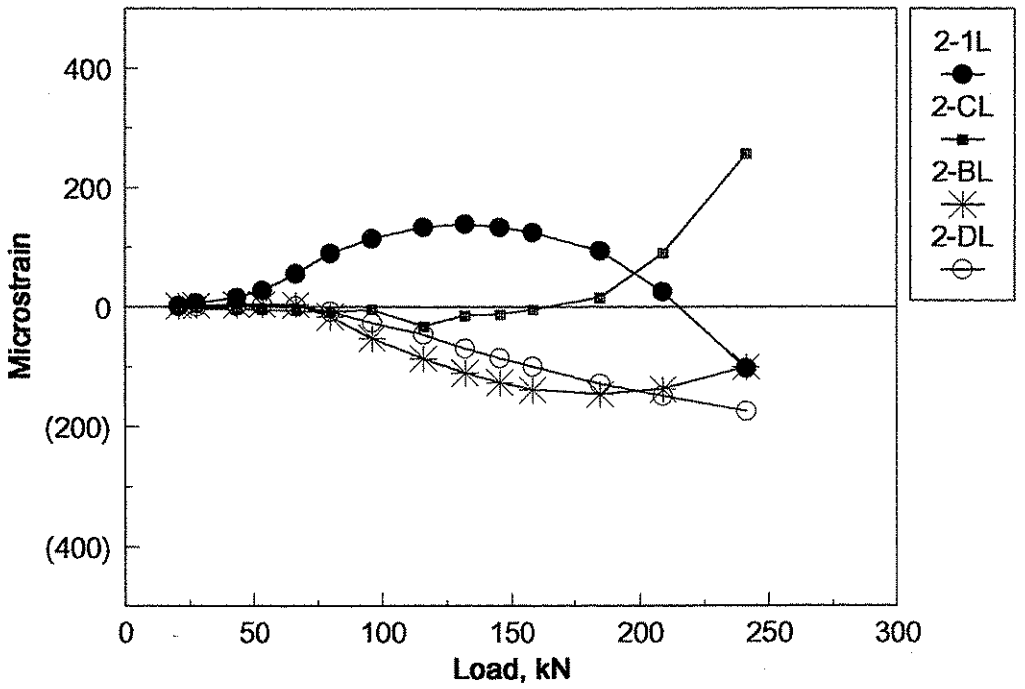

(a) Longitudinal Strain

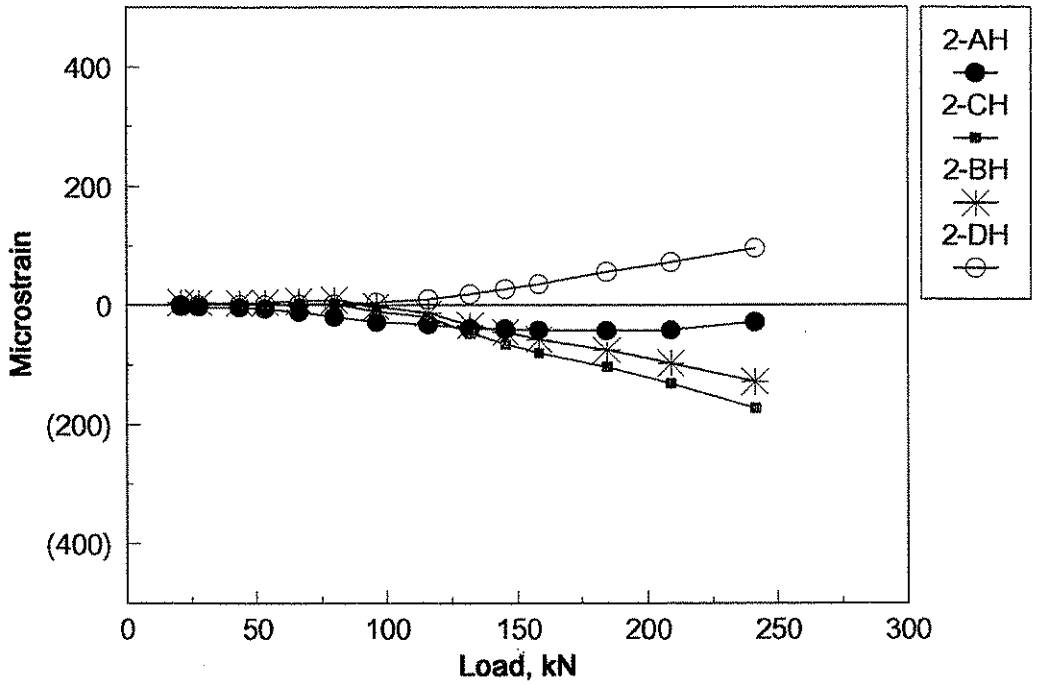

(b) Hoop Strain

Figure 3.24. Test 8R strain readings at section 2.

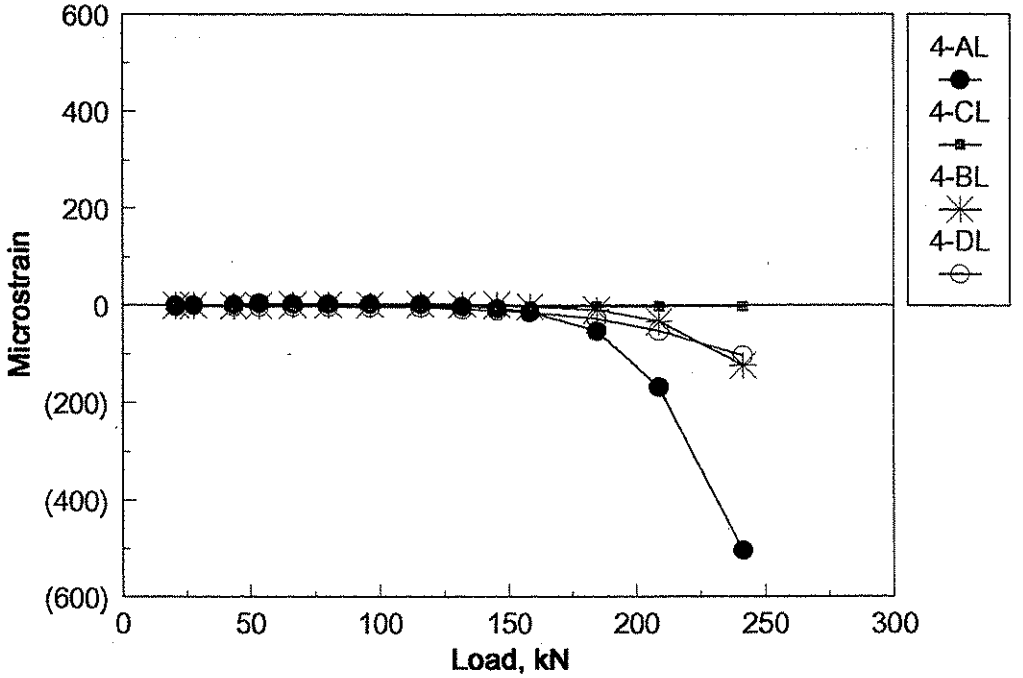

(a) Longitudinal Strain

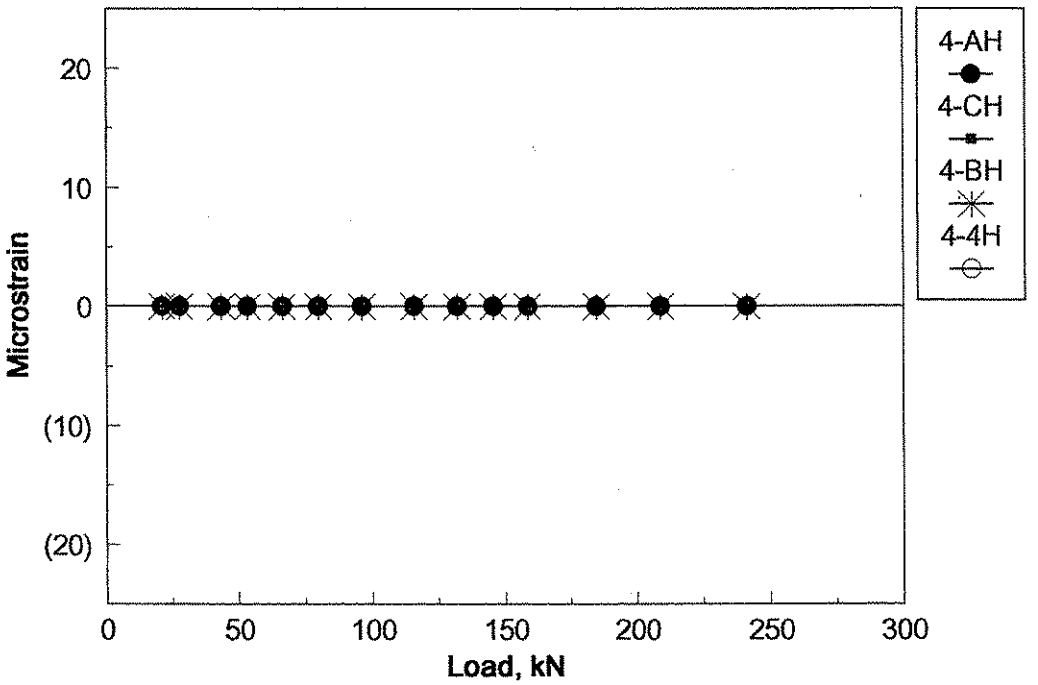

(b) Hoop Strain

Figure 3.25. Test 8R strain readings at section 4.

approximately 6.71 m (22 ft) from the inlet where Section 2 is located. Maximum strains occur where the pipe is bending. This is also evident in Tests 8SC and 8NF.

3.10.3 Cross section deformations

During the uplift portion of the test, the horizontal and vertical diameter changes of the pipe were monitored. Representative data are presented for the various field tests in Figures 3.26 - 3.29 where it can be seen that small deformations occurred during uplift. Note, key same as used in Figure 3.7. In Tests 8SC and 8NF, the sides moved sightly inward while the top moved slightly upward. Deformations in the opposite direction would be expected due to the bending that is occurring. This deformation may be caused by the loading arrangement used in these tests. The loading straps applied load up to the mid height of the pipe which may have confined outward movement. The soil mass also provided confinement for the completely buried section of pipe.

The deformations in Test 8R are opposite to those in Tests 8SC and 8NF. The pipe was restrained at the inlet and confined by the soil mass; therefore, when load was applied, it caused crushing deformations. Test 8NC had no constraints and therefore no deformations occurred during uplift.

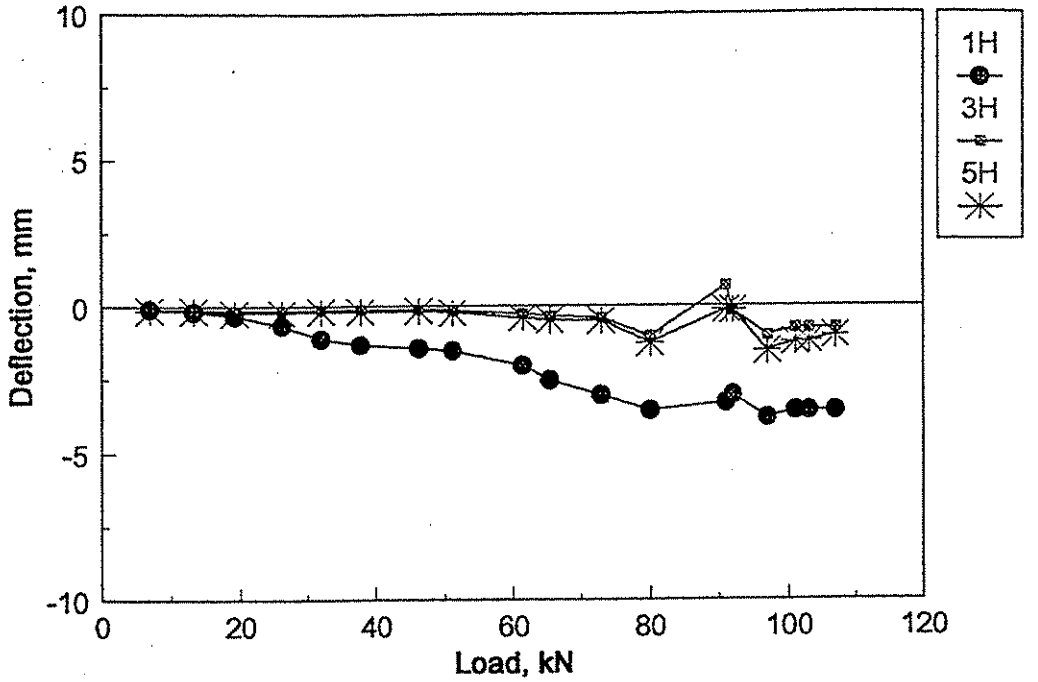

(a) Test 8SC Horizontal Deformations

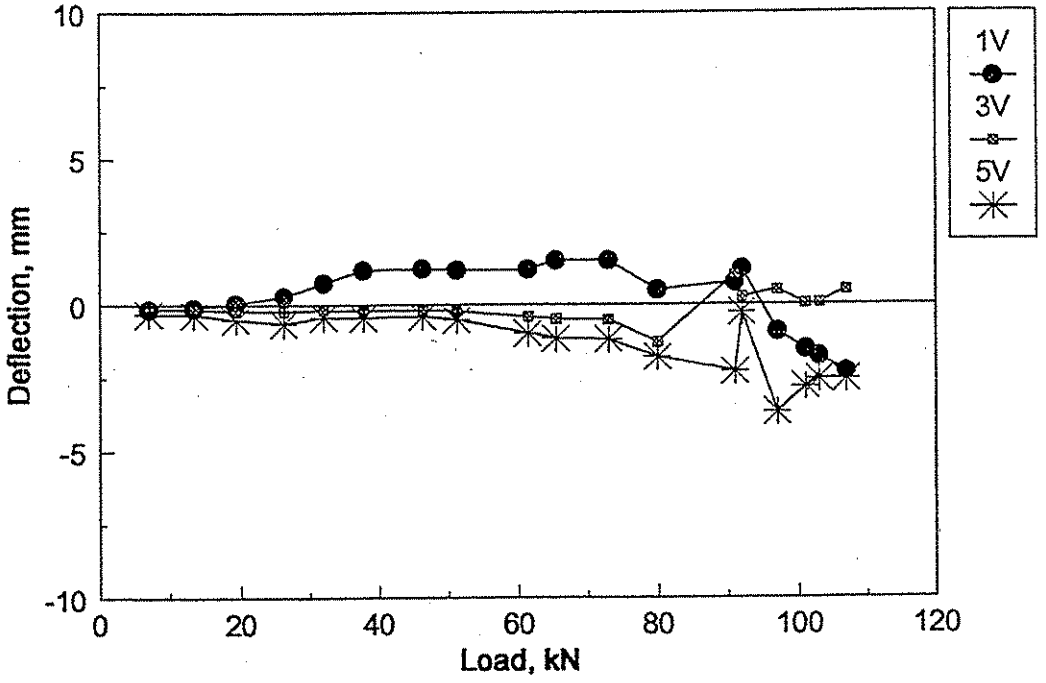

(b) Test 8SC Vertical Deformations

Figure 3.26. Diameter deformations for test 8SC due to uplift.

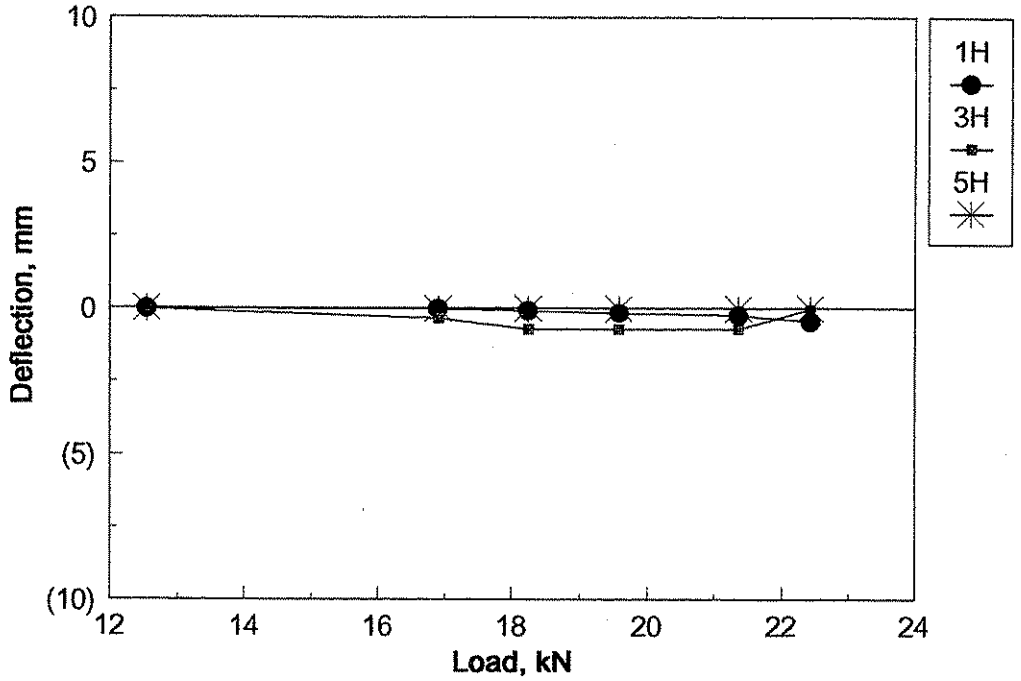

(a) Test 8NC Horizontal Deformations

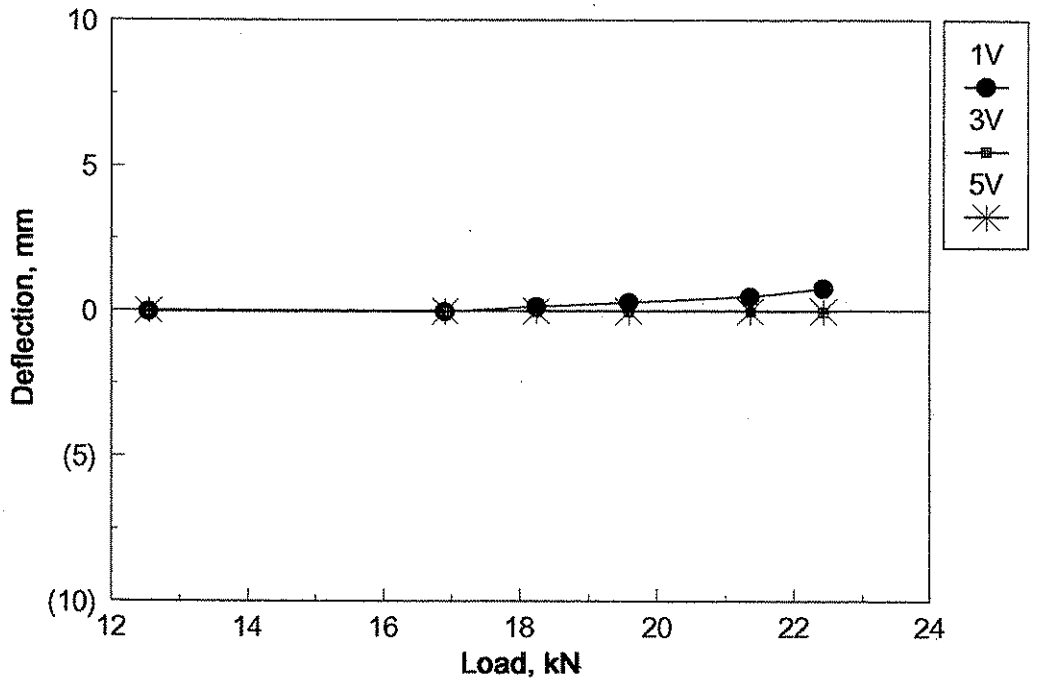

(b) Test 8NC Vertical Deformations

Figure 3.27. Diameter deformations for test 8NC due to uplift.

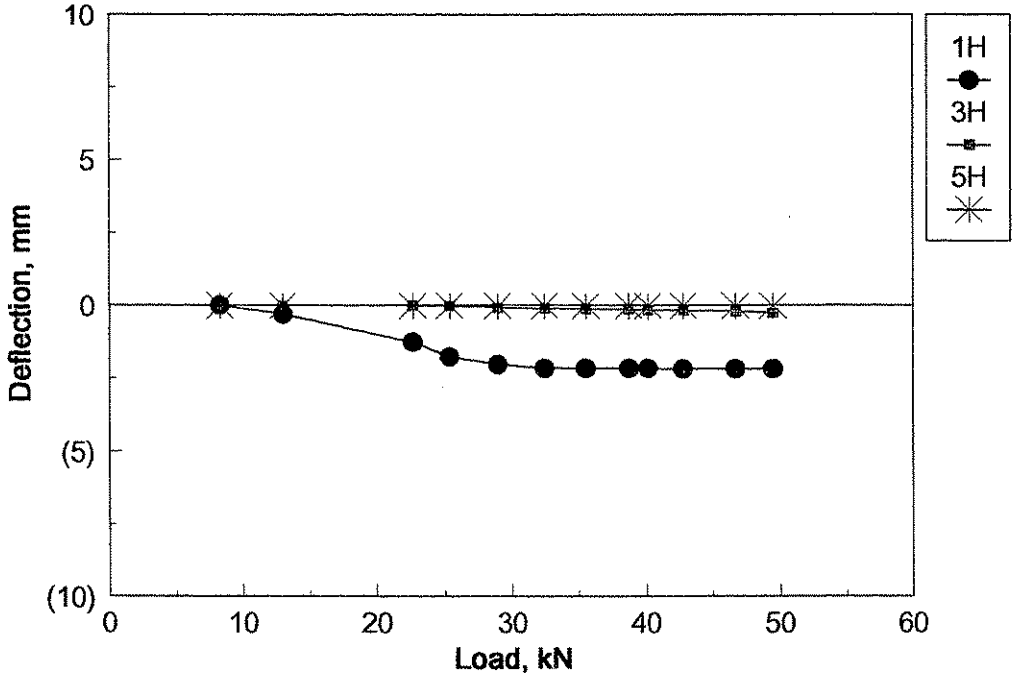

(a) Test 8NF Horizontal Deformations

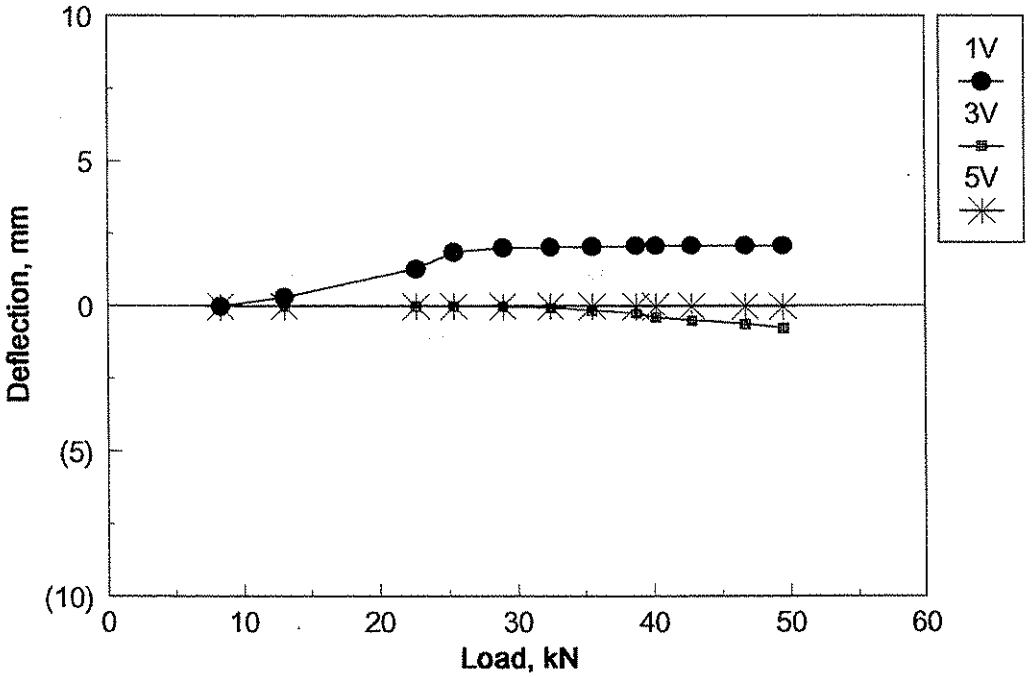

(b) Test 8NF Vertical Deformations

Figure 3.28. Diameter deformations for test 8NF due to uplift.

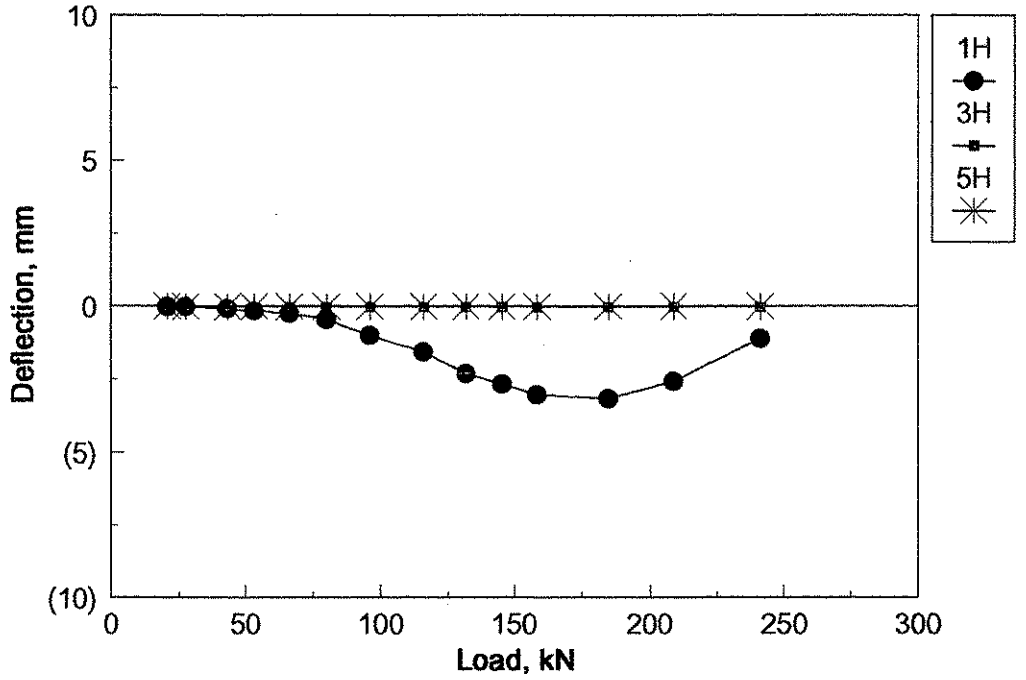

(a) Test 8R Horizontal Deformations

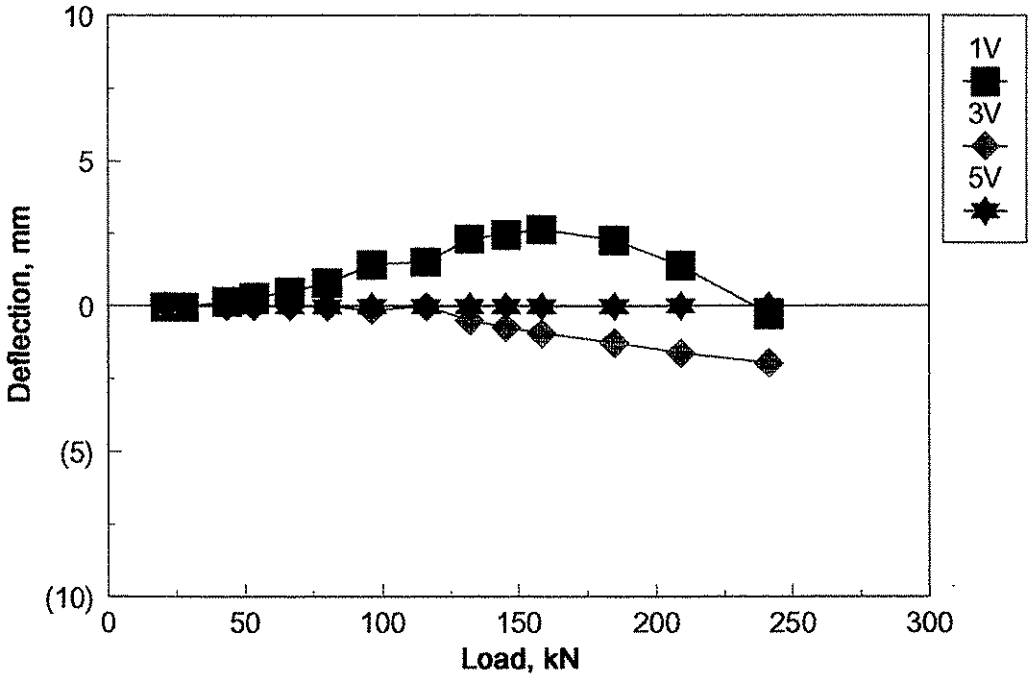

(b) Test 8R Vertical Deformations

Figure 3.29. Diameter deformations for test 8R due to uplift.

3.11 Summary of Field Testing Results

1. During the backfilling process the pipe cross section horizontal diameter decreased due to the horizontal pressure the backfill exerted on the CMP.
2. Strains developed during backfilling are predominantly in the hoop direction while those developed during uplift are predominantly in the longitudinal direction.
3. During uplift small cross sectional deformations occur as compared with backfilling.
4. The soil-structure interaction is evident in the longitudinal bending of CMP. Deflected shapes from Tests 8NC, 8NF, and 8SC indicate the effects of the soil and foreslope.

4. SOIL-STRUCTURE INTERACTION FINITE ELEMENT MODEL

4.1 Scope of this Chapter

This phase of the investigation involved the development and execution of the soil-structure interaction finite element model. In this chapter, the assumptions and theory used to create this model are explained. The material properties and element selection for the complex interface occurring between the CMP and the surrounding soil are also presented.

Results from the finite element analysis (FEA) of the field tests are compared with the experimental data from the field tests described in Chapter 3. This chapter also describes the finite element model and procedure for calculating the force necessary to restrain a CMP from uplift failure. A sensitivity study performed on the finite element model is also presented. A complete treatment of the development of the finite element model may be found in Peiffer (1995).

4.2 Finite Element Models for Tests 8NF, 8SC and 8R

Four noded isoparametric shells were used to idealize the pipe and 2-noded linear beam elements accounted for the loading straps. The soil was modeled using 8-noded isoparametric solid elements. The shell and solid elements worked well for the meshing at the intersection between the pipe and soil since they both have four nodes per face.

The shell elements possess 5 degrees of freedom per node unless attached to a node where a rotational degree of freedom is activated by a boundary condition or another element having 6 degrees of freedom. In the latter case, the node defaults to 6 degrees of freedom to provide compatibility. The solid elements possess 3 degrees of freedom, i.e. 3 displacements only and no rotations, per node. This incompatibility between active degrees for the soil and pipe elements was

not found to be a problem since both elements were never directly joined but were connected by 8-noded interface elements.

FORTRAN programs were written to create the finite element models because a pre-processor was not available for the ABAQUS version. The final models used for the analysis of Tests 8NF and 8SC are shown in Figures 4.1 and 4.2. The meshes used for Test 8R and the restraint design model are essentially identical to the mesh for Test 8SC and therefore are not shown.

The interface elements used in this analysis were two flat 4-noded quadrilateral plates. For the interface between soil and the pipe, one of the plates is attached to the soil element surface and the other to the pipe element. This restricts the faces of the soil and pipe elements attached to the interface element from passing through each other. An important aspect of this element is its ability to allow two surfaces to transmit frictional forces while in contact or allow them to separate freely. This is very useful in general contact problems where the areas of contact are either changing or unknown.

4.2.1 Material properties and constitutive models

The corrugated metal pipe was modeled as an equivalent smooth wall pipe (SWP), with material properties representative of the CMP. Material properties of the equivalent SWP test specimen are presented in Table 4.1. All material properties were considered linear elastic unless specifically stated otherwise.

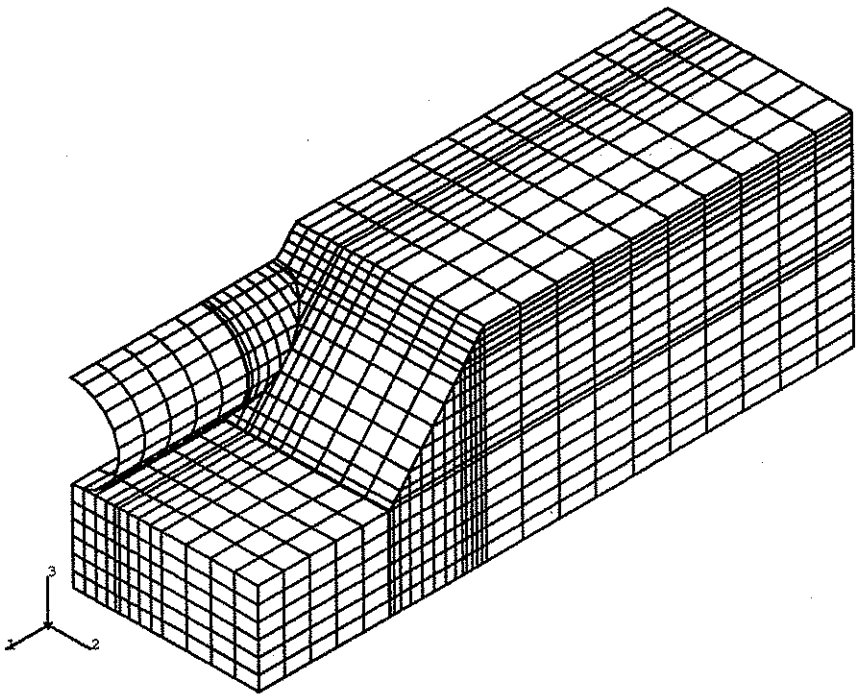

Figure 4.1. 8NF finite element model.

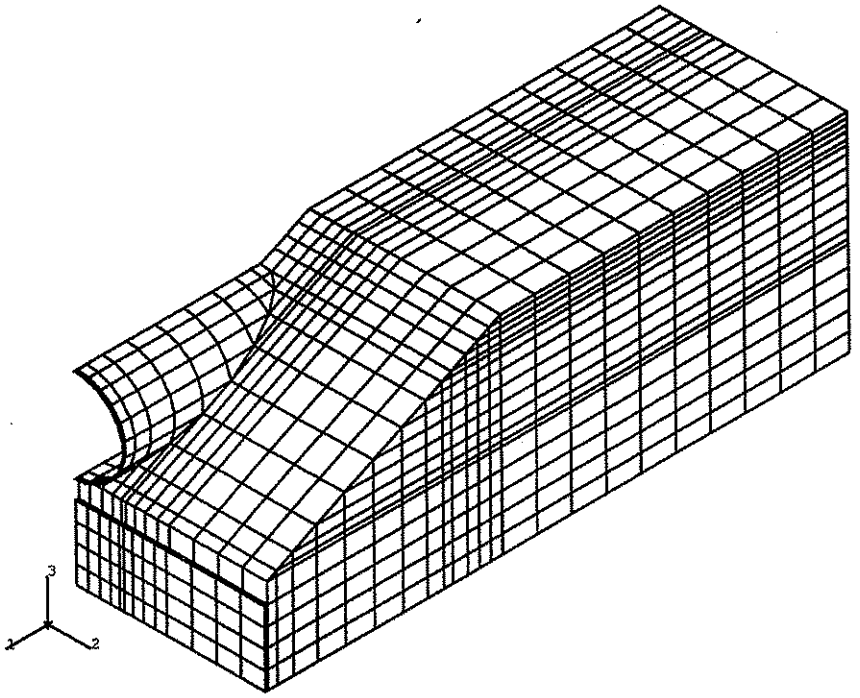

Figure 4.2. 8SC finite element model.

Table 4.1 Geometric and material properties of the SWP pipe model.

Property	SI Units	Imperial Units
Radius m (in.)	1.233	48.5523
Wall thickness mm (in.)	30.34	1.1945
Equivalent density kN/m^3 (lb/in^3)	0.00485	0.0309
Total length m (ft)	15.8496	52
E_{zz} kN/m^2 (ksi)	119,973	17.4
$E_{\theta\theta}$ kN/m^2 (ksi)	21,788,200	3160
$\upsilon_{z\theta}$	0.0016	0.0016
$G_{z\theta}$ kN/m^2 (ksi)	5,460,840	792
G_{zr} kN/m^2 (ksi)	6,784,680	984
$G_{\theta r}$ kN/m^2 (ksi)	8,411,900	1220
Weight kN/m (lb/ft)	1.8972	130

E = Young's modulus, G = shear modulus and υ = Poisson's ratio.

The subscript θ denotes the circumferential direction and z the longitudinal direction. The yield moment of the pipe was calculated as 5.49 m-kN/m^2 (81 ft-kips) based on a 227,535 kN/m^2 (33 ksi) yield stress.

The soil was assigned a Young's modulus of 16,548 kN/m^2 (2400 psi) and a Poisson's ratio of 0.35. Young's modulus was based on in situ field tests (Heilers, 1994). Poisson's ratio was chosen from values commonly accepted for soil analysis. The linear elastic constitutive model is a simplification of the medium's true behavior which is nonlinear elastic with plastic deformation capabilities. For small strains, however, the linear elastic model is commonly implemented. Other more sophisticated soil models are available including: the Drucker-Prager, Cam-Clay, and Duncan-

Chang hyperbolic stress-strain model. All of these models, however, required additional soil properties in exchange for their more realistic portrayal and it is difficult to establish material properties that are representative of those in the field. The introduction of nonlinear material models also increases computation time because extra iterations are needed for solution convergence.

A comparison between the fully elastic material model and an elastic-plastic material model was made for arbitrary load steps in the 8NF and 8SC models. The Drucker-Prager plasticity model, that requires two material parameters in addition to those used in the linear elastic model, was used for this analysis. The additional parameters are calculated from Mohr-Coulomb parameters of cohesion, c, and the angle of internal friction, ϕ_s. The subscript "s" is used here to distinguish the soil property from the corrugation property.

Triaxial tests conducted on samples taken from the CMP site produced a cohesion of 51.71 kN/m^2 (7.5 psi) and a friction angle of 16 degrees (Heilers, 1994). This analysis used a conservative cohesion of 10.34 kN/m^2 (1.5 psi) and the friction angle recorded by Heilers of 16 degrees. The material was set so that no dilation occurred during deformations.

The interface elements in this analysis contributed two important capabilities. First, the elements provided contact and separation capabilities. This is important during the longitudinal uplift because it allow gaps to form between the pipe and soil. Secondly, when the pipe is in contact with the soil it can transfer shear forces across the interface. This was accomplished using an anisotropic Coulomb friction model. This model transfers shear forces whose maximum sliding stresses are functions of the contact pressures at the interface boundaries and a coefficient of friction for the direction of sliding.

Two separate friction coefficients were used in orthogonal directions within the sliding plane. This allowed a better representation of the interface by having a higher friction coefficient in the longitudinal direction (z) (i.e. perpendicular to the corrugations) than in the circumferential direction (θ) (parallel to the corrugations).

Friction coefficients were determined from laboratory tests (Morgan, 1995). Corrugated sections two wavelengths long and three inches wide were fitted flush against soil samples taken from the CMP test site. The corrugated sections were pressed against the soil with varying normal forces and shear forces parallel and perpendicular to the corrugations were applied unit the soil shear strength was mobilized or the frictional forces between the soil and corrugated sample were exceeded. In general, the samples interlocked with the soil in the direction perpendicular to the corrugations and resulted in the soil "riding up" the corrugations so shear progressed and the shear strength of the soil-corrugation system was mobilized. This behavior was recreated in the soil-structure interaction model with a longitudinal friction coefficient, μ_{zz}, of 1.0. In the direction parallel to the corrugations, failure was governed by the friction of the soil against the metal surface. The resulting circumferential coefficient of friction, $\mu_{\theta\theta}$, used in the soil-structure model was 0.6.

4.2.2 Geometry of the finite element models

The pipe model was identical to that used for 8NC. The dimensions are listed in Table 4.2.

Table 4.2. Pipe Geometry.

Pipe Characteristic	SI Units	Imperial Units
Diameter m (ft)	2.44	8
Helical angle degrees	6	6
Gage	12	12
Uncoated thickness mm (in.)	2.6568	0.1046
Corrugation depth mm (in.)	25.4	1.0
Corrugation pitch mm (in.)	76.2	3.0
Radius of curvature mm (in.)	14.2875	0.5625
Tangent length mm (in.)	22.5806	0.889

When the pipe and soil elements were combined, their boundaries were set so that the pipe would fit flush inside of the soil model, i.e. initial interface gaps were zero. The back soil boundary was set flush with the back end of the pipe. The upper boundary was 0.61 m (2 ft) above the top of the pipe to be consistent with the experiments. The lower boundary was 2.44 m (8 ft) below the bottom of the pipe. This created a buffer zone needed to minimize the interference the soil boundary would have on the pipe displacements. The side boundary for the soil was set at 2 pipe diameters away from the pipe's axis. This removed the effects of the boundary from the displacements occurring around the pipe but did not widen the model's dimensions so much as to burden the solution time. The front face, or foreslope, of the soil was set at the proper angle for each test. The foreslope for 8NF started at the bottom of the pipe a distance approximately 3.66 m (12 ft) from the inlet and rose at an angle of 50 degrees from the horizontal. The slope leveled off after a cover of 0.61 m (2 ft) was established. The foreslopes for 8SC and 8R started at the bottom of the pipe inlet

and rose at an angle of 27 degrees from horizontal until the 0.61 m (2 ft) of soil cover was established. The soil cover was constant (0.61 m (2 ft)) for the remaining length of the pipe.

4.2.3 Boundary conditions

Boundary conditions for all soil-structure interaction models were prescribed using a global Cartesian coordinate system. The coordinate system is referenced using numbers 1 through 6. The coordinate axis (shown in Figures 4.1 and 4.2) had the global 1 direction running parallel with the pipe axis. The 3 direction was vertical (up) and 2 was placed in a manner consistent with the right-hand rule. The numbers 4, 5, and 6 denote rotations about global axes 1, 2, and 3, respectively.

The models were given symmetric boundary conditions for all vertical faces. For the front and back faces, no displacements in the longitudinal (1) direction were allowed. On the side faces, the displacements in the lateral (2) directions were restrained. At the back face of the model, the pipe had additional restraints for rotations 5 and 6. Also, the pipe nodes located in the plane of symmetry (which intersected the pipes's axes) were restrained from rotating about the global 1 axis (4) and the global 3 axis (6) in addition to the lateral restriction stated earlier. The underside of the soil model was pinned in all directions (1, 2 and 3).

Additional boundary conditions were applied to 8R at the inlet to create the restraining effect of the concrete mass. Rigid beam elements were used to maintain the cross section shape at the inlet throughout the loading. For each load case modeled, the corresponding vertical displacement and rotation measured at the CMP's inlet during the experiment was applied to the model inlet. The inlet was then held in the vertical direction at this location.

4.2.4 Loading

The construction sequence is typically included in a culvert analysis. In this step, the soil elements are added layer by layer in the same manner as the backfill. Each layer is then subjected to a vertical pressure that simulates the compaction process. After the solution has converged, the procedure is repeated by adding another stress-free layer. This continues until the culvert model is complete. The entire process can be very time consuming and is usually implemented when cross-section distortions and bending moments from surcharges are examined.

In this analysis, the construction procedure was bypassed and an initial geostatic stress state for the soil was substituted for it. A gravitational load was then applied to the entire model. The program was allowed to iterate until residual forces and moments and incremental displacements fell below specified tolerances. This placed the entire model in a dead load condition.

The final step was the strap loading. The loading on the pipe was applied in the same manner as in the 8NC test analyses. The front and rear straps were given the actual loads applied during the field experiments. This allowed displacements to be compared at all desired load levels.

4.2.5 Results and discussion for 8NF

Load steps 1 though 10 for 8NF were modeled using FEA. The resulting deflected shapes are plotted in Figures 4.3 and 4.4. along with the deflections obtained from the field tests. In general, the deflected shapes produced by the FEA were similar to those produced by the experiment. At low loads, the FEA over-predicted deflections (see Figure 4.3). At the high loads, the FEA tended to under-predict deflections (see Figure 4.4).

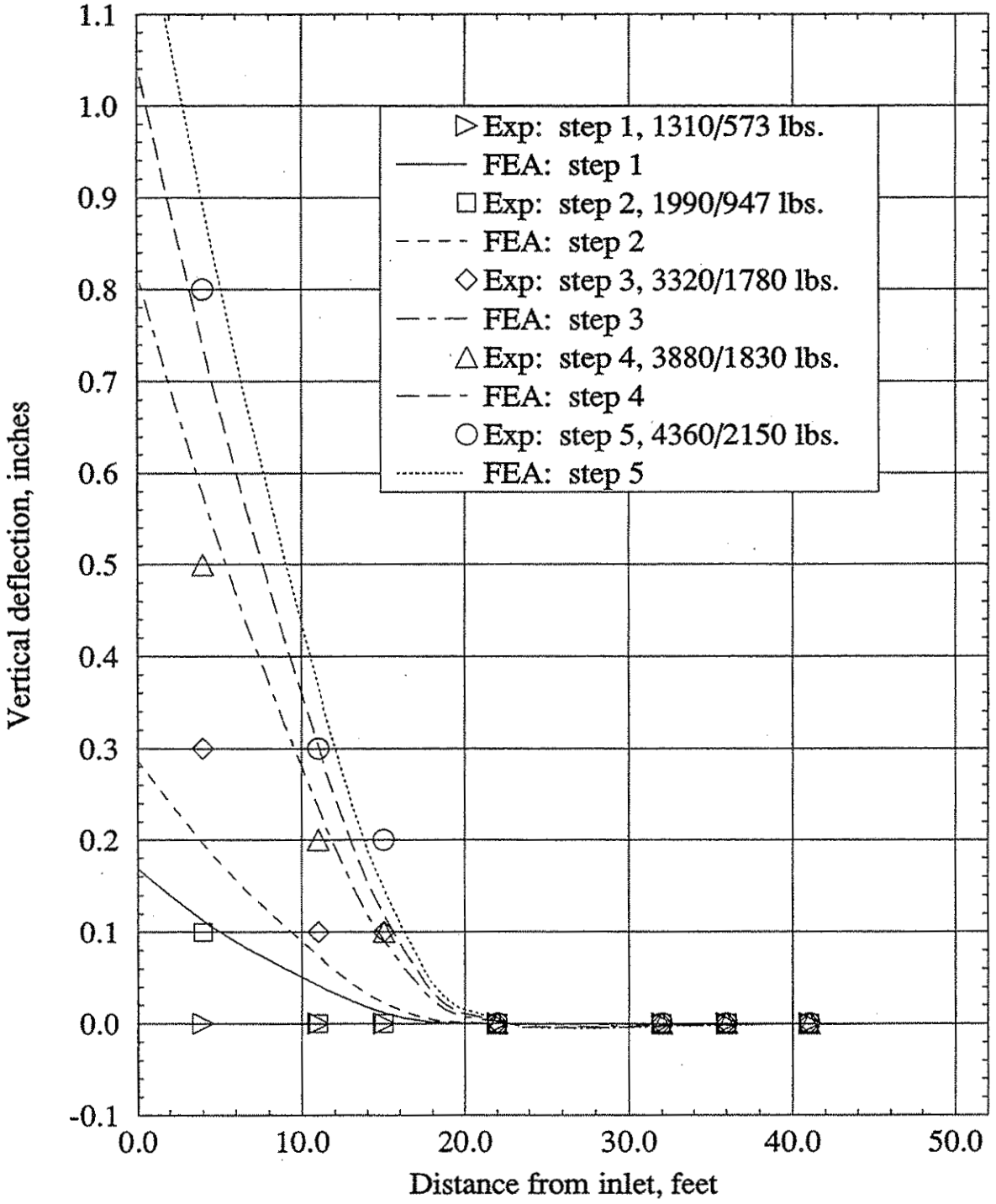

Figure 4.3. Comparison of 8NF FEA with experimental results. Steps 1 through 5 presented. Strap 1/Strap 2 loads given.

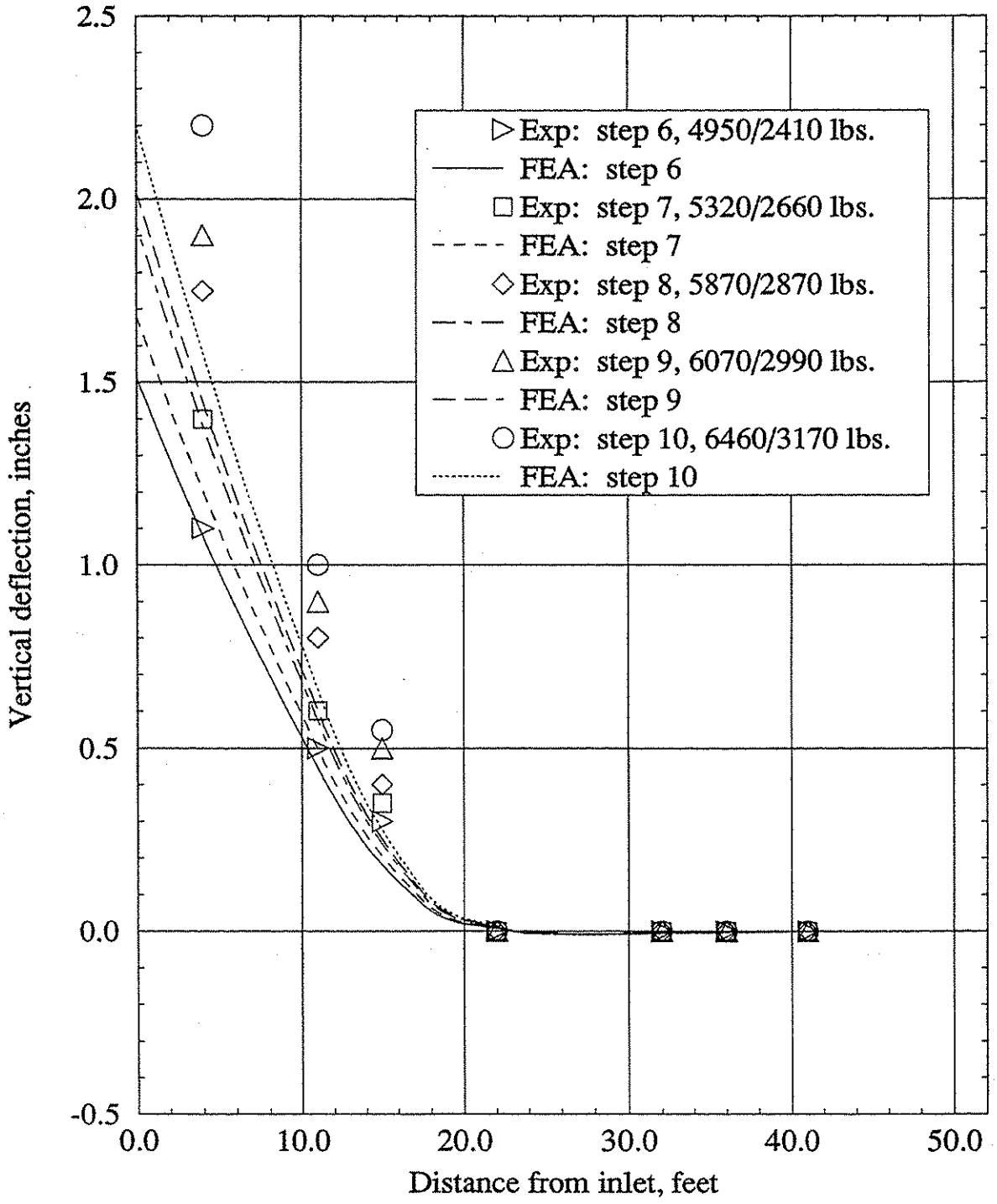

Figure 4.4. Comparison of 8NF FEA with experimental results. Steps 6 through 10 presented. Strap 1/Strap 2 loads given.

One possibility for the discrepancy between the deflections measured in the field, and the FEA deflections may be the weight of the loading system. Although the masses for the steel members (dywidag tendons, straps, transfer blocks, etc.) were consistent between 8NC, 8SC and 8R, the amount of grout placed between the straps and the CMP varied. In this test, the total mass of grout was unknown so the strap weights used for the 8NC test were an approximation. If the straps' weights were lower than the actual system weights, the pipe model would have the tendency to overestimate the deflections. This would be especially apparent at lower loads where the uplift resistance is created more through dead loads than pipe bending and soil deformations.

Another source of differences between FEA and test results at the lower loads could be adhesion occurring between the soil and CMP. Even small adhesive stresses at the soil-structure interface would have to be overcome before the CMP could lift. If no adhesion existed at the interface, the CMP would separate from the soil at much lower loads; therefore, the FEA would tend to overestimate deflections at lower loads. The adhesion characteristic was not included in the interface properties in the analysis because the phenomenon was not proven and would cause further complexities in the FEA.

The maximum curvature of the pipe was located approximately 5.5 m (18 ft) from the inlet for both the analytical model and the test specimen. This location was also the region of the highest vertical forces produced in the soil model as shown in Figure 4.5. This figure shows how the pipe loads, both self weights and uplift forces, were transferred into the soil model. Several load steps are shown.

Loads along the pipe model were created using the interface elements. Each interface element covered a unique length along the circumference of the pipe model that produced shear and normal

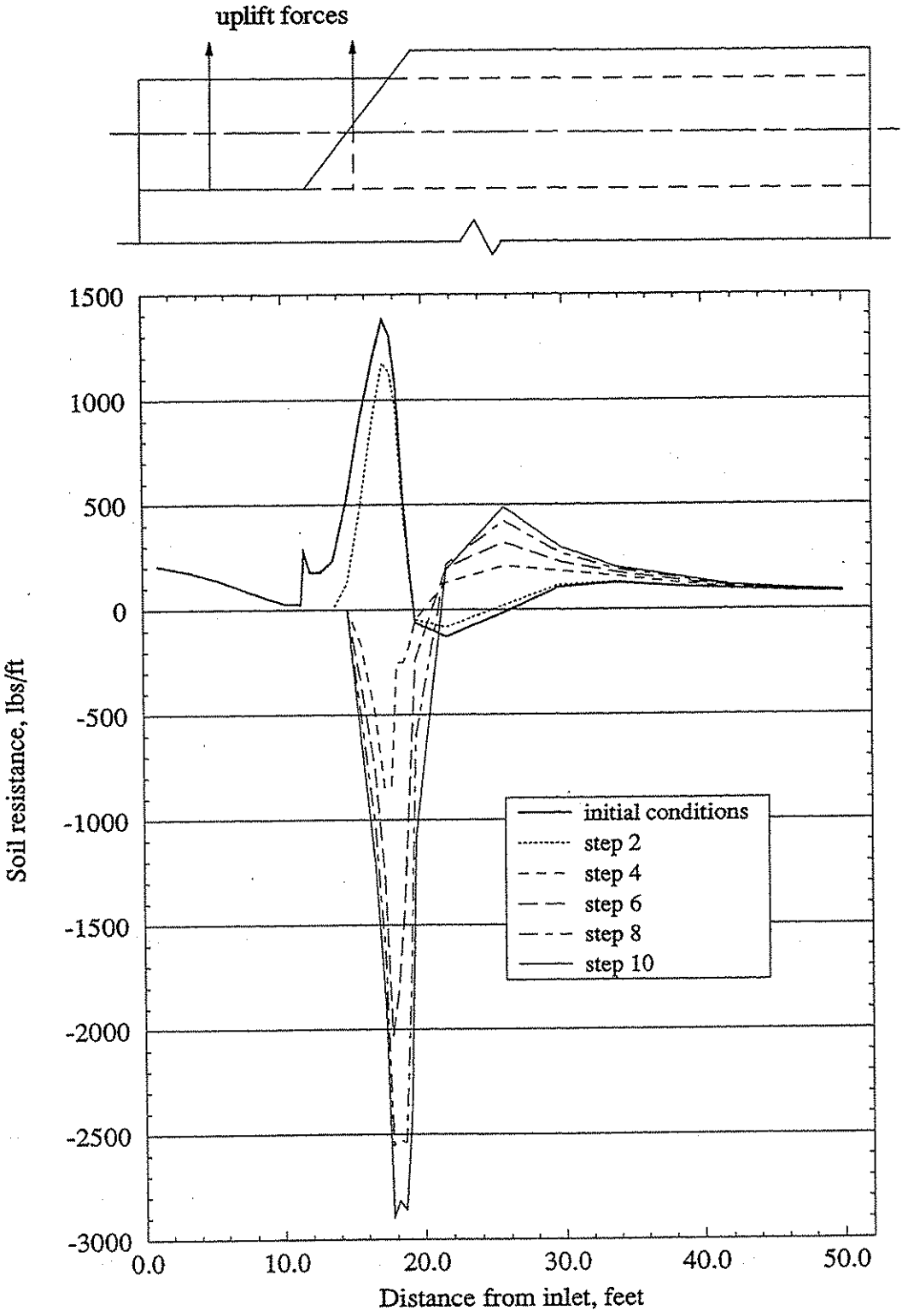

Figure 4.5. Soil resistance per foot length of 8NF SWP model.

stress data. Using the circumferential length of the element along with its position and stress information, the resultant normal and shear force vectors per unit length were calculated. Summing the vertical components of the force vectors at a pipe cross section produced the load per unit length applied to the pipe by the soil. The loads were then multiplied by 2 to account for the other half of the pipe not included in the FEA model. The initial load distribution along the pipe peaks about 5.5 m (18 ft) from the inlet indicating the soil is applying a large upward force on the pipe at this location. This is partly the result of the differential settlement that occurred during the gravitational loading step in the FEA. Also, the high strap weight in this region is a contributor to the magnitude of the peak. This graph indicates that the maximum soil resistance occurs only a small distance into the embankment. Most of the uplift load is, therefore, absorbed by the soil model within the foreslope region above the pipe. In a length of approximately 1.8 m (6 ft), the soil is producing all of the downward force needed to resist the uplift loads.

The analytical model indicates that almost all of the downward forces in the soil develop in the foreslope. Full cover occurs at 6.07 m (20 ft) from the inlet. This means that increasing the soil cover above the minimum specified 0.61 m (2 ft) has no effect on the uplift response for the given foreslope condition.

Figures 4.6 through 4.8 show comparisons of strains approximated from the FEA with actual longitudinal strains recorded during uplift testing for various cross sections along the CMP. The strains from the test were measured by gages mounted on the crests of corrugations at the top and bottom of the CMP. The FEA strains were calculated using the longitudinal strains from the top and bottom of the pipe model. The strains from the FEA were multiplied by a conversion factor that related the smooth-wall strains to the maximum longitudinal strains in the original corrugations. This

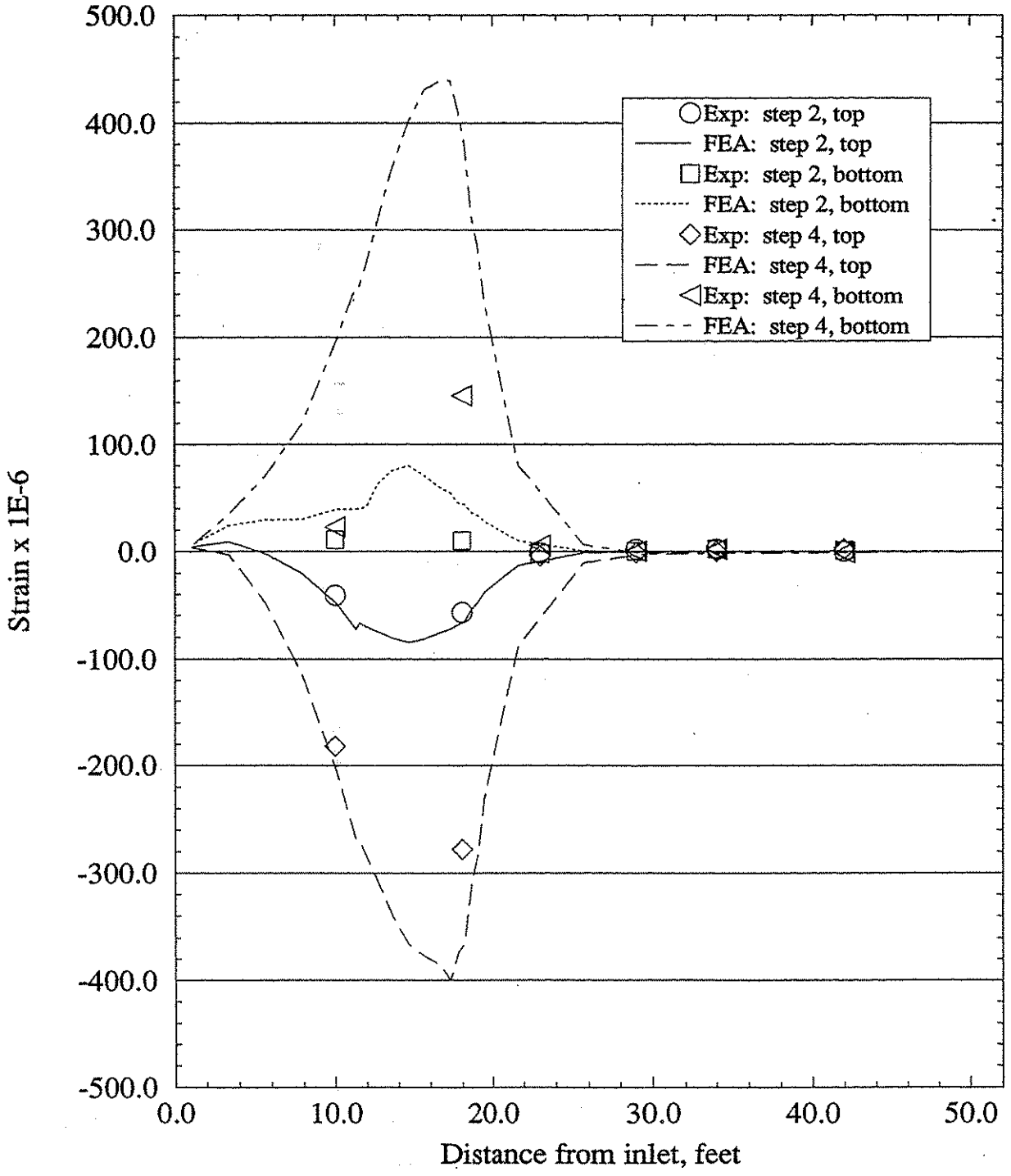

Figure 4.6. Comparison of strains for 8NF test and FEA.

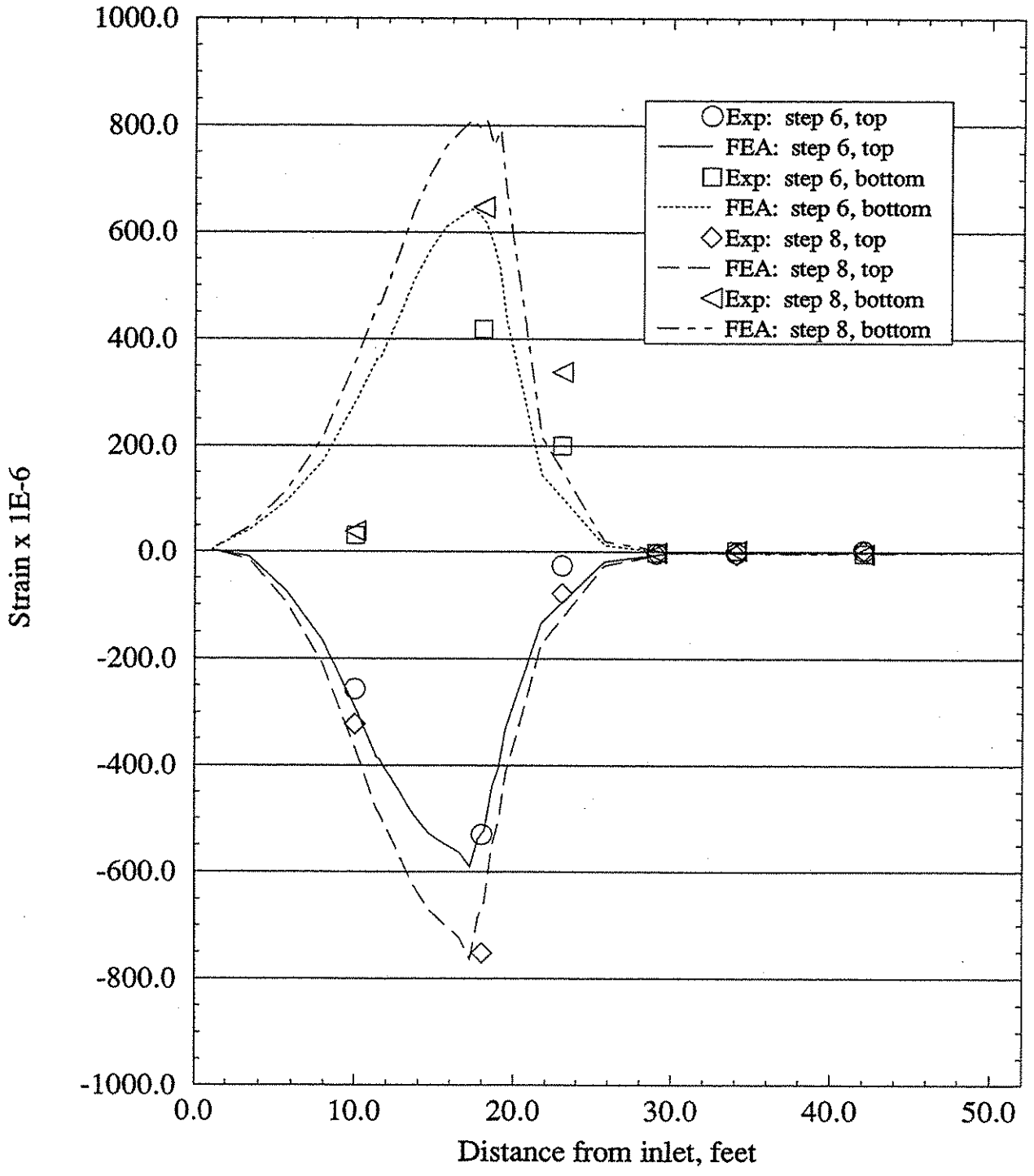

Figure 4.7. Comparison of strains for 8NF test and FEA.

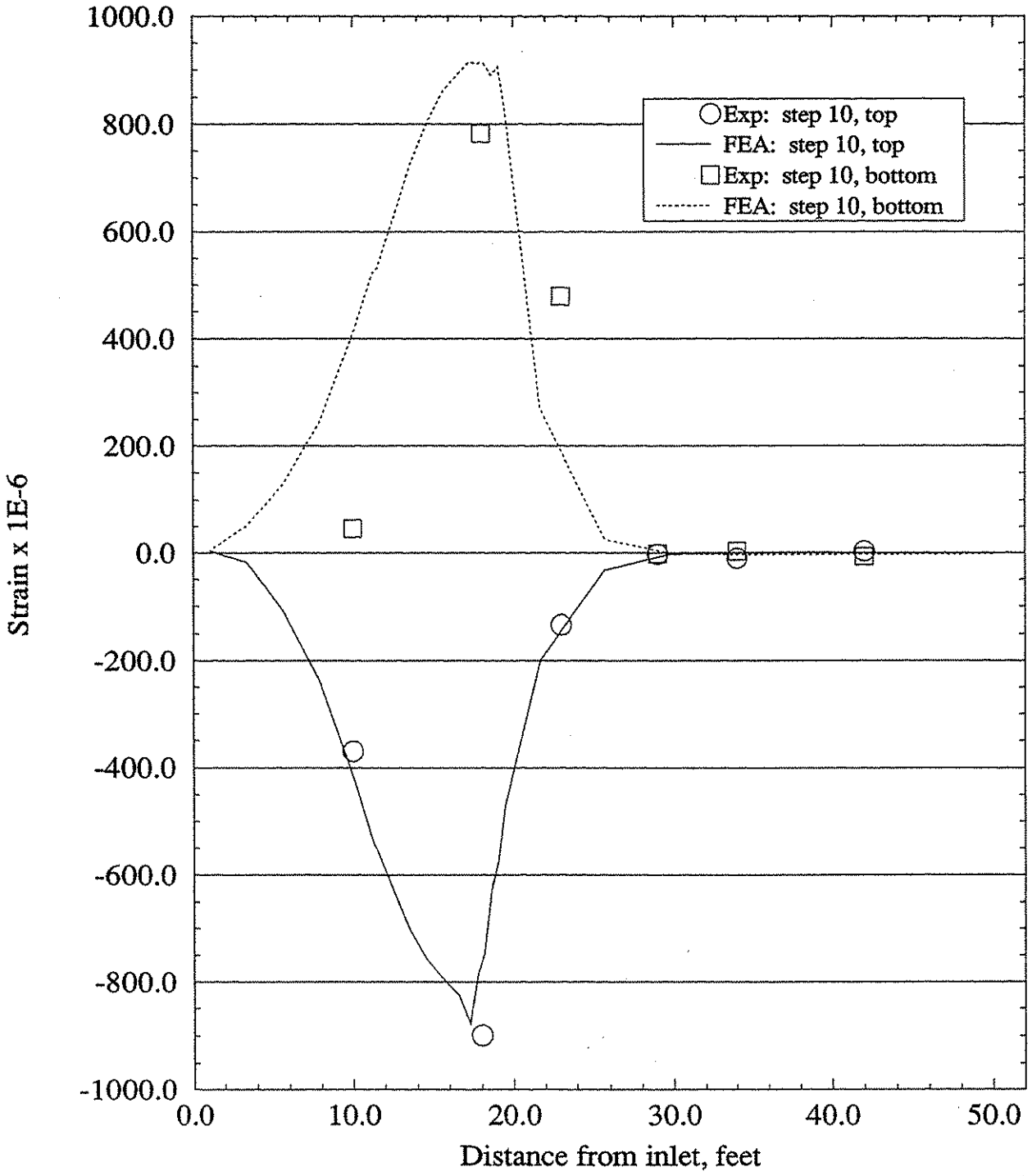

Figure 4.8. Comparison of strains for 8NF test and FEA.

factor was determined by the method of Peiffer (1995). For the corrugation style 3X1 with 12 gage, the conversion factor was 0.2. Positive and negative values of strain indicate tension and compression, respectively. Figure 4.6, for example, shows the top of the pipe in compression (negative) and the bottom in tension (positive).

The strain comparisons for 8NF shown in Figures 4.6 to 4.8 indicate a good correlation between the FEA and test results with the exception of load step 2. This match between analytical and experimental strains is mostly a verification of the pipe model's performance since little soil-structure interaction occurs without the foreslope. It is, however, indicative of the accuracy of the model.

Since the strains recorded in the field for load steps 1 though 10 were all below the yield strain of 1,100 microstrain, it is not likely that the CMP response was affected by yielding. The point of maximum soil resistance stays centered at approximately 5.5 m (18 ft) from the inlet for all loads. If all of the downward soil resistance is assumed to act at this distance from the inlet, an approximation of the bending moment in the pipe model can be made easily. After moments are summed about the 5.5 m (18 ft) point, the resulting moment at load step 10 is 43 m-kN (68.6 ft-kips). This is below the limiting moment of 110 m-kN (81.5 ft-kips) calculated using FEA. Using the applied and limiting moments, an estimation of the maximum Mises stress occurring at this location can be made. By multiplying the limiting stress of 227,535 kN/m^2 (33 ksi) by the ratio of applied and limiting moments, the stress existing at a corrugation crest is estimated at 193,060 kN/m^2 (28 ksi). The Mises stress calculated from strains measured at this location in the field specimen is also 193,060 kN/m^2 (28 ksi). The finite element model for the pipe appears to predict behavior quite well.

The discrepancies between the FEA and test results at the highest load levels are most likely due to the soil model. As stated previously, a linear elastic constitutive model is incapable of reproducing all of the nuances in soil's behavior. The excessive deflections of the FEA at low load levels and underestimated deflections at high load levels suggest that a nonlinear elastic model would produce much more consistent results. A model such as Duncan-Chang's hyperbolic stress-strain model is capable of producing a stiffer soil at lower load increments and a softer soil at the higher loads. Models such as these have very slow convergence, however, and may prove too formidable for three-dimensional analysis where model sizes can be quite large.

The feasibility of using nonlinear constitutive models for the soil was explored by running one load step with the Drucker-Prager plasticity model. The material properties used in this model are given in Section 4.2.1. The response from this model was compared with the response of the linear elastic soil model to examine the effects of limiting plastic deformations. The deflected shape produced for load step 6 is shown in Figure 4.9 along with the linear elastic FEA and the test results. At these loads, the analysis with the elastic-plastic soil produces 5% greater inlet deflections than the FEA with the elastic soil. A better match between the elastic-plastic FEA and field results also exists. It is quite possible that at higher loads, the elastic-plastic soil model might produce even better correlations with the test results.

A difficulty with elastic-plastic FEA is the computational effort needed. Higher load levels were attempted, but the convergence proved to be too slow. In some cases, the automatic incrementation procedure in ABAQUS would stop at a fraction of the total load where the analysis would be terminated due to convergence problems in the plasticity algorithm.

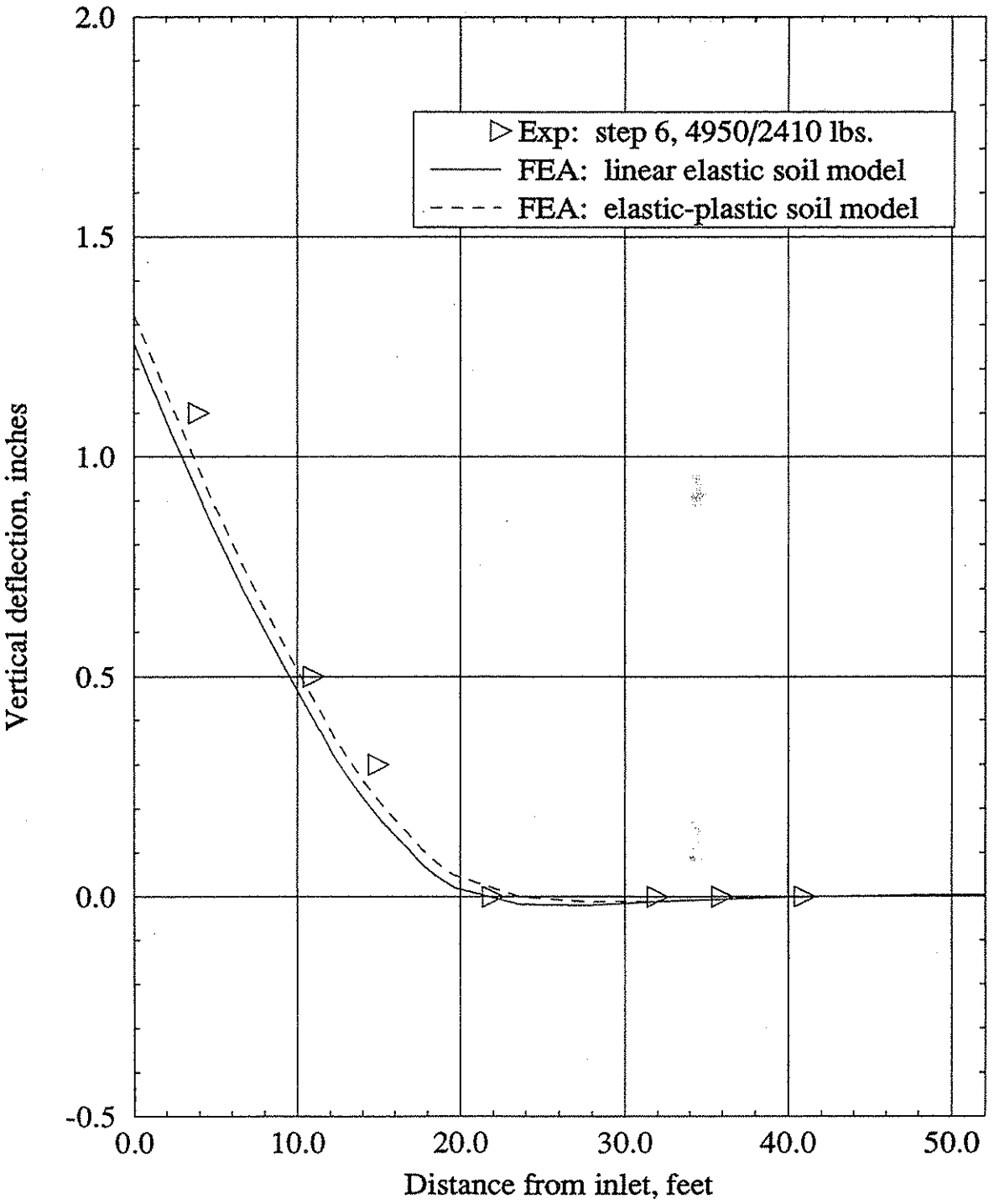

Figure 4.9. Comparison for linear elastic and linear elastic-plastic constitutive soil models for 8NF FEA. Strap 1/Strap 2 loads given.

Another difficulty with elastic-plastic FEA is that it is dependent on the stress history in the model. This caused complications in the FEA. Typically, the construction phase is modeled in culvert and buried pipe analysis. This step, as stated earlier, was bypassed for this analysis and the effect was simulated by declaring initial stresses in the soil model. Doing so created a somewhat unrealistic stress distribution throughout the soil after the initial dead load was applied. The approximate initial stresses caused the pipe to be forced vertically up while the surrounding soil was relatively unchanged. This caused the soil above the pipe to be in tension before uplift loads were applied. The soil in this area should be in a state close to geostatic conditions. Because the soil was in tension, there were premature tension failures at high loads. Load step 6 did not produce failures here, however. Tension failures for load step 6 were confined to a region in the foreslope where it intersects the top of the pipe.

4.2.6 Results and discussion for 8SC

Deflected shapes produced by the FEA of 8SC are shown in Figures 4.10 through 4.12 where load steps 1 through 11 are represented. Deflections shown were taken from the top of the pipe for both the experimental data and FEA. The general trend for the FEA is overestimation of the deflections at lower load levels, approximate matching at the middle load steps, and underestimation of deflections at the higher loads.

Figure 4.13 shows how the uplift loads and the pipe weight are distributed into the soil model. The general trend is much like that for 8NF except the width of the region where the soil is resisting the uplift loads is wider here. This is a result of the 2:1 foreslope and its increased region of contact with the pipe when compared with the foreslope of 8NF. The region of the soil's downward

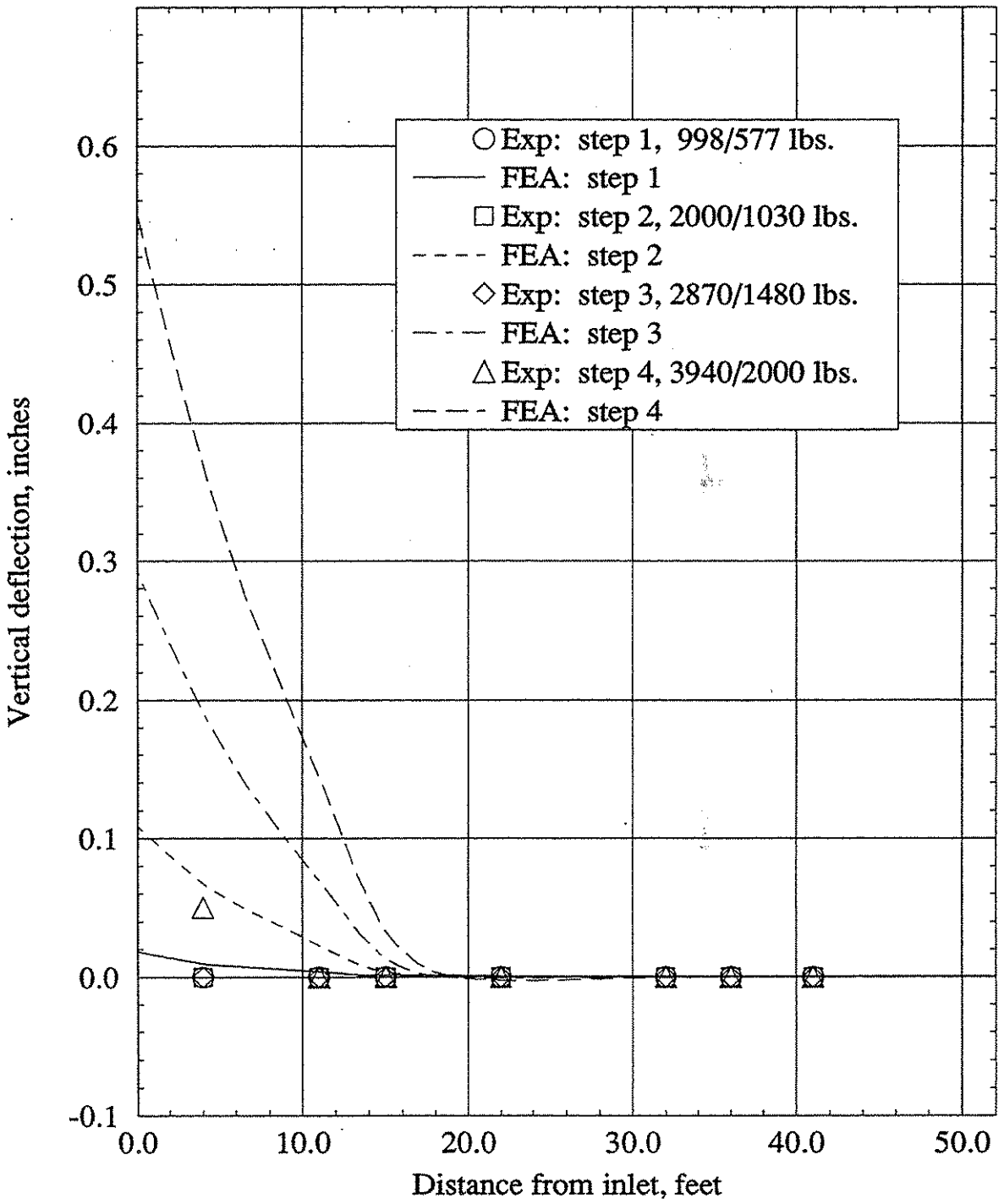

Figure 4.10. Comparison of 8SC FEA with experimental results. Steps 1 through 4 presented. Strap 1/Strap 2 loads given.

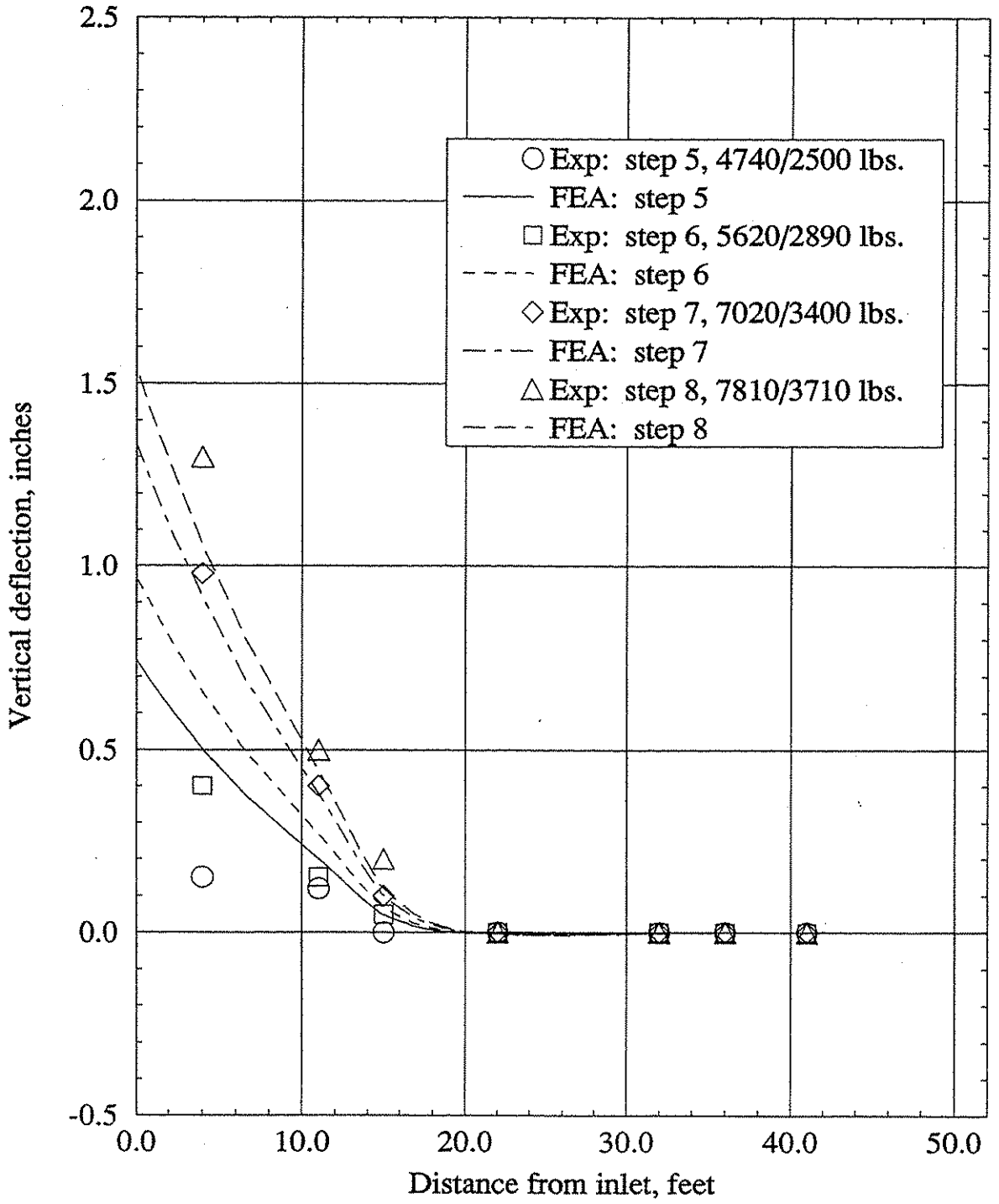

Figure 4.11. Comparison of 8SC FEA with experimental results. Steps 5 through 8 presented. Strap 1/Strap 2 loads given.

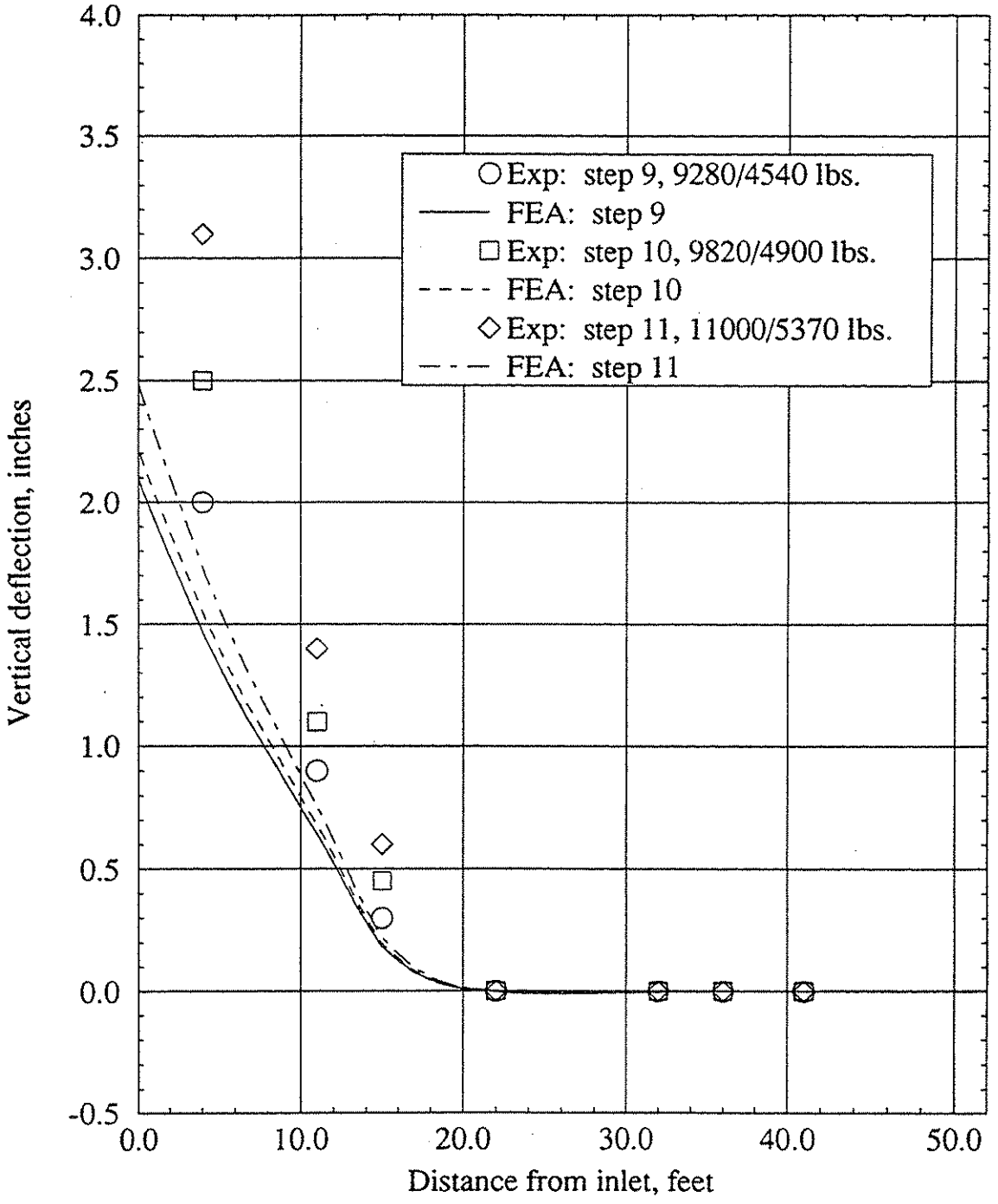

Figure 4.12. Comparison of 8SC FEA wtih experimental results. Steps 9 through 11 presented. Strap 1/Strap 2 loads given.

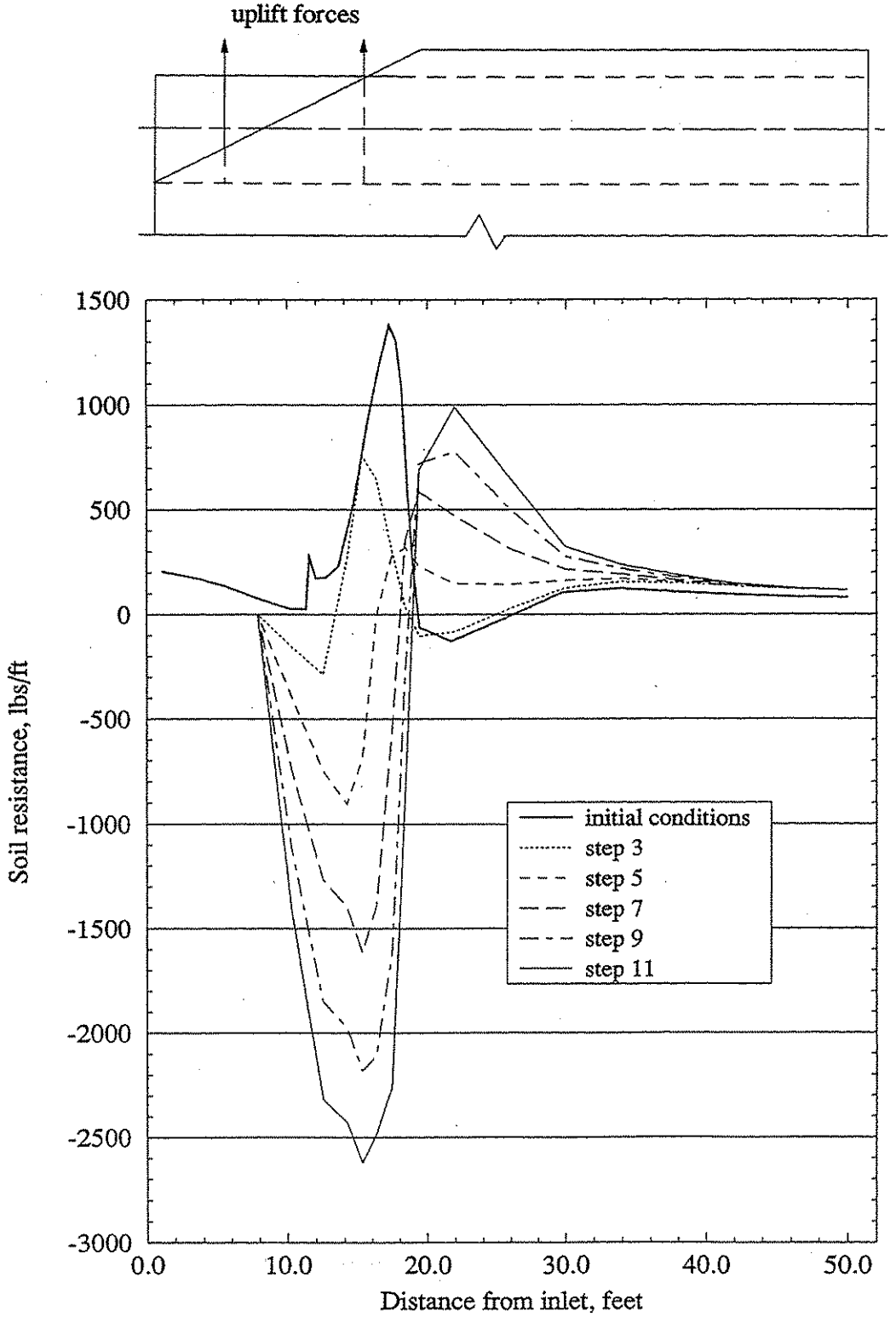

Figure 4.13. Soil resistance along CMP length for 8SC.

resistance runs from approximately 2.74 m to 6.10 m (9 ft to 20 ft) from the inlet. Again, all of the soil's resistance to the uplift forces is generated within the foreslope.

Figures 4.14 through 4.16 show the strains predicted by the FEA and those recorded in Test 8SC where various load steps are plotted. The analytical strains were converted using the conversion factor of 0.2 previously described in Section 4.2.5. Unlike the comparisons of the FEA and test strains for 8NF, more discrepancies exist between the analysis and test results. At the lower load increments, the FEA over-predicts strains. This follows the same pattern as the deflection data in Figures 4.10 and 4.11. At load steps 9 and 11 shown in Figure 4.16, the strains compare rather well. It is apparent that the foreslope in the field test is affecting the CMP's behavior more than the foreslope in the FEA.

There are several possibilities as to why the FEA is over-predicting deflections and strains at lower loads. Confining stresses from FEA in the foreslope region could be lower than those that existed in the field prior to uplift. This would cause the pipe model to slide more freely in the vertical direction. Or, the coefficient of friction for the circumferential direction may be low creating the same effect as low confining stresses. Also, the presence of adhesion between the soil and CMP could be restraining the vertical displacements as suggested in the interpretation of 8NF discrepancies. Even a small amount of adhesion causes a significant uplift resistance because the contact between the soil and structure is large. Adhesion was not used in interface elements; therefore, the FEA has a tendency to overestimate deflections at lower loads.

Another source of error in the FEA most certainly lies in the isotropic linear elastic constitutive model used for the soil. As a comparison, an elastic-plastic constitutive model was run

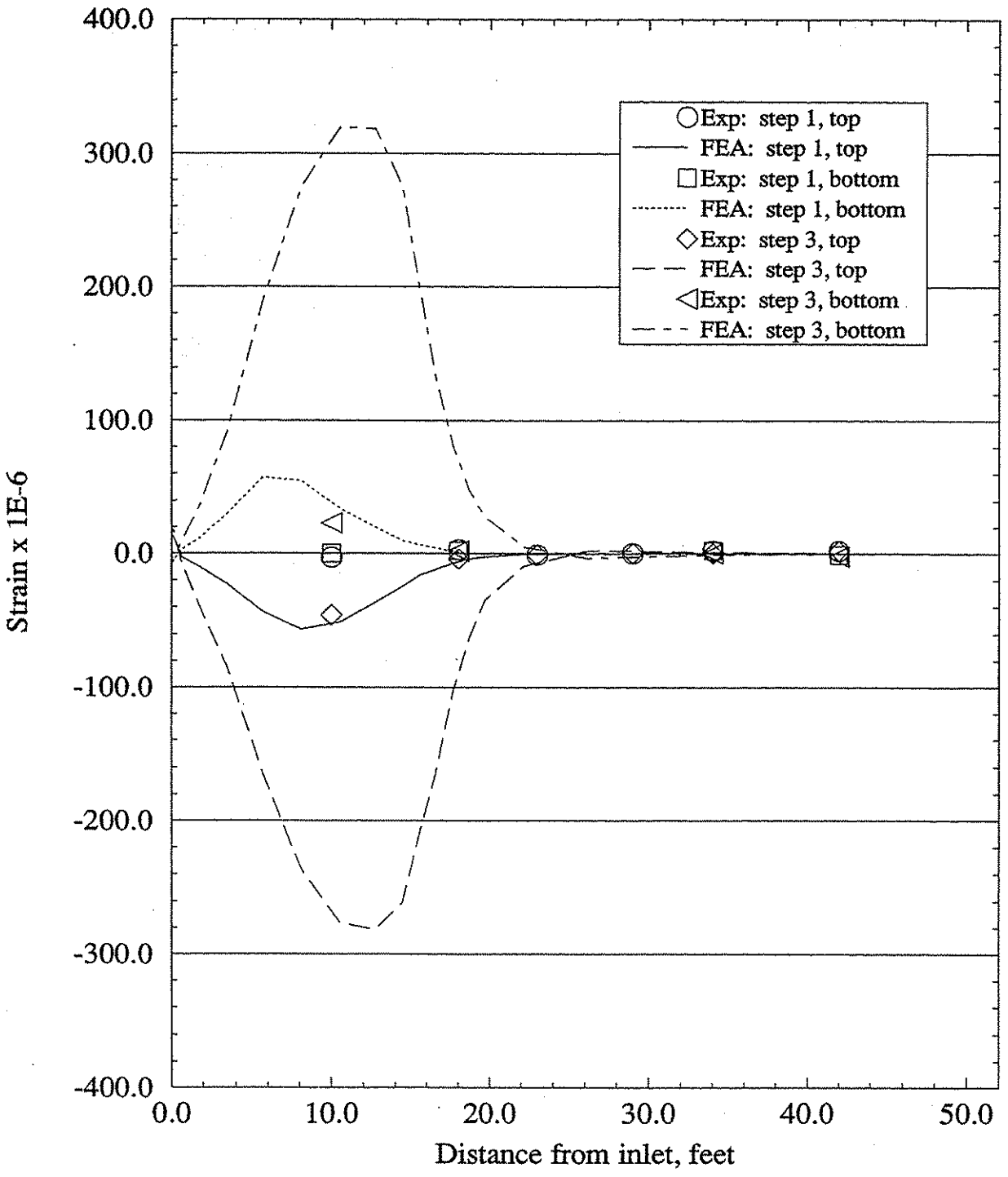

Figure 4.14. Comparison of experimental and FEA strains for 8SC.

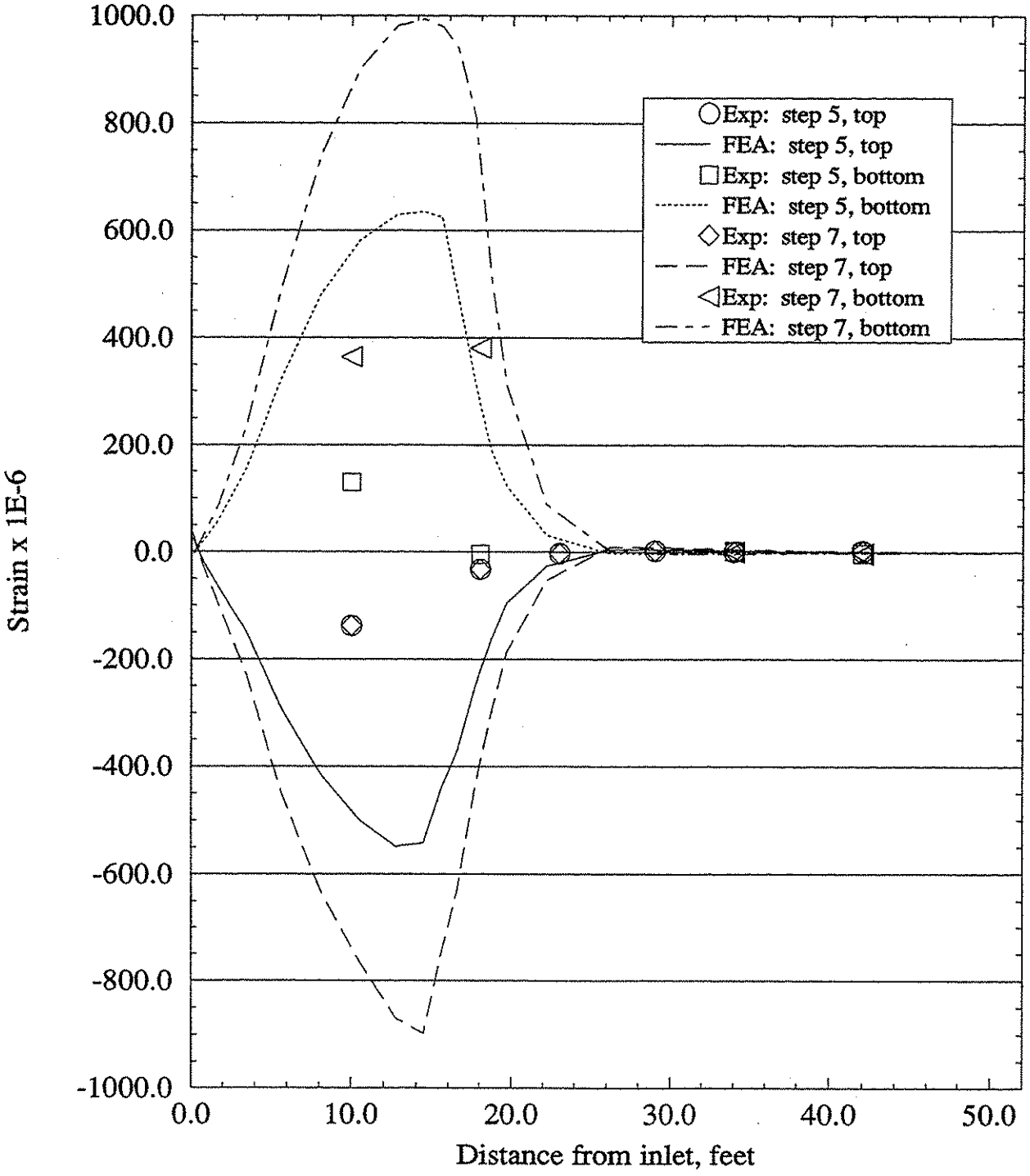

Figure 4.15. Comparison of experimental and FEA strains for 8SC.

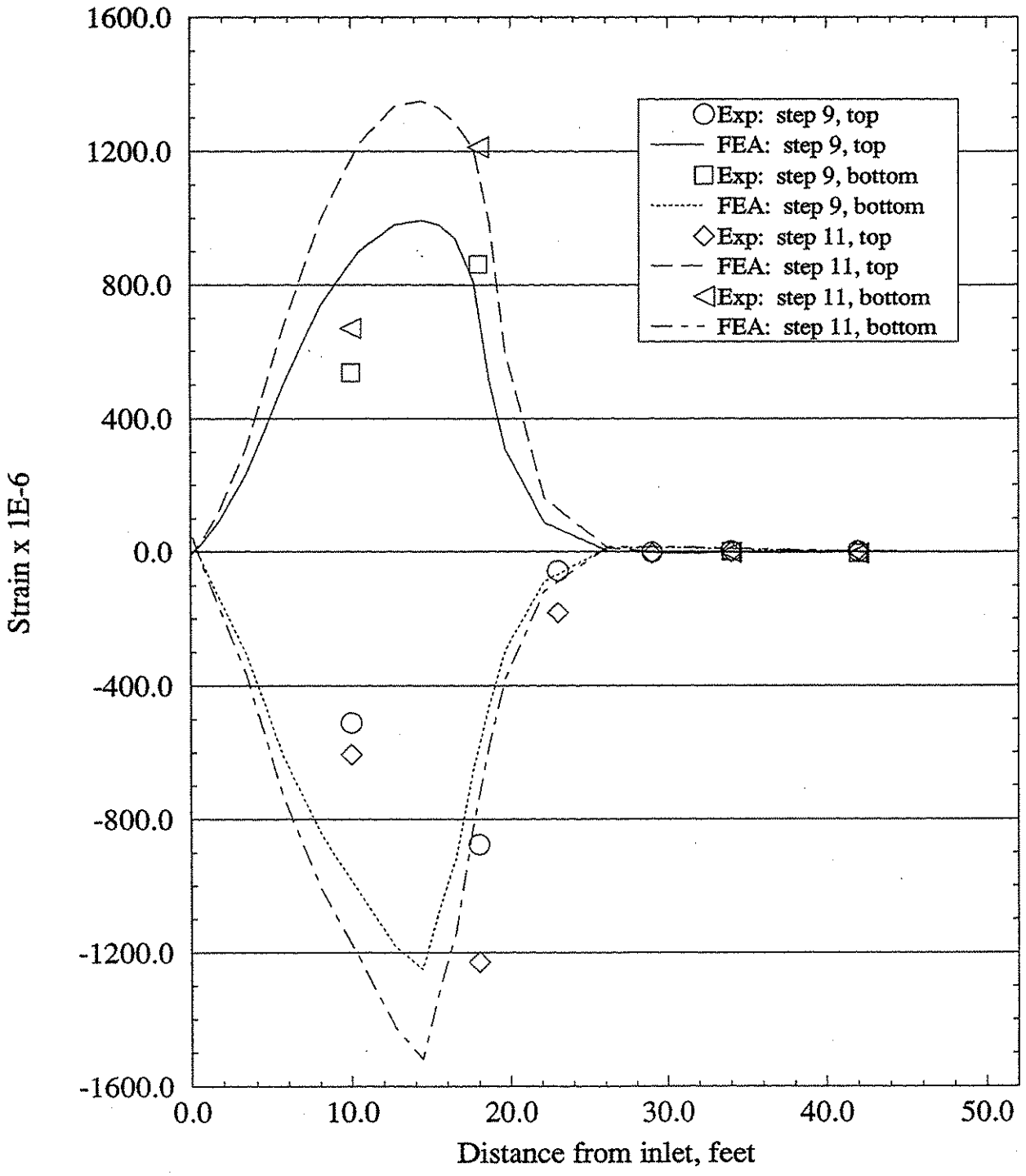

Figure 4.16. Comparison of experimental and FEA strains for 8SC.

for load step 6. The deflected shape from the elastic-plastic analysis, shown in Figure 4.17, is plotted with the deflections from the experiment and the linear elastic FEA.

The introduction of the Drucker-Prager model resulted in a 52% increase in the deflections at the CMP inlet. The magnitude of the increase must be viewed with care, however. The stress distribution in the soil model prior to the application of the uplift load was most likely in error because the construction phase was not modeled in this analysis. This phase is typically modeled in culvert analysis when more specific FEA programs such as CANDE (Culvert Analysis and Design, Katona et al., 1976) are used. This is to obtain an accurate representation of the stresses in the soil. This step, although not as important in the linear elastic analysis conducted for this study, is very important in plastic analysis or nonlinear elastic material models because the soil behavior is stress history dependent. Like the 8NF FEA, a problem arose when excessive tensile stresses develop in the soil model prior to uplift loading. This resulted in premature tensile failures above the pipe. If the construction phase were modeled, it is likely that the deflections would be somewhat lower than those from the elastic-plastic analysis shown in Figure 4.17.

The soil stresses prior to the application of the uplift loads also have an effect on the interface elements and their contribution to the CMP's deflections. This analysis produced confining stresses which are thought to be larger than those around the field specimen. This may have led to problems in the interface model. If confining stresses are too great, the allowable shear stresses would be overestimated and the pipe model would be overly constricted from displacements. This is not considered a problem, however, since behavior at the interface was similar to that observed in the full-scale test.

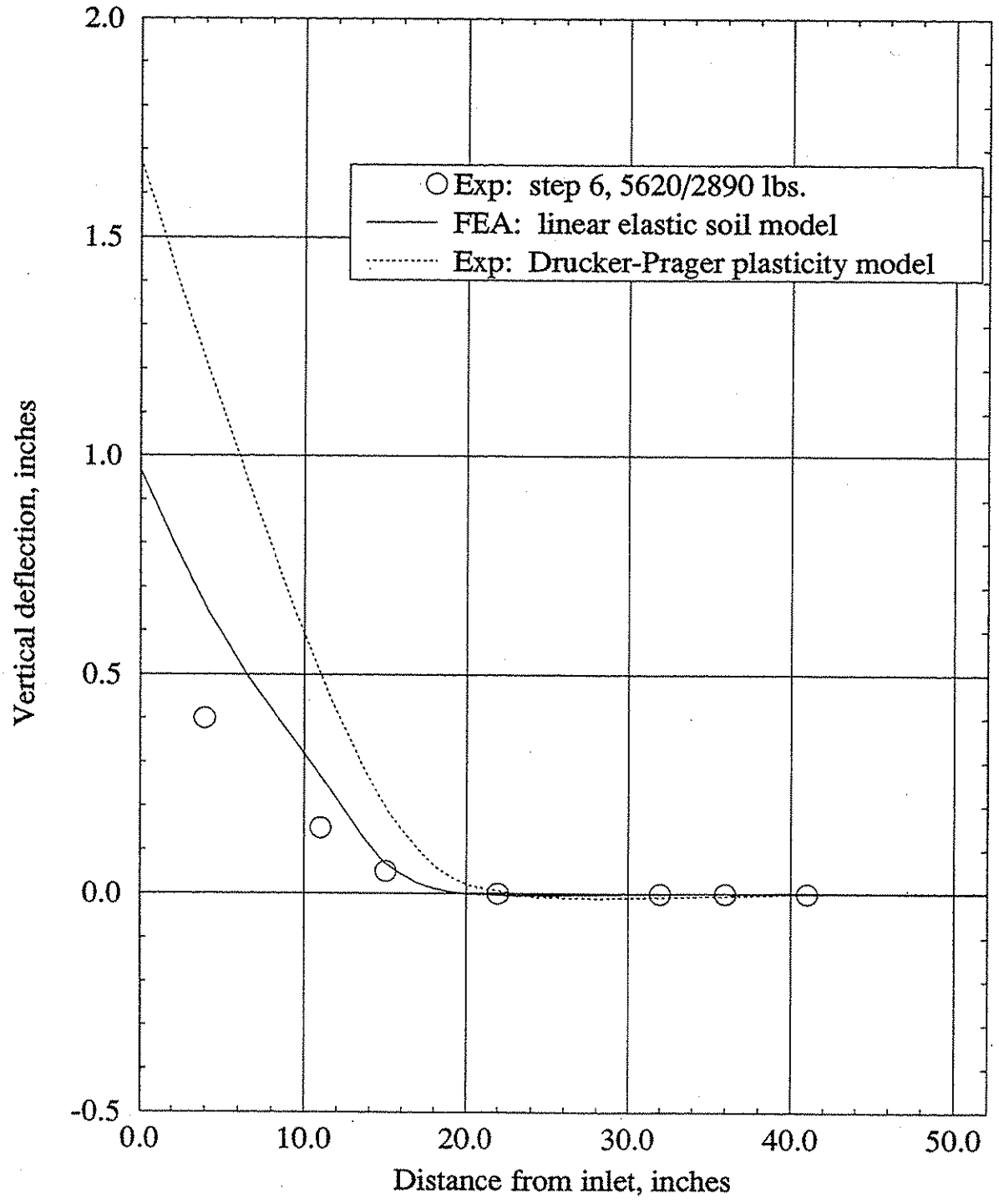

Figure 4.17. Comparison of 8SC FEA linear-elastic, elastic-plastic, and experimental results.

4.2.7 Results and discussion for 8R

Deflected shapes from Test 8R produced by FEA are plotted against test results in Figure 4.18. All deflections shown are relative to the original dead load state. In general, the analytical model's deflections reflect the behavior observed in the field quite well. Load steps towards the center of the loading range tend to have better matching between field and analytical results. The highest increment represented has a combined load of 145.5 kN (32,700 lbs). For this step, the FEA over-predicted the pipe deflections. This is atypical behavior when compared to all of the analysis previously presented in this chapter. One would expect the FEA to be below the field results at the highest load levels based on the previous results. One reason for this could be an error in the inlet's rotation measured in the field test. It appears that the rotation applied to the finite element model was slightly high. Another possibility might be the load levels run for the FEA are not high enough to show this behavior. The lower load steps exhibit the behavior common in this investigation, i.e. over-predicting deflections at the lower load levels. Possible explanations for the difference are: the adhesion, the soil model and the possibility that the rotations prescribed at the restraint location are in error. If the inlet was forced to rotate excessively at any of the load increments modeled, the pipe model would most definitely deflect more than the field specimen.

Figure 4.19 shows how the system's self weight and uplift loads are transferred into the soil. In the dead loading step, a large peak develops around 4.6 m (15 ft) from the inlet. This is most likely a combination of two things: differential settlements in the soil mass and the weight of the rear loading strap. These phenomena were also encountered in the analysis performed on 8NF and 8SC. The general trend is for the peak to progressively invert as loads are increased. This shows the soil resists more load as the total uplift force is increased. The maximum load the soil achieves is

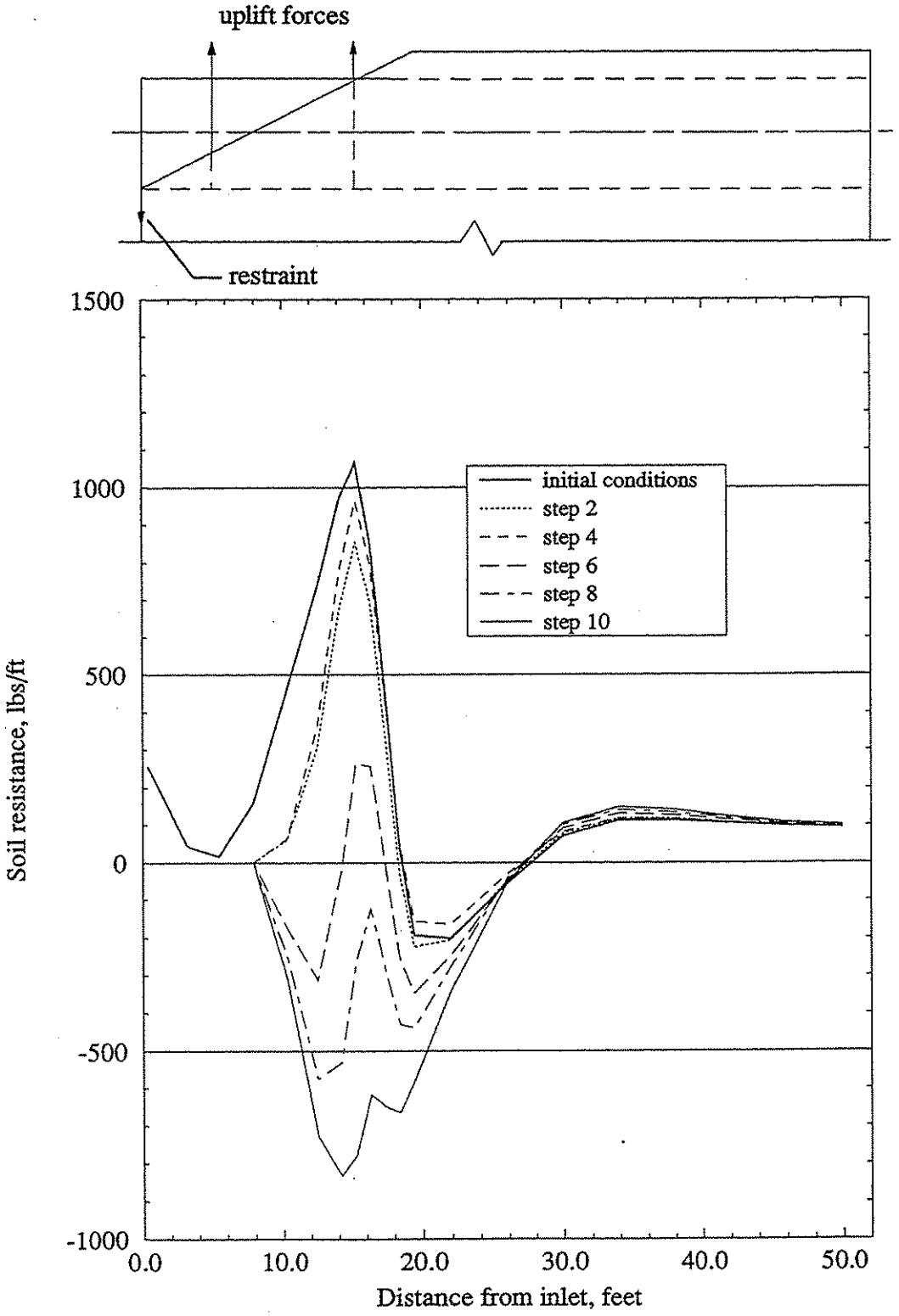

Figure 4.19. Soil resistance per foot length of 8R SWP model.

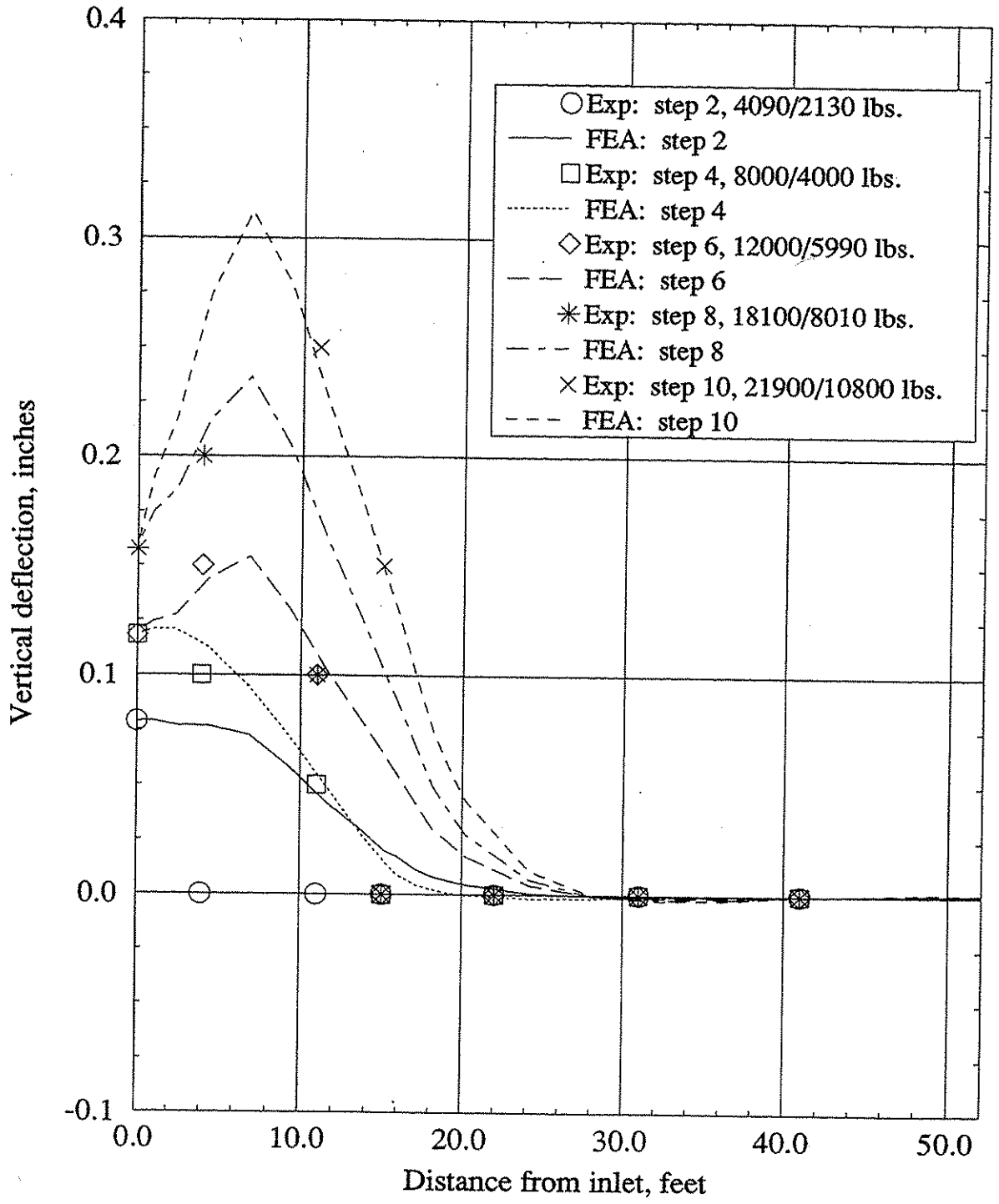

Figure 4.18. Comparison of 8R FEA and test deflected shapes. Strap 1/Strap 2 loads given.

approximately 12 kN/m (820 lb/ft) of the pipe. Most of the uplift loads are resisted by the soil in the foreslope as is the case with Tests 8NF and 8SC results. Beneath the soil embankment, the effects of the uplift loads are diminished until all that remains is the pipe self-weight of 1.9 kN/m (130 lbs/ft).

Strain comparisons for four load steps are shown in Figures 4.20 and 4.21. The strains predicted by the FEA do not match well with those recorded in the test. The general trend for the two sets of results is similar but the FEA tends to over-predict strains. This could be a result of the end restraint. In the field tests, the concrete mass was approximately 0.61 m (2 ft) in length and reached from the mid height of the CMP to approximately 1.22 m (4 ft) below the pipe (see Figure 3.11). The FEA was conducted with the restraint conditions applied at the very end of the pipe model. This would tend to put the strains calculated using the FEA higher than would be expected if the analysis had placed the restraining force at the center of the tiedown. Also, the test results show the top and bottom surfaces almost always in tension. For this to occur the end restraint must resist axial deflections. The FEA allowed the restraint to move freely along the longitudinal axis and therefore created more symmetric bending behavior than that recorded in the field.

4.3 Finite Element Model for Determination of Restraint Force

The model developed for determining restraint forces is referred to as 8RF. It was created much like the 8SC model but with an alternate loading and an added restraint at the inlet. The loading straps modeled in previous FEA were excluded; the remaining elements were the soil, pipe, and interface elements. All soil, pipe, and interface material properties had base values equivalent to those used in the previous analysis. Material properties thought to be important in the overall model behavior were varied to perform a sensitivity study.

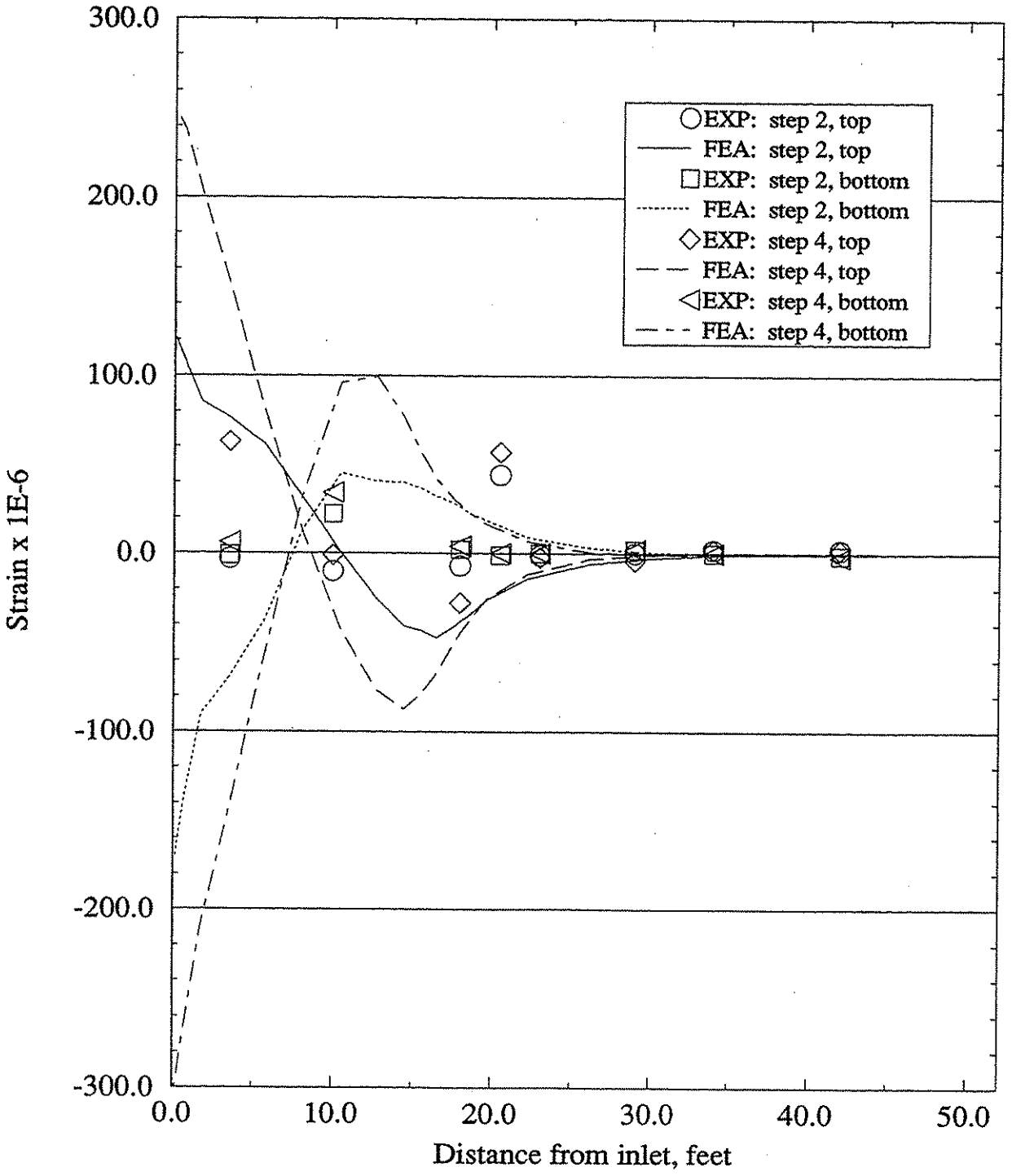

Figure 4.20. 8R strain comparisons between FEA and test results.

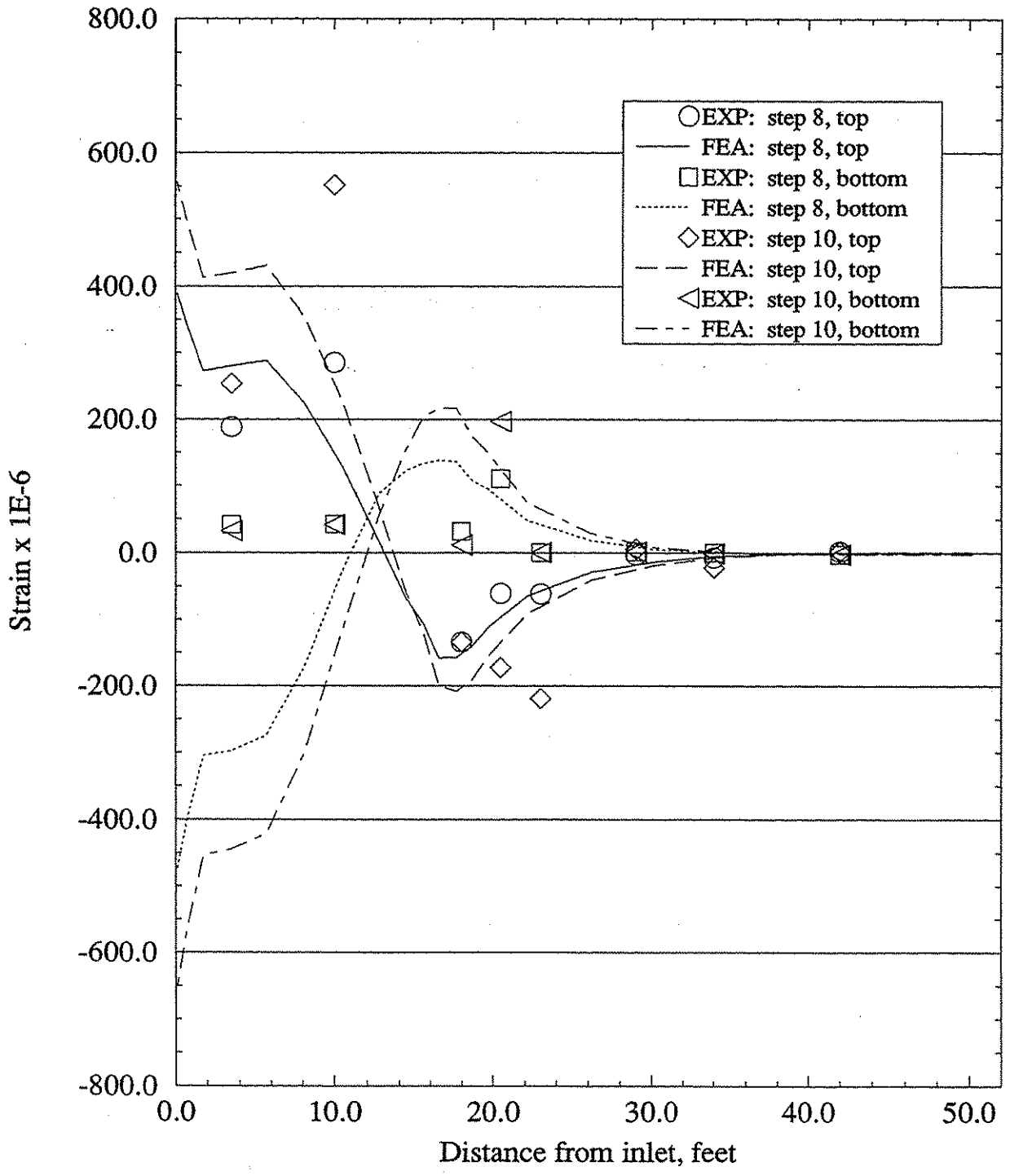

Figure 4.21. 8R strain comparisons between FEA and test results.

4.3.1 Loading and restraint procedure

The loading applied to 8RF was performed in two steps. The first step was a gravitational loading. This was necessary to put the entire model into a dead load condition and is important because the system mass aided in countering the applied uplift forces.

After step 1 had reached an equilibrium condition, the inlet boundary condition was applied along with the hydraulic loading. The restraint at the inlet was applied to the bottom of the pipe model and was used to control vertical movement. The node at this location can either be held in its current position or given an arbitrary vertical displacement. The act of prescribing a vertical displacement is intended to simulate movement of the restraint device. When a dead weight such as the concrete in 8R is used for uplift restraint, the mass will move before all of its weight is mobilized. An allowable displacement of ½ of a corrugation's depth was specified on the basis that vertical movement less than this would not allow piping beneath the CMP. In this analysis, this value was 12.7 mm (0.5 in.). This prescribed displacement also allowed more of the pipe's own flexural strength to mobilize and counteract the uplift.

At the location of the uplift restraint, rigid beam elements were added around the circumference of the pipe to prevent cross section distortions and avoid stress concentrations in the pipe model. This procedure increased the pipe hoop rigidity much like the concrete formed around the CMP in the 8R field test.

After the proper restraint condition had been applied, the load step was completed by applying the hydraulic load. As previously described, a triangular pore pressure distribution was used to determine this load. The inlet of the pipe was exposed to a full hydraulic head equal to the pipe diameter and the pressure was then decreased linearly to zero load at the outlet of the CMP. The

effect of the full hydraulic load created a buoyancy force equivalent to the mass of water the pipe is displacing.

For the finite element model used in this analysis, the slope area in the region around the outlet was not modeled in order to decrease the solution time. It should not affect the restraint value since the deflections occurring around the inlet have diminished before the back boundary is reached. The hydraulic load at the right side of the diagram in Figure 4.22 is shown as non-zero since it is not at the outlet of the pipe.

4.3.2 Results and discussion

A vertical force of 40.7 kN (9,150 lbs) was obtained from the restrained node after allowing the prescribed 12.7 mm (0.5 in.) of deflection at the inlet of the base of model 8RF. Multiplying the force by a factor of 2 to account for the other half of the finite element model, because of symmetry, produced a uplift restraint force of 81.4 kN (18,300 lbs).

Figure 4.22 shows the soil resistance along the length of the pipe model when the triangular hydraulic load is applied. The resistance developed by the soil model is similar to that produced in the 8R finite element model. Larger soil loads, however, are required to resist the hydraulic load. Like 8R model, the loads applied to the exposed pipe in the foreslope area in 8RF extend further into the soil embankment than in 8NF and 8SC. For 8RF, the soil resistance is affected by the pipe in the foreslope area to a point approximately 8.5 m (28 ft) from the inlet. At this location, the soil resistance developed is only that needed to resist the hydraulic load minus the pipe weight.

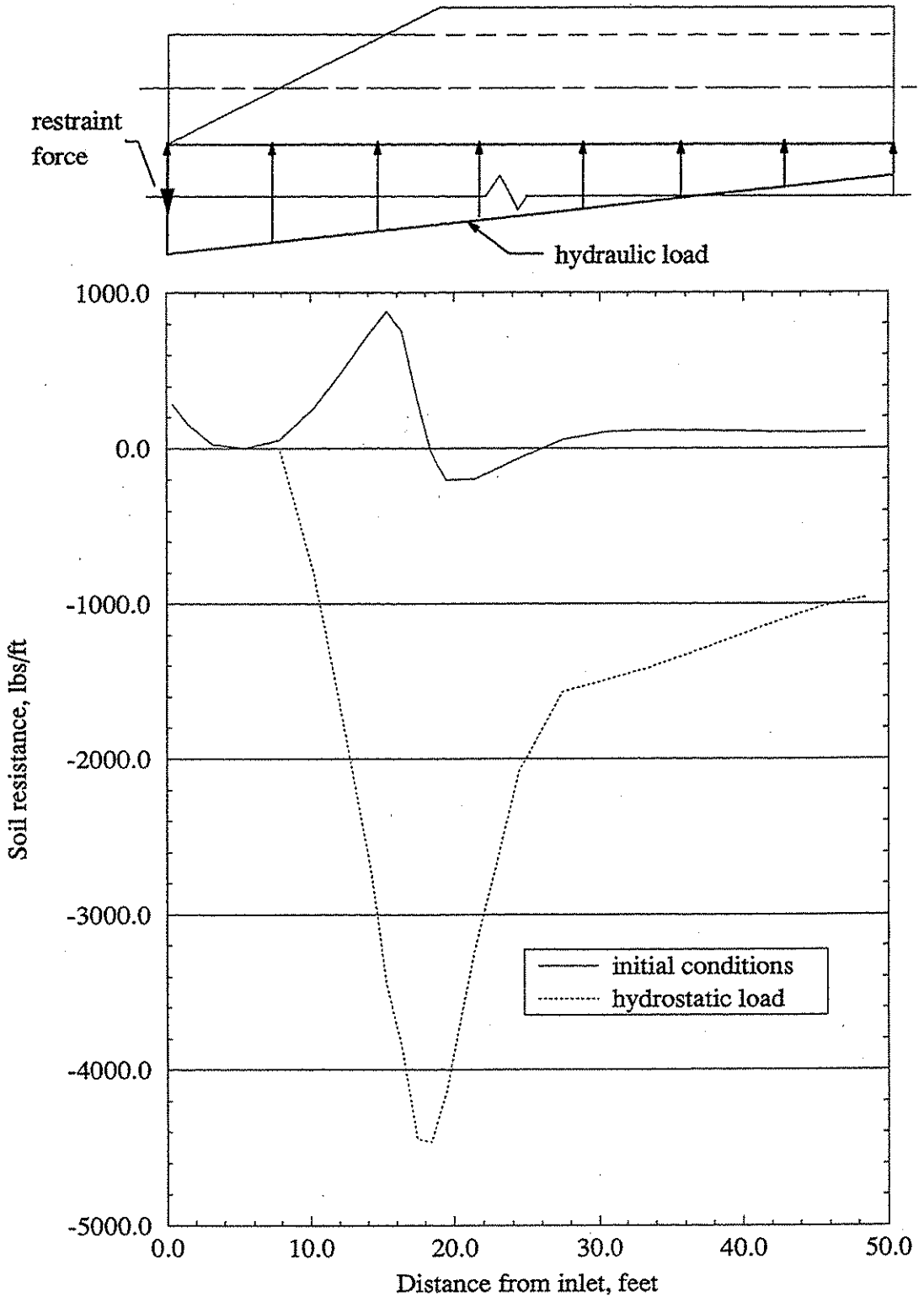

Figure 4.22. Soil resistance per foot length along SWP finite element model with hydraulic load.

Table 4.3 shows the results of varying the four main variables controlling the uplift behavior. The first four table entries are variables decreased by 50%. Of these, the soil modulus, E_{soil} has the largest effect on restraint force.

Table 4.3 Sensitivity analysis results.

Parameter	Original Value (psi)	Final Value (psi)	Change of Parameter (%)	Calculated Restraint Force (lb)	Change of Restraint Force (%)
E_{11}	17,400	8,710	-50	17,500	-4.4
E_{soil}	2,400	1,200	-50	19,400	+6.0
μ_{zz}	1.0	0.5	-50	18,800	+2.2
$\mu_{\theta\theta}$	0.6	0.3	-50	18,700	+2.2
μ_{zz}, $\mu_{\theta\theta}$	1.0, 0.6	0.0, 0.0	-100, -100	20,600	+12.6

Note: 1 psi = 6.89 kPA; 1 lb = 4.45 N.

Although variation of all properties had an effect on the required restraint force, the change is not substantial when one considers the assumptions required to arrive at this final model. The final model is relatively insensitive to material parameters.

5. CONCLUSIONS

Many factors are involved in the soil-CMP interaction and the bending characteristics of CMP including the influence of the backfill properties. In comparing the response for different foreslope conditions during the field tests, it has been shown that the presence of the foreslope has a significant effect on the CMP bending characteristics . This was further verified by two and three dimensional numerical analyses (Heilers, 1994 and Peiffer, 1995)

Another factor that significantly affects the required tiedown force is the amount of water flowing in the pipe. The influence of flow in the pipe on the restraining force is shown in Figure 5.1 where the restraint forces for 14 gage pipe and clayey alluvium backfill are plotted versus the amount of flow in the pipe. The results indicate a decrease in the restraining force from 60 kN (13,490 lb) to 1.2 kN (270 lb) as the flow level increases from 0 to 75% of the pipe diameter.

Klaiber et al (1993) presented data on tiedown forces required by seven different DOT's as a function of pipe diameter. In Figure 5.2, these curves are compared with the equivalent design curve developed in this study assuming a moderately stiff alluvium. The guidelines presented from this study have no safety factors and that safety factors, if applied, for the other curves in Figure 5.2 are not known. This comparison shows that Agencies 4, 8, 11 require larger forces for all pipe diameters. Agencies 9 and 6 have higher forces up to diameters of approximately 2.5 m (8 ft) where they become lower than the standards presented here. The forces required by Agencies 7 and 10 standards follow these recommendations up to a diameter of 1.5 m (5 ft) where they are lower than the force recommended here. This comparison indicates that several agencies' requirements may be

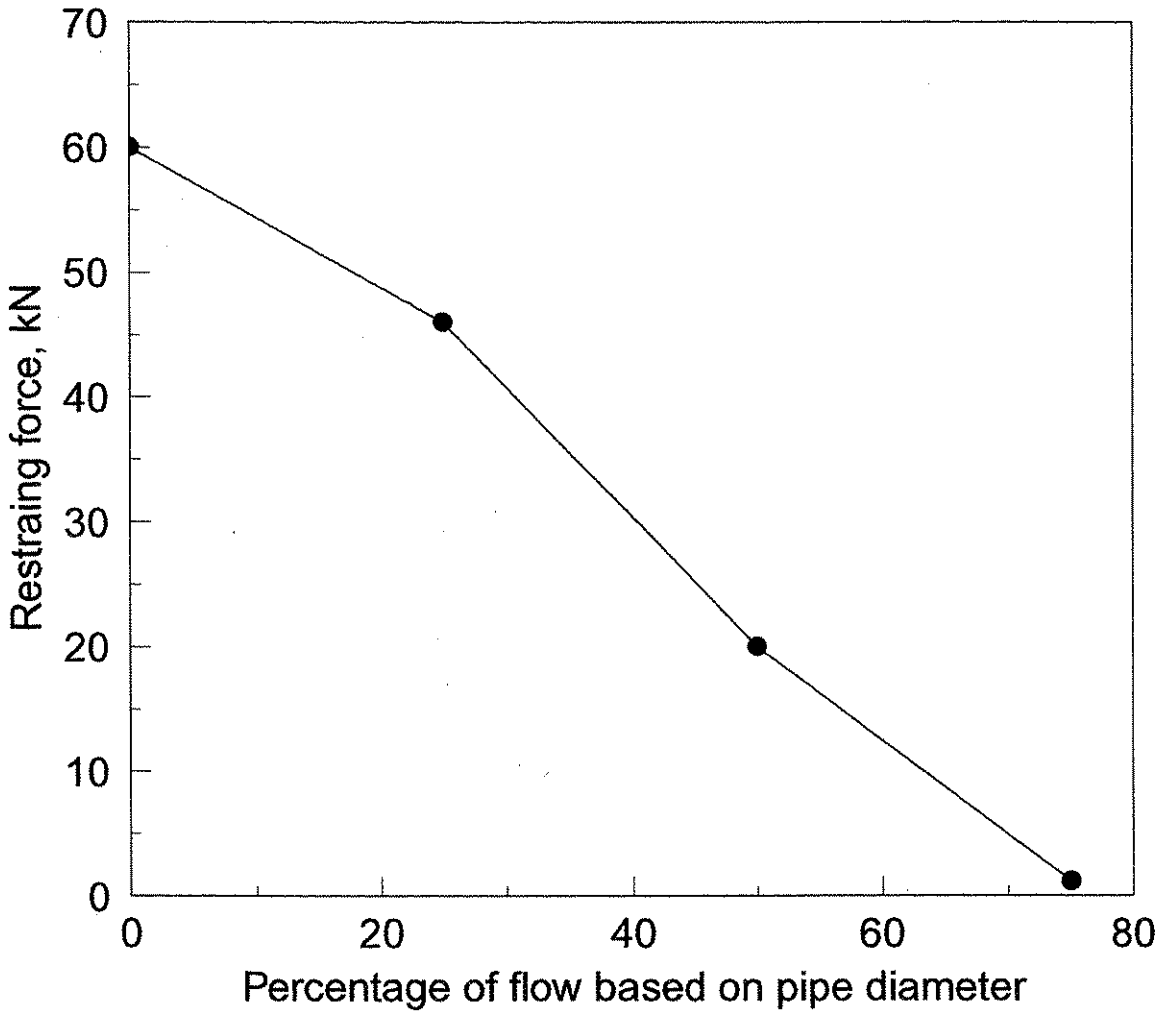

Figure 5.1. Influence of flow condition on restraining force.

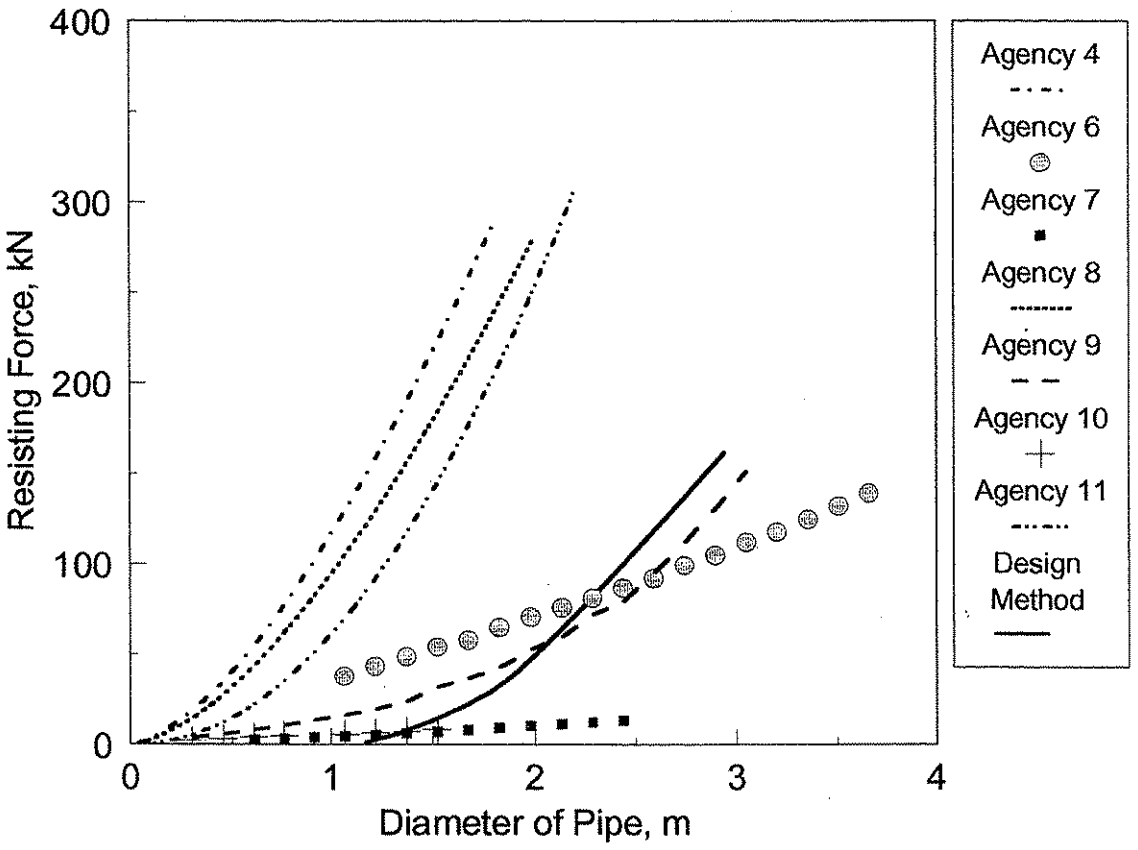

Figure 5.2. Comparison of various DOT design curves with design method presented here.

somewhat conservative. This also suggests that some agencies may be overlooking expanded use of CMP by limiting the maximum diameter pipe that they allow.

The design process suggested here provides an easy to follow procedure based upon experiment and analysis and allows the engineer to make final design considerations based on their judgment and experience. The method also indicates that in situations where the soil and/or pipe is sufficiently stiff or where total blockage of the pipe is unlikely, tiedowns may not be required.

6. ACKNOWLEDGEMENTS

This study was funded by a research grant (HR-362) from the Highway Research Board and the Highway Division of the Iowa DOT. The standards were developed with the help of an advisory board of practicing engineers including: Brad Barrett, Darrell Coy, Jim Christensen, Gary Harris, Mark Naraha, and John Steddom. The authors are grateful to the Iowa DOT for the financial support and to the committee for their advice and suggestions. A special thanks is extended to the numerous undergraduate students who assisted with the field testing portion of this investigation.

The opinions, findings, and conclusions expressed in this publication are those of the authors and not necessarily those of the Highway Division of the Iowa Department of Transportation.

7. BIBLIOGRAPHY

Abdel-Sayed, G., "Stability of Flexible Conduits Embedded in Soil," Canadian Journal of Civil Engineering, Vol. 5, September, 1978, pp. 324-333.

Abdel-Sayed, G., Bahkt, B., and Jaeger, L. G., Soil-Steel Bridges Design and Construction, McGraw-Hill, New York, 1994.

American Iron and Steel Institute, Handbook of Steel Drainage and Highway Construction Products, AISI, New York, 3rd Edition, 1983, Chapter 3.

Armco Drainage and Metal Products, Handbook of Drainage and Construction Products, Armco, Middletown, Ohio, 1955.

Austin, T. A., Lohnes, R. A., and Klaiber, F. W., "Investigation of Uplift Failures in Flexible Pipe Culverts," Final report to the Iowa Department of Transportation, March, 1990.

Austin, T. A., Lohnes, R. A., and Klaiber, F. W., "Investigation of Uplift Failures in Flexible Pipe Culverts," Abridgment of Final Report to the Iowa Department of Transportation, October, 1990.

Bathe, Klaus-Jűrgen, Finite Element Procedures in Engineering Analysis, Prentice-Hall, Inc., Englewood Cliffs, New Jersey, 1982.

Boresi, A. P., Schmidt, R. J. and Sidebottom, O. M., Advanced Mechanics of Materials, John Wiley and Sons, Inc., New York, 5th Edition, 1993.

Boulon, M. and Nova, R., "Modeling of Soil-Structure Interface Behaviour - A Comparison Between Elastoplastic and Rate Type Laws," Computers and Geotechnics, Vol. 9, pp. 21-46, 1990.

Bulson, P. S., Buried Structures-Static and Dynamic Strength, Chapman and Hall, New York, 1985.

Das, B. M. and Seeley, G. R., "Breakout Resistance of Shallow Horizontal Anchors," Journal of Geotechnical Engineering Division, ASCE, Vol. 101, No. GT9, September, 1975, pp. 999-1003.

Edgerton, R. C., "Culvert Inlet Failures-A Case History," Highway Research Board Bulletin 286, 1960, pp. 13-21.

Federal Highway Administration, "Pipe Culvert Inlet and Outlet Protection," FHWA Notice N 5040.3, April 26, 1974.

Federal Highway Administration, "Hydraulic Charts for the Selection of Highway Culverts," FHWA Hydraulic Engineering Circular #5, December 1965.

Federal Highway Administration, "Hydraulic Design of Highway Culverts," FHWA IP-85-16, September 1985.

Fourie, A. B. And Beer, G., "An Illustration of the Importance of Soil Non-Linearity in Soil-Structure Interaction Problems, Computers and Geotechnics, Vol. 11, No. 3, pp. 219-241, 1990.

Girges, Y., Abdel-Sayed, G., "Design of Multi-Span Soil-Steel Bridges," Developments in Short and Medium Span Bridge Engineering, The Canadian Society for Civil Engineering, Montreal, Canada, 1994.

Havens, B. T., "Determination of the Longitudinal Strength and Stiffness of Corrugated Metal Pipe," M.S. Thesis, Iowa State University, Ames, Iowa, 1993.

Heilers, G. A., "Numerical Analysis of Soil Response Due to Longitudinal Uplift of Corrugated Metal Pipe", M. S. Thesis, Iowa State University, Ames, Iowa, 1994.

Hibbitt, H. D., Karlsson, B. I., and Sorensen, E. P., "ABAQUS Version 4.8, Finite Element Program," Hibbitt, Karlsson, and Sorensen, Inc., Providence, Rhode Island, 1994.

Hibbitt, H. D., Karlsson, B. I., and Sorensen, E. P., "ABAQUS Version 5.3, Finite Element Program," Hibbitt, Karlsson, and Sorensen, Inc., Providence, Rhode Island, 1994.

Iowa Department of Transportation, Standard Specifications for Highway and Bridge Construction, Ames, Iowa, 1990.

Kardestuncer, H., Editor in Chief, and Norrie, D. H., Project Editor, Finite Element Handbook, McGraw-Hill, Inc., New York, 1987.

Katona, M. G. et al, "CANDE-A Modern Approach for Structural Design and Analysis of Buried Culverts," FHWA-RD-77-5, October 1976.

Kelkar, V. S., and Sewell, R. T., Fundamentals of the Analysis and Design of Shell Structures, Prentice-Hall, Inc., Englewood Cliffs, New Jersey, 1987.

Kennedy, J. and Laba, J. T., "Suggested Improvements is Designing Soil-Steel Structures," Transportation Research Record 1231, 1989, pp. 96-104.

Klaiber, F. W., Lohnes, R. A., Zachary, L. W., Austin, T. A., Havens, B. T., and McCurnin, B. T., " Design Methodology for Corrugated Metal Pipe Tiedowns: Phase I," Final Report to the Iowa Department of Transportation, February, 1993.

Kolář, V., and Němec, I., Modelling of Soil-Structure Interaction, Developments in Geotechnical Engineering Vol. 58, Elsevier Science Publishing Co., Inc., New York, 1989.

Lane, W. W., "Comparative Studies on Corrugated Metal Culvert Pipes," Report No. EES-236, Engineering Experiment Station, Ohio State University, February 1965.

Lange, K., Handbook of Metal Forming, McGraw-Hill Book Company, New York, 1985.

Linger, D. A., "Historical Development of the Soil-Structure Interaction Problem," Highway Research Record 413, 1972, pp. 5-12.

Luscher, U. and Höeg, K., "The Action of Soil Around Buried Tubes," Proceedings, 6th International Conference on Soil Mechanics and Foundations Engineering, Montreal, Canada, Vol. II, 1965, pp. 396-400.

Luscher, U. and Höeg, K., "The Beneficial Action of the Surrounding Soil on the Load-Carrying Capacity of Buried Tubes," Proceedings of the Symposium on Soil-Structure Interaction, University of Arizona, Tucson, Arizona, 1964, pp. 393-402.

Marston, A., "The Theory of External Loads on Closed Conduits," Bulletin No. 96, 1930, Iowa Engineering Experimental Station, Ames, Iowa, pp. 5-8.

Matyas, E. L. and Davis, J. B., "Prediction of Vertical Earth Loads on Rigid Pipes," Journal of Geotechnical Engineering, ASCE, Vol. 109, No. 2, February, 1983, pp. 190-201.

McCurnin, B. T., "Investigation of Soil-Structure Interaction of Corrugated Metal Pipe," M.S. Thesis, Iowa State University, Ames, Iowa, 1993.

Moore, I. D., and Brachman, R. W., "Three-Dimensional Analysis of Flexible Circular Culverts," Journal of Geotechnical Engineering, ASCE, Vol. 120, No. 10, October 1994, pp. 1829-1844.

Moore, I. D., "Local Strain in Corrugated Pipe: Experimental Measurements to Test a Numerical Model," Journal of Testing and Evaluation, JTEVA, Vol. 22, No. 2, March 1994, pp. 132-138.

Moore, I. D., "Response of Buried Cylinders to Surface Loads," Journal of Geotechnical Engineering, ASCE, Vol. 113, No. 7, July 1987, pp. 758-773.

Morgan, B., "Design Methodology for the Prevention of Longitudinal Uplift in Corrugated Metal Pipe," M.S. Thesis, Iowa State University, 1995.

Moser, A. P., Buried Pipe Design, McGraw-Hill, New York, 1990.

Nielson, F. D., "Experimental Studies in Soil-Culvert Interaction," Highway Research Record 413, 1972, pp. 30-44.

Peiffer, E. A., "Numerical Modeling of Corrugated Metal Pipe Uplift with Soil-structure Interaction," M.S. Thesis, Iowa State University, Ames, Iowa, 1995.

Pestotnik, C., A Letter to County Engineers on "Report on Flexible Culvert Inlet Flotation Failures Survey," Iowa DOT Ref. No. 521.1, February 20, 1976.

Poulos, H. G., "Analysis of Longitudinal Behavior of Buried Pipes," Proceedings of the Conference on Analysis and Design in Geotechnical Engineering, ASCE, June, 1974, pp. 199-223.

Riley, W. F., and Zachary, L., Introduction to Mechanics of Materials, John Wiley and Sons, Inc., New York, 1989.

Rowe, R. K., and Davis, E. H., "The Behavior of Anchor Plates in Clay," Geotechnique, Vol. 32, No. 1, March, 1982, pp. 9-23.

Rowe, R. K. and Davis, E. H., "The Behavior of Anchor Plates in Sand," Geotechnique, Vol. 32, No. 1, March, 1982, pp. 25-41.

Spangler, M. G. and Handy, R. L., Soil Engineering, Harper and Row, New York, NY, 4th Edition, 1982.

Spangler, M. G., Soil Engineering, The International Textbook Company, Scranton, PA, 1st Edition, 1951.

Spangler, M. G., "The Structural Design of Flexible Pipe Culverts," Engineering Experiment Station, Iowa State University, Bulletin 153, 1941.

Syed Ahmed, A. M., McMickle, R. W., and Brassow, C. L., "Soil-Pipe Interaction and Pipeline Design," Transportation Engineering Journal, ASCE, Vol. 107, No. TE1, January, 1981, pp. 45-58.

Timoshenko, S., Woinowsky-Krieger, S., Theory of Plates and Shells, McGraw-Hill Book Company, Inc., New York, 2nd Edition, 1959.

Trautman, C. H., O'Rourke, T. D., and Kulhawy, F. H., "Uplift Force-Displacement Response of Buried Pipe," Journal of Geotechnical Engineering Division, ASCE, Vol. 111, No. 9, September, 1985, pp. 1061-1076.

Trautman, C. H., and O'Rourke, T. D., "Uplift Force-Displacement Response of Buried Pipe," Journal of Geotechnical Engineering Division, ASCE, Vol. 111, No. 9, September, 1985, pp. 1077-1092.

Vesic, A. S., "Expansion of Cavities in Infinite Soil Mass," Journal of Soil Mechanics and Foundations Division, ASCE, Vol 98, No. SM3, March, 1972, pp. 265-290.

Vesic, A. S., "Breakout Resistance of Objects Embedded in Ocean Bottom" Journal of Soil Mechanics and Foundations Division, ASCE, Vol 97, No. SM9, September, 1971, pp. 1183-1205.

Watkins, R. K., "Failure Conditions of Flexible Culverts Embedded in Soil," Highway Research Board Proceedings, Vol. 39, 1960, pp. 361-371.

Watkins, R. K., and Spangler, M. G., "Some Characteristics of the Modulus of Passive Resistance of Soil: A Study in Similitude," Highway Research Board Proceedings, Vol. 37, 1958, pp. 576-583.

Young, W. C., Roark's Formulas for Stress and Strain, McGraw-Hill Book Company, New York, 6th Edition, 1989.

APPENDIX A: Examples of Design Procedure

The following examples are provided to help understand the design process. Data are assumed for the examples. It is up to the user to determine the pipe diameter by using the HEC 5 design process. The examples are for the installation of a new culvert, not retrofitting an existing culvert.

Example 1.

Given: $Q = 5\ m^3/s$ (175 cfs) Channel cross section: see Figure A.1a.
pipe diameter = 1.2 m (4 ft)
pipe gage = 8
backfill material is a stiff glacial till

Step 1. Determine critical depth, d_c, using Figure 2.2.
$d_c = 3.75$ ft (1.7 m)

Determine normal depth, Dn, using iterative process:
From assumed channel cross section, $A = (10)Dn + 2(2(Dn))$
and the wetted perimeter $10 + 2(Dn^2 + (2Dn)^2)^{1/2}$

Dn, m	A, m^2	Wetted perimeter, m	R, m	$AR^{2/3}$	$Qn/1.0s^{1/2}$
0.15	1.5	10.7	0.14	0.42	0.74
0.2	2.1	10.89	0.68	0.68	
0.22	2.3	10.98	0.80	0.80	
0.21	2.2	10.93	0.75	0.75	

From the iterative process, the normal depth, Dn = 0.21 m.

Step 2. Determine assumed depth of flow in pipe.
The depth of flow in the pipe will be assumed to be 50% of the pipe diameter, which is equal to the depth of critical flow.

Step 3. Check adequacy of selected gage using Table 2.3.
Knowing the pipe diameter of 1.2 m and flow at 50% of the pipe diameter, Table 2.3 indicates that the 8 gage steel selected will be adequate to prevent yielding.

Step 4. Determine required restraining force.
Using 8 gage pipe and 50% flow, use Figure 2.6.
From Figure 2.6, No restraint is required for a 1.2 m diameter 8 gage steel pipe backfilled with a stiff glacial till and 50% flow in the pipe.

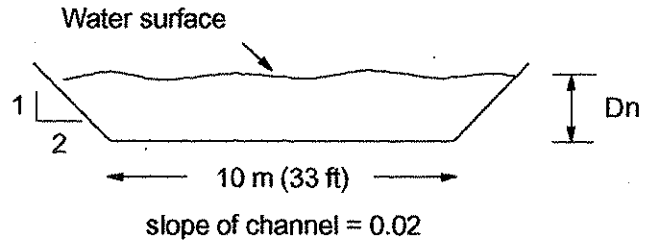

(a) Assumed channel cross section for Example 1.

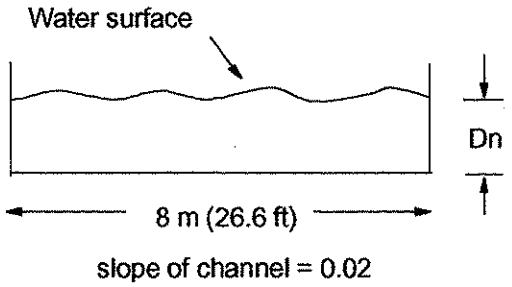

(b) Assumed channel cross section for Example 2.

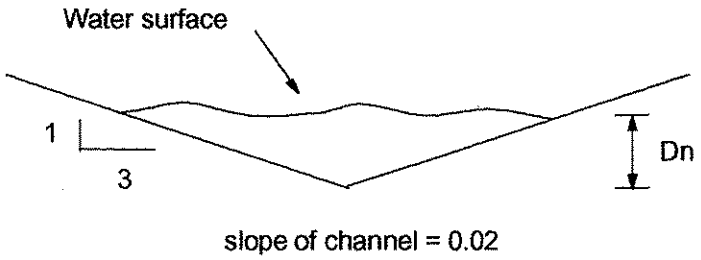

(c) Assumed channel cross section for Example 3.

Figure A.1. Assumed channel cross sections for example problems.

Example 2.

Given: Q = 20 m^3/s (700 cfs) Channel cross section: See Figure A.1b.
pipe diameter = 2.1 m (7 ft)
pipe gage = 14
backfill material is clayey alluvium

Step 1. Determine critical depth, dc, using Figure 2.2. dc = 6.7 ft (2.0 m)

Determine normal depth, Dn, using iterative process:
From assumed channel cross section, A = 8Dn
and the wetted perimeter 8 + 2Dn

Dn, m	A, m^2	Wetted perimeter, m	R, m	$AR^{2/3}$	$Qn/1.0s^{1/2}$
0.405.5	10.8	0.37	2.06	2.95	
0.50	4.32	11.0	0.45	2.96	
0.6	6	11.5	0.53	3.95	

From the iterative process, the normal depth, Dn = 0.5 m.

Step 2. Determine assumed depth of flow in pipe.

The depth of flow in the pipe will based on the normal depth of 0.5 m, which is approximately 25% of the pipe diameter.

Step 3. Check adequacy of selected gage using Table 2.3

Based on the flow of 25% and a pipe diameter of 2.1 m, Table 2.3 indicates the 14 gage steel selected will be sufficient.

Step 4. Determine required restraining force.

Using 14 gage pipe and 25% flow, use Figure 2.17.

From Figure 2.17, the restraining force required for a 2.1 m diameter 14 gage steel pipe backfilled with clayey alluvium and 25% flow in the pipe is 46 kN (10 kips).

Example 3.

Given: Q = 15 m^3/s (530 cfs)
Channel cross section: See Figure A.1c.
pipe diameter = 2.7 m (8 ft)
pipe gage = 14
backfill material is between clayey alluvium and till.

Step 1. Determine critical depth, dc, using Figure 2.2. dc = 5.8 ft (1.7 m)

Determine normal depth, Dn, using iterative process:

Dn, m	A, m^2	Wetted perimeter, m	R, m	$AR^{2/3}$	$Qn/1.0s^{1/2}$
1	3.0	6.3	0.47	1.82.06	2.27
1.1	3.63	6.9	0.52	2.35	
1.05	3.3	6.6	0.50	2.07	
1.08	3.5	6.8	0.51	2.24	

From the iterative process, the normal depth, Dn = 1.08 m.

Step 2. Determine assumed depth of flow in pipe.

It is assumed that this culvert is located in a area which may possibly produce enough debris to completely plug the pipe.

Step 3. Check adequacy of selected gage using Table 2.3.

Based on the pipe diameter, flow condition, and 14 gage steel, Table 2.3 indicates that the 14 gage steel will not be adequate. To provide adequate steel, Table 2.3 suggests using steel between 8 and 12 gage. Use 10 gage steel to determine restraining force required.

Step 4. Determine required restraining force.
Using 10 gage pipe with no flow, use Figure 2.8.

From Figure 2.8, the restraining force based on a 2.7 m diameter 10 gage steel pipe backfilled with a material between clayey alluvium and till with no flow in the pipe is 142 kN (32 kips).